HYBRID FLUIDIC HEADING REFERENCE SYSTEM
AND
THE CONTROL OF SYSTEMS WITH PURE TIME DELAY

Sinh Lequoc

A THESIS
in the
Faculty of Engineering

Presented in Partial Fulfilment of the Requirements for
the Degree of Doctor of Engineering at
Sir George Williams University
Montreal, Canada

August, 1972.

Sinh Lequoc

HYBRID FLUIDIC HEADING REFERENCE SYSTEM
AND
THE CONTROL OF SYSTEMS WITH PURE TIME DELAY

ABSTRACT

A heading reference system which could have application in navigational systems has been implemented by introducing a negative rate feedback loop around a fluidic vortex rate sensor to continuously maintain zero rotational rate of the sensor, and hence a fixed orientation about its axis of sensitivity. The existence of an inherent pure time delay of appreciable magnitude in the fluidic rate sensor results in stability problems in the closed loop system.

This thesis investigates different linear feedback compensation circuits which may be readily implemented fluidically for stabilizing the heading reference system. The system dynamic performance with proportional-integral-derivative, proportional-integral and integral controller types of compensation is evaluated using hybrid computer simulation techniques. Initially, the system angular rate response is optimized using the Ziegler-Nichols criterion to demonstrate the feasibility of attaining acceptable system transient duration and rate error. The results are experimentally verified using a 5.0 inches coupling diameter vortex rate sensor, electronically implemented feedback loop and a D.C. sensor drive servomotor. The results indicate that the simulation model adequately represents the experimental heading system, that the system dynamic performance justifies a more appropriate optimization technique, and

that a proportional-integral controller offers the best compromise between hardware complexity and system performance in the presence of substantial system noise.

The parameter settings for the proportional-integral controller are theoretically developed for both stability limit and minimum time-integral of error for a generalized negative feedback control system containing two first-order lags plus a pure time delay. The derived optimization equations are verified in the case of the heading reference system both by hybrid computer simulation and experimental system performance in terms of minimizing the system heading error. The closed loop frequency response for the heading reference system with optimum controller setting is also theoretically determined.

The derived complex set of equations defining the optimum controller parameter settings are approximated over a wide range of system transfer function parameter values by a much simplified set of equations using numerical curve fitting techniques. The approximation is verified by hybrid computer simulation and experimental heading system performance. The dependency of the heading error upon the system transfer function parameters is numerically determined over an extended range of parameter values. The results indicate that the optimized heading error varies linearly with the system time delay and non-linearly with the time lags.

ACKNOWLEDGMENT

The author is deeply indebted to his thesis supervisors, Dr. C. K. Kwok and Mr. W. F. Hayes, for their invaluable advice and assistance with this research.

Research facilities offerred to the author by the National Research Council of Canada, in particular by the Control Systems Laboratory, during this investigation are greatly appreciated.

The author is also grateful to the Université du Québec at Chicoutimi and its mechanical engineering staff for the leave of absence and to his wife Louise for her constant support in achieving the fulfilment of this thesis.

TABLE OF CONTENTS

LIST OF FIGURES

NOMENCLATURE

t	Time, sec.
s	Laplace operator (sec^{-1})
G_1	Rate sensor gain ($in.H_2O/deg./sec.$)
G_2	Sensor drive motor gain (deg./sec./volt)
K_c	Feedback controller proportional gain
Θ_i	Angular heading input (degree)
Θ_o	Angular heading output (degree)
Θ_e	Angular heading error (degree)
T_L	Rate sensor pure time delay (sec.)
T_1	Rate sensor time constant (sec.)
T_2	Sensor drive motor time constant (sec.)
T_I	Feedback controller integration time constant (sec.)
K_2	$= (1/T_I)$ (sec^{-1})
T_D	Feedback controller derivative time constant (sec.)
ω_{co}	Uncompensated system crossover frequency (rad./sec.)
G_{co}	Uncompensated system overall gain at crossover frequency
ΔP	Rate sensor differential pressure output ($in.H_2O$)
E_m	Sensor motor drive voltage input (volt)
J	Rate sensor polar inertia (in^2-lbs)
g	Acceleration due to gravity ($in./sec^2$)
ΔP_t	Turbine differential pressure input ($in.H_2O$)
G_t	Turbine gain ($deg./sec./in.H_2O$)
N	Rate sensor/turbine drive coupled gear ratio

ω_i Angular rate input (deg./sec.)

ω_o Angular rate output (deg./sec.)

ω_e Angular rate error (deg./sec.)

K_1 Compensated overall system proportional gain = $G_1 K_c G_2$

q Laplace auxiliary variable

Φ Phase shift (deg.)

f Input frequency (cps)

δ Real part of the characteristic equation's root

Ω Imaginary part of the characteristic equation's root

M Ratio of two successive absolute amplitude values

(δ/Ω) System response damping ratio

ψ_n Rate sensor natural frequency (rad./sec.)

ζ Rate sensor damping coefficient

ΔP_∞ Rate sensor differential pressure at steady-state ($in.H_2O$)

Dimensionless quantities:

$$\tau = \frac{t}{T_L} \quad , \quad A = \frac{K_1 T_L^2}{T_1 T_2} \quad , \quad B = K_2 T_L$$

$$C = \frac{T_1+T_2}{T_1 T_2} T_L \quad , \quad D = \frac{T_L^2}{T_1 T_2} \quad , \quad E = \frac{T_1+T_2}{\sqrt{T_1 T_2}}$$

CHAPTER 1

INTRODUCTION

1.1 General

The potential environmental capability, reliability and, eventually, low cost of fluidic devices leads one to conceive many fluidic systems to compete directly with or to complement their electrical and mechanical counterparts. Particularly in spacecraft control, extensive effort has been made to develop a hybrid fluidic-mechanical equivalent of the conventional direction gyro. References 1, 2, 3, 4, 5 and 6 describe some typical hybrid fluidic-mechanical gyros which consist principally of a pneumatically supported and driven spinning spherical free rotor and a fluidic pick-off, as illustrated in figure 1.1. Such hybrid gyros operate on conventional gyrodynamic principles wherein the rotor spin axis remains fixed in inertial space in the absence of external disturbing torques. The gyro relative rotor angular displacement is generally sensed with a stator referenced fluidic pick-off which normally utilizes the relative movement between the rotor spin axis and the stator to attain a variable orifice or a flapper valve operation. The heading reference signal is proportional to the pick-off differential pressure signal. This heading signal, as

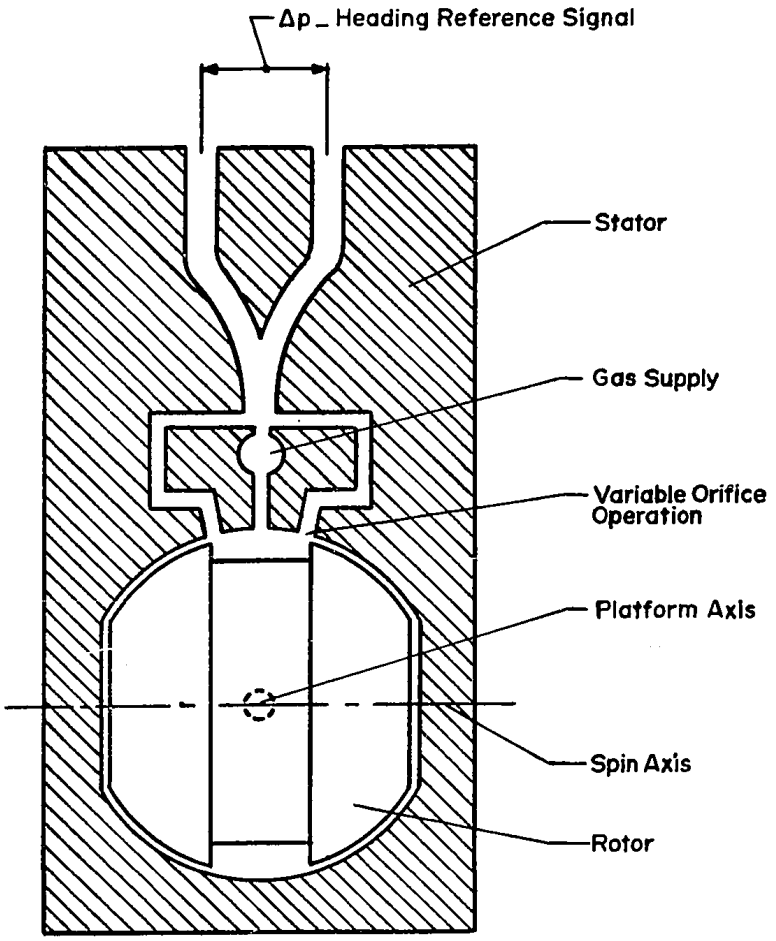

FIGURE I.I TYPICAL HYBRID DIRECTIONAL GYRO CONFIGURATION

mentionned in references 1, 4 and 5, is obtained over a relatively limited angular deviation, normally in the order of ± 5 to 10 degrees. Such pneumatically supported gyro rotors typically exhibit increasingly higher drift rates with increasing rate of stator angular deviation relative to the rotor spin axis. The precession results directly from a torque applied to the rotor about the platform axis through the mechanism of viscous shear within the fluid boundary layer which supports the rotor.

Such hybrid fluidic-mechanical gyros exhibit characteristics which are ideally suited for a nulling directional servo loop in short duration guidance systems where heading deviations are minimal. The heading variation capability as limited by acceptable linearity of the gyro heading reference signal as well as high drift rates at appreciable rates of change of heading, largely discount the adaptability of the hybrid gyro in navigation systems which normally are required to generate an accurate heading reference over appreciable durations and all points of the compass.

The development of a practical, all-fluid angular rate sensor brought a possible alternative to realize a pneumatic navigational system heading reference without moving parts. The general configuration of a rate sensor, as

shown in figure 1.2, consists of a thin cylindrical chamber with a perforated wall or "coupling ring". Flow is fed through the perforated wall across the chamber to exit through a centrally located outlet. As the differential pressure output signal is proportional to the sensor rotational rate, it is sufficient to integrate this signal to obtain the angular displacement, as shown in figure 1.3. The fluidic rate sensor exhibits performance comparable with conventional spinning rotor single axis rate gyros but without the use of moving parts. Fluidic rate sensor threshold limits are typically in the order of 0.1 deg./sec. (References 1 and 4) to 0.05 deg./sec. (Reference 10) for 5 to 6 inches diameter units.

The fluidic rate sensor has been used in a number of pneumatic control system applications where its inherent features of simplicity, reliability and environmental tolerance are exploited, such as TIM (Test Instrumentation Missile) roll attitude control system shown in figure 1.4 (References 7, 8 and 9). Angular motion of the vehicle is sensed by the vortex rate sensor, output signals from the vortex rate sensor are combined and amplified in a suitable fluidic amplifier network and then fed into a two-stage supersonic reaction amplifier. The final outflow emerges tangential to the missile skin and the system limit cycles in a dead band around zero attitude error.

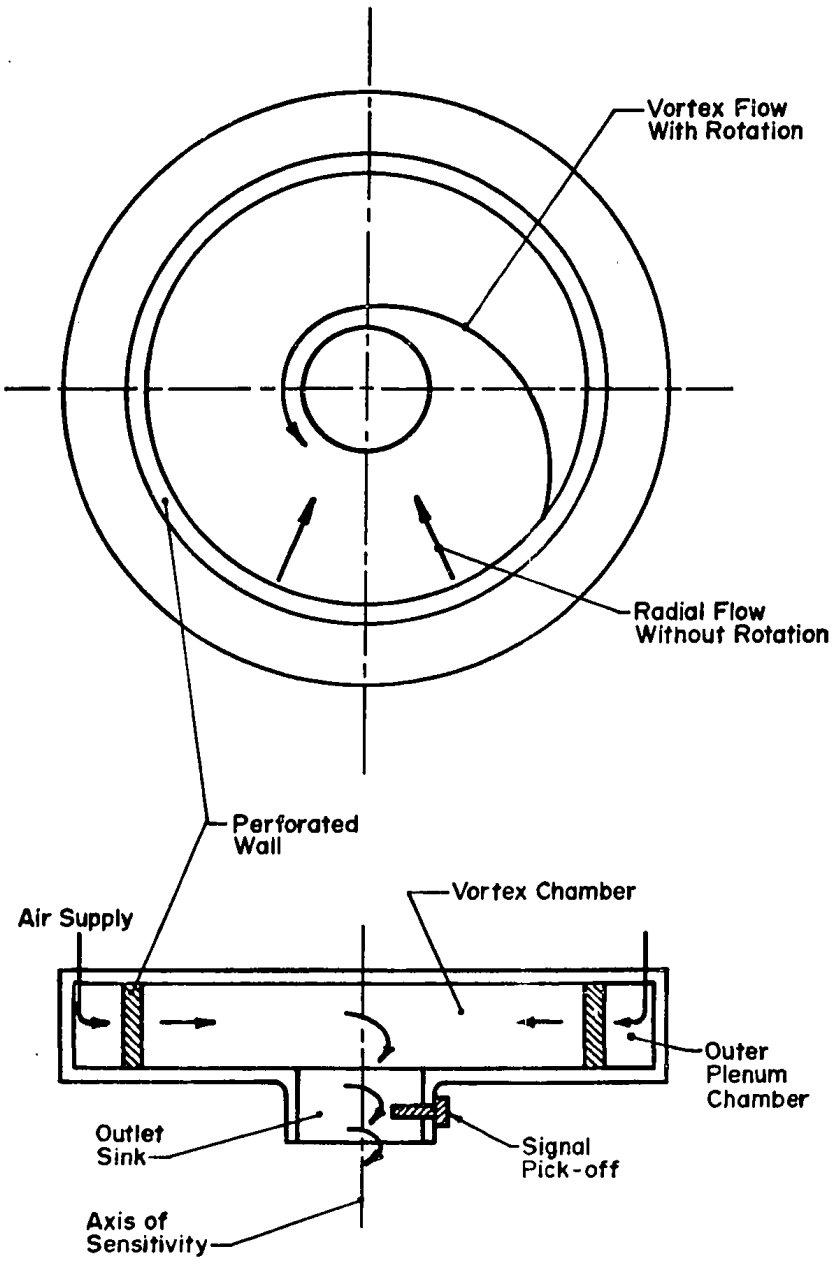

FIGURE 1.2 FLUIDIC VORTEX RATE SENSOR SCHEMATIC

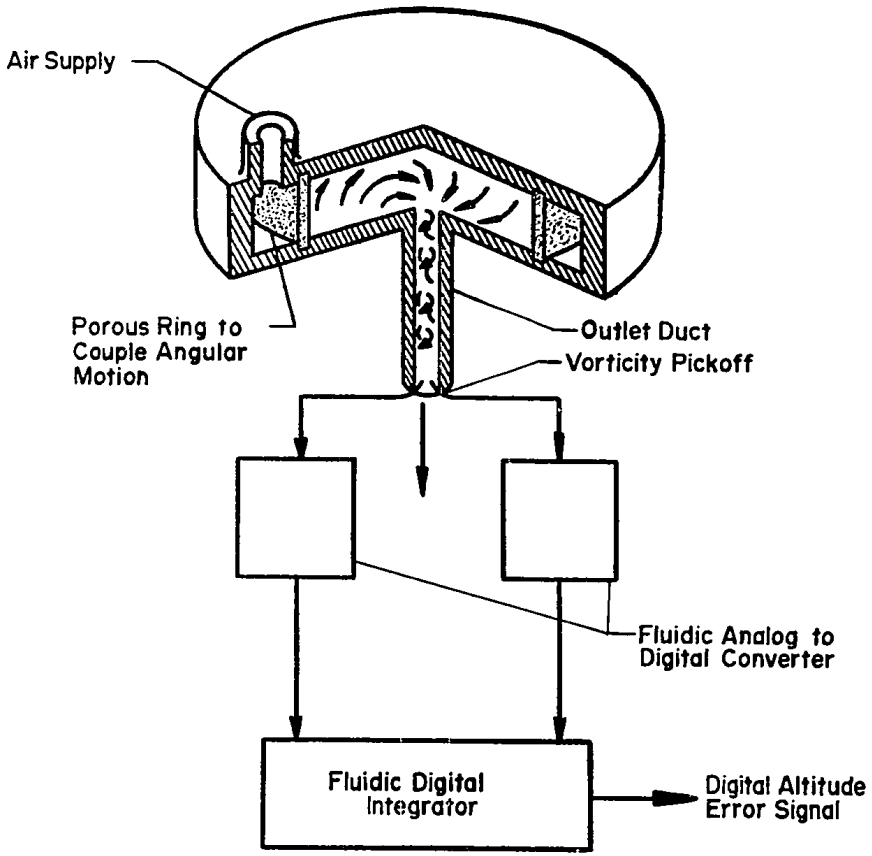

FIGURE I.3 HEADING REFERENCE BY DIRECT INTEGRATION OF RATE SENSOR OUTPUT SIGNAL

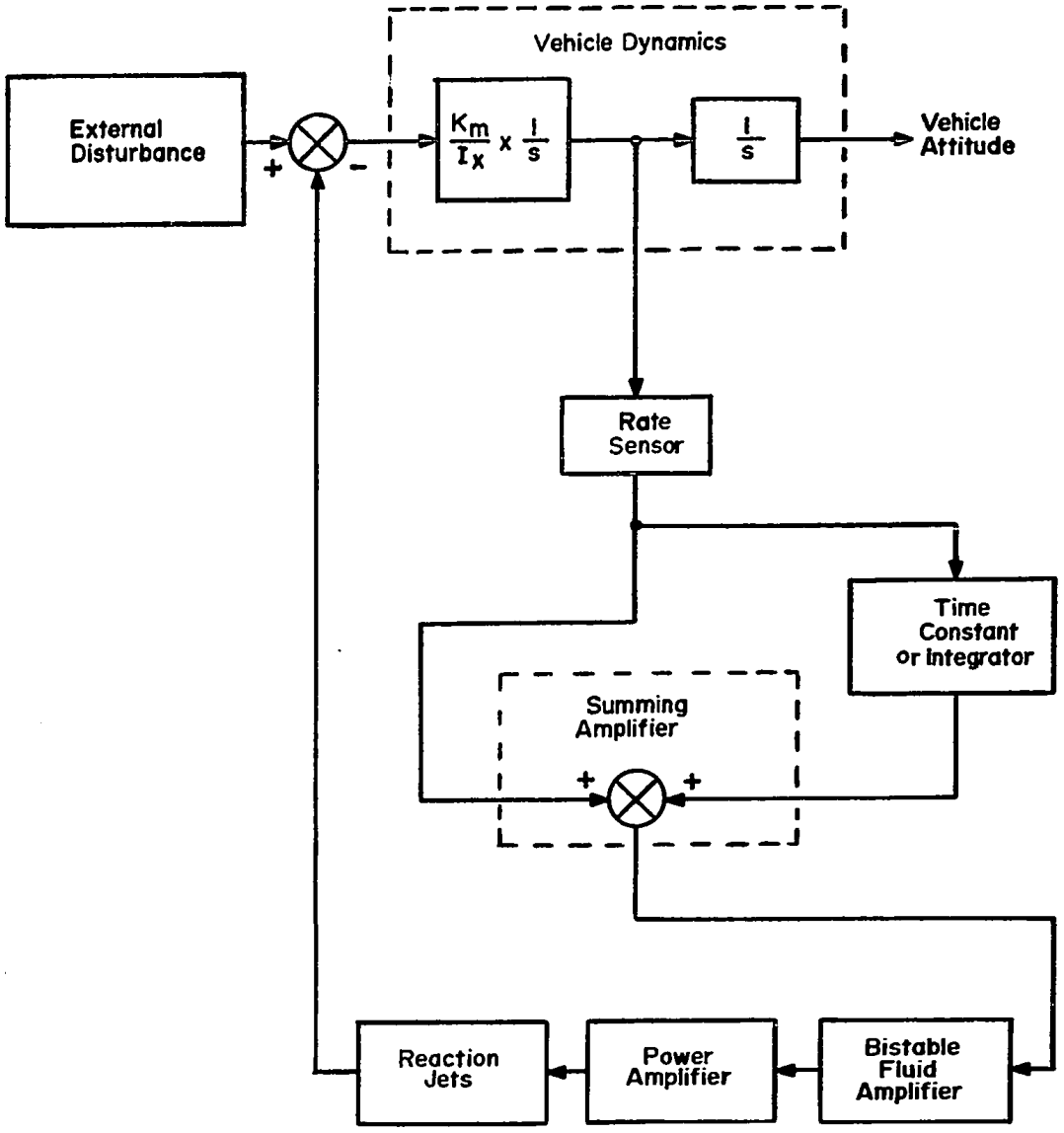

FIGURE 1.4 TIM ROLL ATTITUDE FLUID CONTROL SYSTEM

The substitution of vortex rate sensors and fluidic integrators for conventional directional gyros would appear to offer an attractive alternative which avoids the mechanical complexity and high speed moving parts. However, practical considerations of rate sensor gain, drift and linearity limitations, coupled with fluidic integration inaccuracies tend to limit the attainment of angular heading by direct integration of the rate sensor output to short duration and relatively inaccurate reference systems.

An alternative approach was considered to minimize the limitation associated with the rate sensor signal quality. The initial concept, as proposed by Aviation Electric Limited, Montreal, consisted of an electromechanical negative feedback servo loop around the rate sensor as illustrated in figure 1.5. The differential pressure output of the fluidic rate sensor due to vehicle frame rotation is converted into an electrical signal. This signal is amplified and fed into a servomotor to form a feedback loop which acts to maintain the rate sensor at a fixed orientation about its rotational axis, irrespective of the vehicle frame rotation. Such a single axis heading reference system might provide an attractive low cost alternative to a conventional gyro in navigation and/or stabilization system applications where the absolute heading deviation of the rate sensitive sensor axis would be minimal. A typical application for this

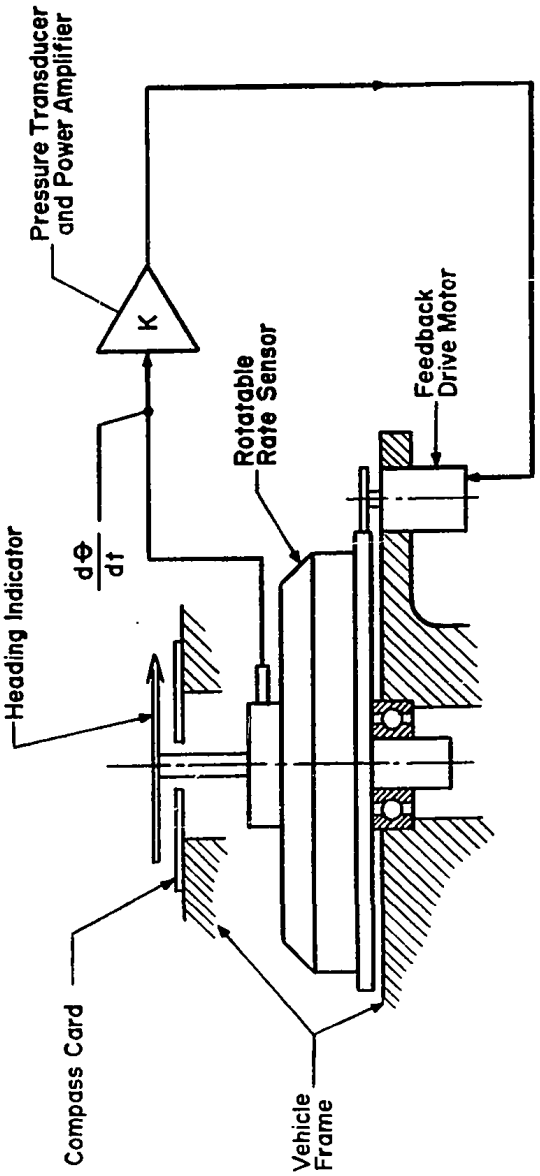

FIGURE I.5 SERVOED HEADING REFERENCE SYSTEM

sensor rate feedback approach would be to provide a heading direction reference in cross-terrian vehicles such as heavy duty trucks, tracked snow caterpillars and air cushion vehicles for navigational purposes.

1.2 Objectives of the Project

The primary objective of this project is to investigate different possible compensation techniques which reduce the system heading steady-state error while maintaining acceptable stability margin and transient response. No attempt has been made to improve the gain/response characteristics of the commercial fluidic rate sensor used in this investigation in order to optimize the overall system performance. Further, there is an advantage to implement the heading reference system entirely with fluidics to avoid the necessity for electro-fluidic interfaces. Accordingly, particular attention will be given to those compensation networks which are practically realizable with commercially available fluidic devices.

Efforts are directed to developing a sophisticated optimization technique to minimize the system steady-state heading error. The stabilization of the heading reference system with a vortex rate sensor induced pure time delay of appreciable relative magnitude is a problem common to many

industrial processes, particularily in petroleum and chemical plants where the pure time delay is usually associated with material and/or fluid signal propagation in long transmission pipes. Accordingly, the optimization of the heading reference system has been extended to cover the more general case of the industrial process control system.

CHAPTER 2

DIFFERENT SYSTEM FEEDBACK COMPENSATION SCHEMES

2.1 General

The initially conceived heading reference system outlined in the previous chapter could be represented by the block diagram illustrated in figure 2.1. Shown is, the rate sensor differential pressure output/angular rate input transfer function, which had been experimentally determined using a servoed hydraulic rate table (Reference 10), incorporates a first order lag and a pure time delay. From the block diagram, it could be easily seen that the overall system open loop transfer function consists of a second order lag and a pure time delay. According to the theory of linear control systems (Reference 11), a zero system rate error, which is the principal objective of the feedback loop, will be attained only at an infinite value of system overall gain (i.e. infinite value of $G_1 K_c G_2$). However, the system phase shift introduced by the rate sensor delay time, being proportional to input signal frequency, will result in system instability at an appropriate value of system loop gain. For example, with a time constant $T_1 = 0.011$ second and a delay time $T_L = 0.010$ second, which are the characteristics of the commercial fluidic rate sensor used in the experimental program (Aviation Electric Type 1600

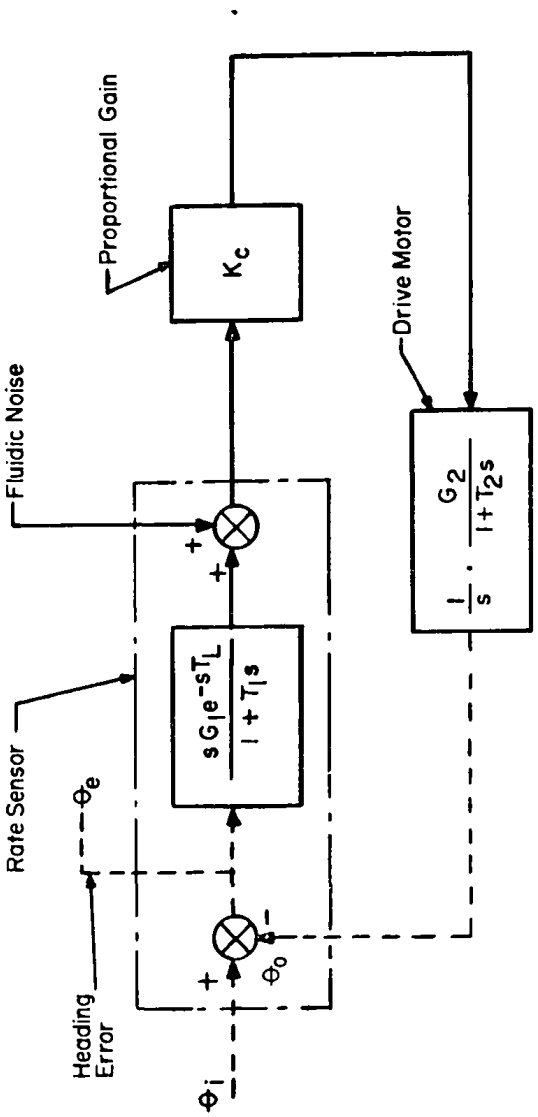

FIGURE 2.1 PRELIMINARY HEADING SYSTEM BLOCK DIAGRAM

RSOI, Reference 10), it had been shown that, with a drive motor time constant T_2 = 0.020 second, the system becomes unstable at the loop gain value of approximately $G_1K_cG_2$ = 4.0 and at this condition the heading system steady-state drift rate is 20% of the step rate input (Reference 12). This large system drift rate is obviously unacceptable for a heading reference system. Thus, some compensation networks are necessary to reduce the system steady-state rate error while maintaining acceptable stability margin and transient response.

Some appropriate compensation circuits in the form of linear lags combined with a pure time delay have been investigated in reference 12. Such compensation techniques, which have been advocated by several authors to stabilize industrial process control loops containing transportation lag (References 13, 14, 15), are essentially devised to remove the effect of time delay from the feedback loop thereby permitting the forward loop gain to be increased, without encountering the instability limit associated with the time delay. Such compensation circuits theoretically offer a great improvement on the system performance. However the hardware implementation of a perfect pure time delay required in the control loops introduces some serious practical limitations. Electronically, a pure time delay simulation could be achieved by using Padé approximation analog circuits, reflection of ultrasonic waves in crystals, capacitors wheels, tape recorder and digital

computer storage (Reference 16), even though such methods tend to be expensive and unwieldy, particularly when the time delay magnitudes are significant. Fluidically, the time delay might be generated by acoustic signal propagation down a transmission line. However, the relatively high speed of sound and the frictional attenuation which occurs in transmission lines undermine the practical feasibility of this method. An alternative for delaying fluidic signals has been described in references 17 and 18, where bubbles are injected into a tube containing water flowing at a constant rate. The bubbles are sensed at a point downstream and the delay period is determined by the water flow rate and by the tube length between the injector and the sensor. This bubble tube simulation technique provides an attractive means to fluidically implement the pure time delay in the control loop, although it can only be used for delaying frequency modulated signals.

A number of other techniques for compensating systems with pure time delay including feedforward compensation (References 15, 19, 20), sampled control (References 21, 22, 23) and modern optimal control (References 24, 25, 26) have been investigated in the literature. Although theoretically they offer means for handling processes having a pure time delay, actual application of those techniques is largely discounted in the case of the heading reference

system by practical considerations. For instance, a feed-forward compensation loop is physically unrealizable since the system input, in being the relative angular movement between the vehicle and the ground reference, is not detectable in the practical system. Additionally, sampled control is not recommended for systems with an inexactly defined time delay (Reference 21), as in the case of the rate sensor where the time delay magnitude has been approximated (Reference 44) and varies as a weak function of the supply pressure. Bang-bang control type as described in reference 24 would probably result in system self-oscillation with zero input due to the significant noise content of the fluidic rate sensor output switching relay devices. Other modern control techniques using an iterative algorithm which generates an optimal feedback control (References 25, 26) require the implementation of a large memory digital computer for performing necessary computation in the feedback loop. This approach is obviously impractical in the case of the heading reference system.

From the above discussion, it is evident that a relatively conventional compensation scheme which offers a good compromise between control effectiveness, manageability, hardware implementation complexities and cost should be investigated. In this regard, several control possibilities using different combinations of proportional, integral and derivative actions in the feedback loop of systems with dead

time are cited in references 15, 27, 28, 29. Although it had been shown that the conventional linear compensation control techniques do not offer the same degree of system performance improvement as some other more advanced schemes previously cited (References 15, 19), the trade-off between performance, cost, reliability, and maintenance considerations has resulted in the continuing wide spread industrial use of both pneumatic and electronic linear controllers. In addition, the required linear controllers can be realized using commercially available no-moving parts fluidic devices such as operational amplifiers, resistances and capacitances, as demonstrated in references 30 et 31.

For those reasons, the possibilities of improving the performance of the initially proposed heading reference system by introducing in the system feedback loop different combinations of linear control actions, such as proportional-integral-derivative, proportional-integral and integral control have been investigated.

2.2 Different Linear Control Schemes

2.2.1 Proportional-Integral-Derivative Control

The destabilizing effects of the rate sensor pure time delay could be eliminated by compromising the system response through the addition of an integral function in the

proportional feedback loop. The resultant oscillatory transient response of the proportional-integral control could be minimized with the addition of a derivative control function. With such combined control scheme, the heading reference system could be represented by the block diagram as shown in figure 2.2, where the transfer function of the ideal proportional-integral-derivative controller is given by:

$$\frac{\text{Controller output}}{\text{Controller input}} = K_c\left(1 + \frac{1}{T_I s} + T_D s\right) \qquad (2.1)$$

Different criteria for setting the controller parameters (K_c, T_I, T_D) to obtain a so-called optimum system response have been reported in the literature. Some of the optimization criteria were developed by trial-and-error procedure (References 27, 28, 32), while others were established using a theoritical analysis (References 33, 34, 35, 36, 37). Typically, such optimization criteria are applicable only to the given type of control system considered during the investigation. One exception is the Ziegler-Nichols criterion (Reference 32) which has been developed for a more generalized case where only the open loop system amplitude-phase plots are required to determine a set of optimized controller parameters.

It is convenient initially to evaluate the system performance using the Ziegler-Nichols criterion to determine

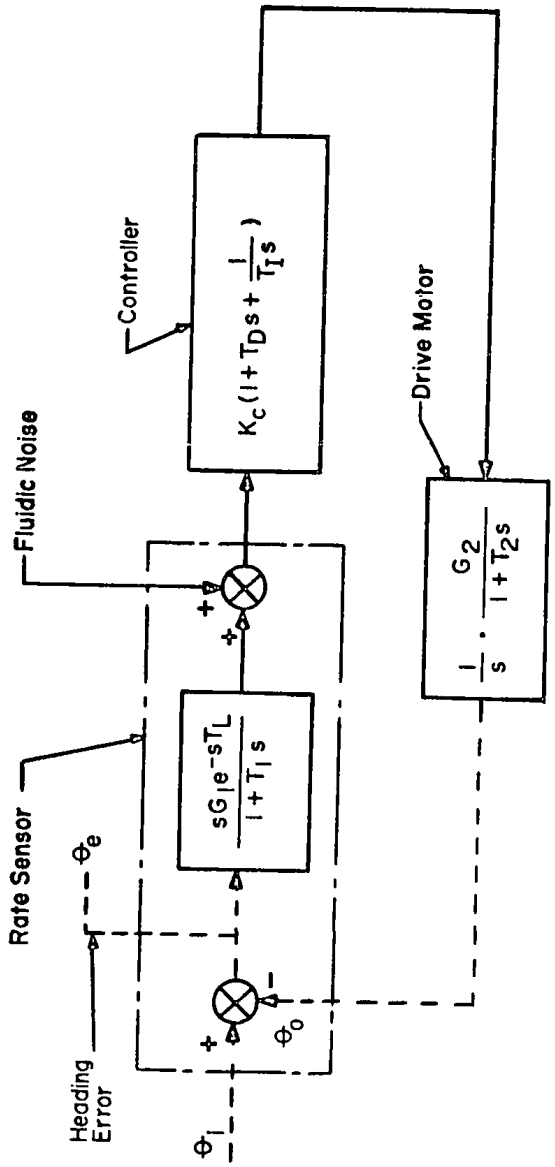

FIGURE 2.2 HEADING SYSTEM BLOCK DIAGRAM WITH THREE MODE CONTROLLER

the feasibility of attaining acceptable order of magnitude of system transient response while appreciating that the "angular rate error" rather than the "heading error" will be optimized. The use of this criterion will result in an "angular rate error" overshoot of approximately 25% and a reasonable compromise between the area under the "angular rate error" curve and the transient oscillatory period.

The optimum controller parameters are estimated by Ziegler-Nichols as follows:

$$K_c = \frac{0.6}{G_{co}} \tag{2.2}$$

$$T_I = \frac{1}{2} \times \frac{2\pi}{\omega_{co}} \tag{2.3}$$

$$T_D = \frac{1}{8} \times \frac{2\pi}{\omega_{co}} \tag{2.4}$$

The Bode diagram of the open loop system without a compensation circuit is used to evaluate the crossover frequency (ω_{co}) and the corresponding overall gain (G_{co}) as shown in figure 2.3, where the rate sensor and feedback drive motor transfer functions which have been experimentally determined to be (Reference 12):

Fluidic Rate Sensor

$$\frac{\Delta P(s)}{\Theta_i(s)} = \frac{s.G_1.e^{-0.01s}}{1 + 0.011s} \tag{2.5}$$

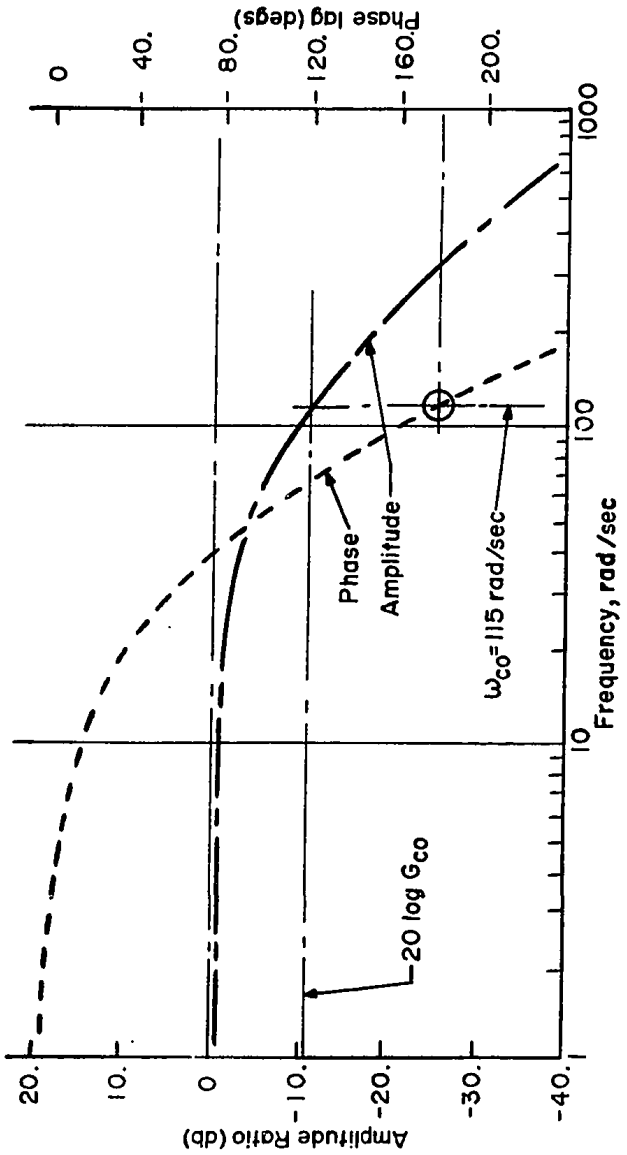

FIGURE 2.3 BODE DIAGRAM OF HEADING SYSTEM WITHOUT CONTROLLER
(G_1G_2=1.0)

Feedback Drive Motor

$$\frac{\Theta_o(s)}{E_m(s)} = \frac{G_2}{s(1 + 0.02s)} \qquad (2.6)$$

The gain at the -180^o phase shift crossover frequency of ω_{co} equal to 115 rad./sec. is given by:

$$20 \log_{10} G_{co} = -10.5 \implies G_{co} = 0.3$$

Hence, from equations (2.2), (2.3) and (2.4):

$$K_c = \frac{0.6}{G_{co}} = \frac{0.6}{0.3} = 2.0$$

$$T_I = \frac{1}{2} \times \frac{2\pi}{\omega_{co}} = \frac{1}{2} \times \frac{2\pi}{115} = 0.0273 \text{ sec.}$$

$$T_D = \frac{1}{8} \times \frac{2\pi}{\omega_{co}} = \frac{1}{8} \times \frac{2\pi}{115} = 0.0068 \text{ sec.}$$

2.2.2 Proportional-Integral Control

In practice, it is often preferable to eliminate the derivative function in controllers where the input signal contains a significant random noise component such as is introduced by the fluidic rate sensor in the heading reference system. The predictive function of the differentiator in reducing transient response overshoot may be more than offset by accentuation of the random noise content of the signal. Accordingly, a proportional-integral controller is investigated, the associated controller transfer function being:

$$\frac{\text{Controller output}}{\text{Controller input}} = K_c \left(1 + \frac{1}{T_I s}\right) \qquad (2.7)$$

Optimized controller parameters (K_c, T_I) are estimated using the Ziegler-Nichols rules for the same optimization criterion as in the PID controller case previously described, the pertinent parameter definitions being:

$$K_c = \frac{0.45}{G_{co}} \qquad (2.8)$$

$$T_I = \frac{1}{1.2} \times \frac{2\pi}{\omega_{co}} \qquad (2.9)$$

Hence,

$$K_c = \frac{0.45}{0.3} = 1.5$$

$$T_I = \frac{1}{1.2} \times \frac{2\pi}{115} = 0.0455 \text{ sec.}$$

2.2.3 Integral Control

Further simplification of the control circuit may be attained by using a simple pure integral controller, the transfer function being given by:

$$\frac{\text{Controller output}}{\text{Controller input}} = \frac{1}{T_I s} \qquad (2.10)$$

By setting of a sufficiently large integral time constant T_I, one can maintain system stability while retaining zero heading rate steady-state error. The optimized controller integration time constant (T_I) estimated by Ziegler-Nichols is:

$$T_I = \frac{1}{1.2} \times \frac{2\pi}{\omega_{co}} = \frac{1}{1.2} \times \frac{2}{115} = 0.0455 \text{ sec.} \quad (2.11)$$

2.3 System Simulation

The performance of the heading reference system was simulated using the hybrid computer EAI 680/640, the fluidic rate sensor delay time being simulated digitally within the limits of the memory storage capability (sampled rate = 100 sampling/sec.) while the remainder of the system was analogue simulated.

For the purpose of the system simulation study, the proportional-derivative part of the controller was replaced by a lead-lag circuit as given by:

$$1 + T_D s \approx \frac{1 + T_D s}{1 + (T_D/\lambda)s} \quad (2.12)$$

This approximation is reasonable for $\lambda \geq 10$ (Reference 29). Figure 2.4 shows the simulation diagram of the heading reference system with a proportional-integral-derivative.

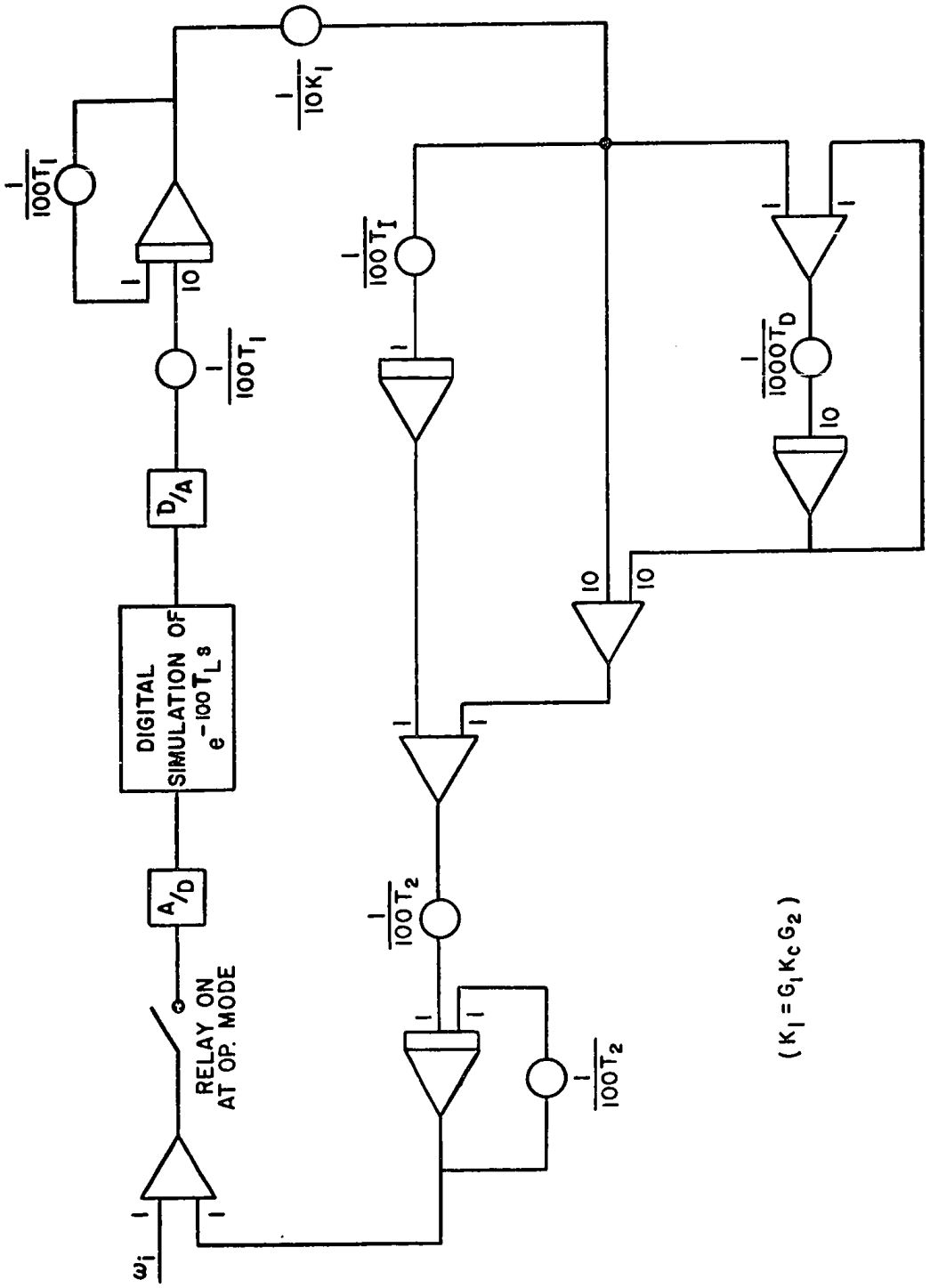

FIGURE 2.4 HYBRID SIMULATION DIAGRAM OF SYSTEM WITH THREE MODE CONTROLLER

controller.

The time domain heading error responses of the simulated system to a 10. degs/sec. step rate input are shown in figures 2.5, 2.6 and 2.7 respectively for each of the three controllers considered above. It could be observed that the system heading transient response overshoot may be reduced or eliminated at the expense of steady-state heading error by suitable adjustment of the controller parameters as examplified in figure 2.5 by the reduction of the proportional gain (K_c) of the PID controller. Conversely, the steady-state heading error may be reduced at the expense of stability by suitable adjustment of the controller parameters as examplified in figures 2.6 and 2.7 by the reduction of the integration time constant of the controller. Progressive reduction of integration time constant or increase of the proportional gain is limited by the onset of rate sensor time delay induced system instability in the form of sustained sensor heading oscillations. A quick comparison between the optimum responses of the system with different controllers demonstrates the compromise between heading error response and controller complexity.

2.4 Experimental System Performance

An experimental hybrid heading reference system

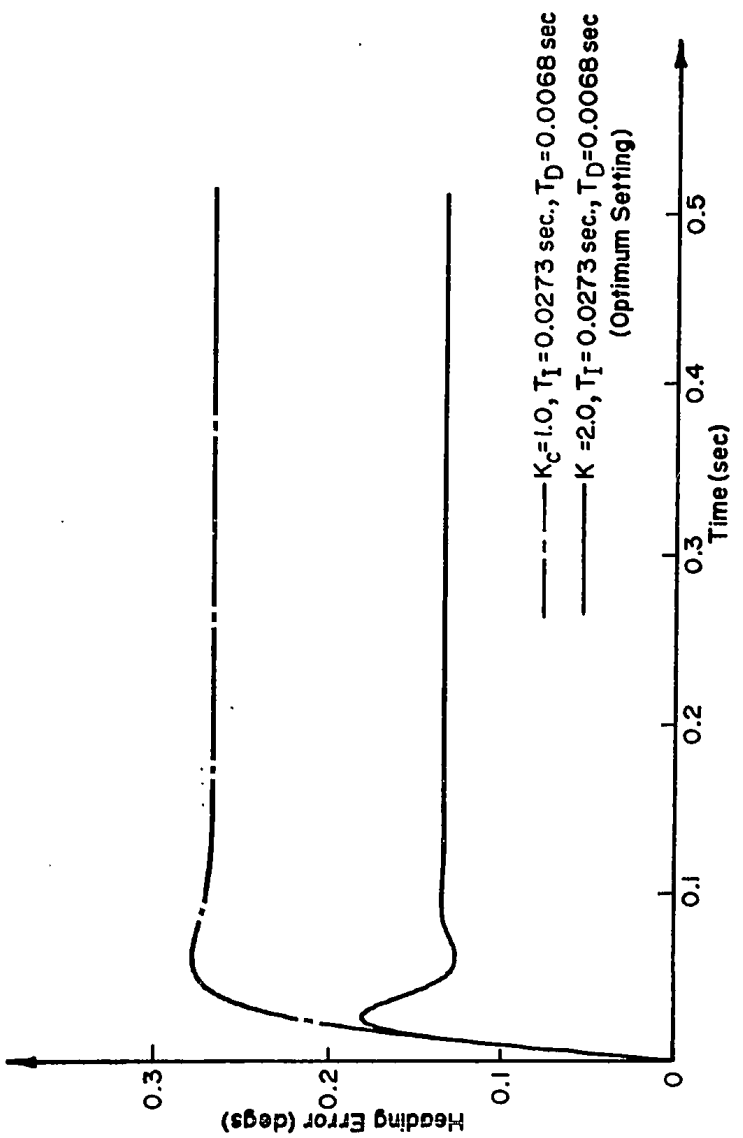

FIGURE 2.5 SYSTEM RESPONSES TO A STEP RATE INPUT OF 10.0 degs/sec
(PID Controller)

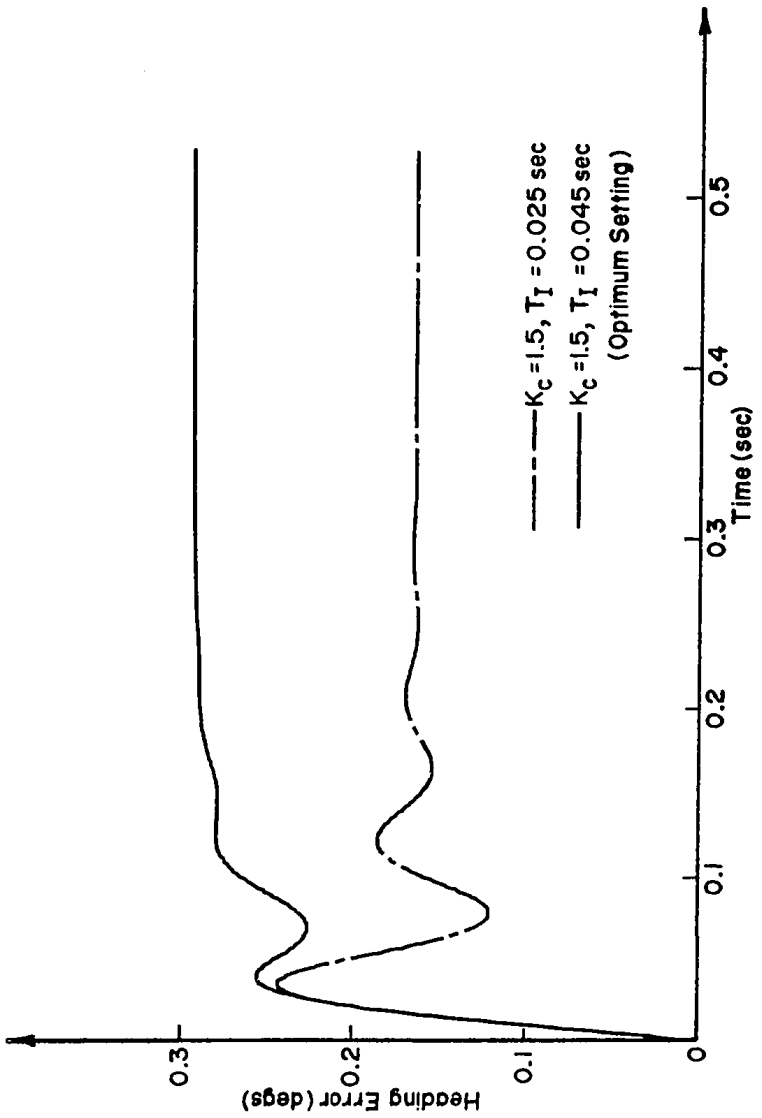

FIGURE 2.6 SYSTEM RESPONSES TO A STEP RATE INPUT OF 10.0 degs/sec
(PI Controller)

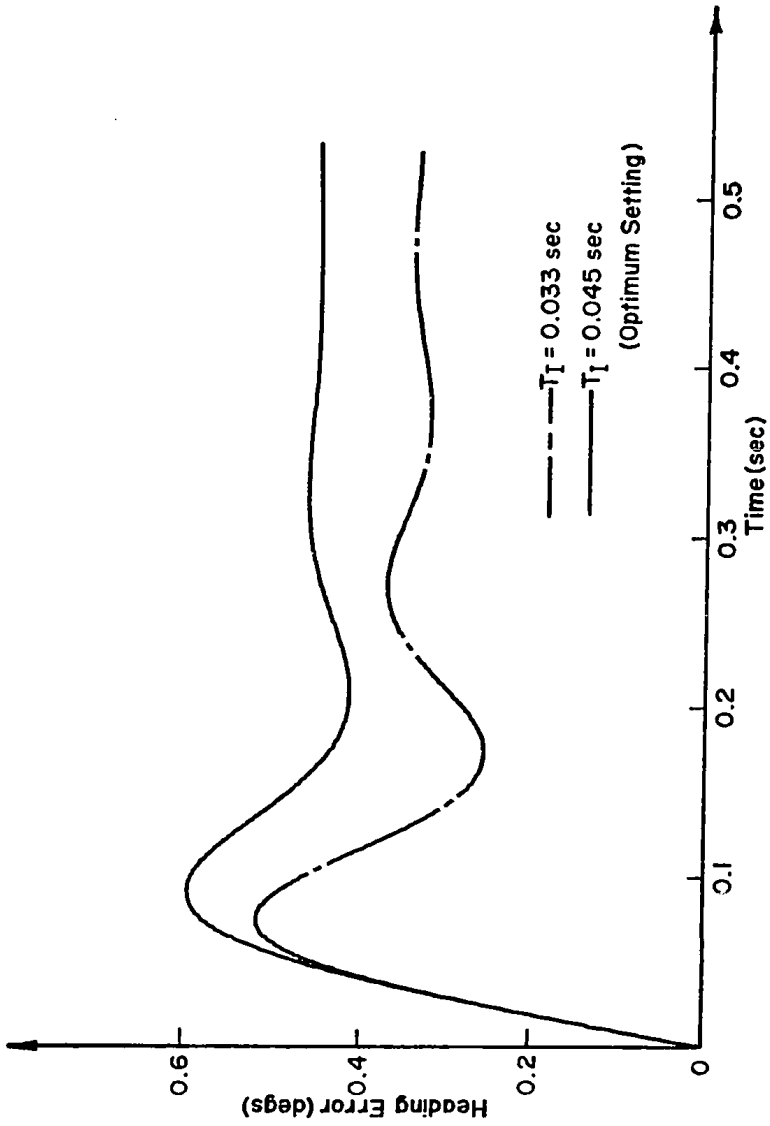

FIGURE 2.7 SYSTEM RESPONSES TO A STEP RATE INPUT OF 10.0 degs/sec
(Integral Controller)

incorporating electrical feedback has been assembled to facilitate performance evaluation. The experimental assembly is shown schematically in figure 2.8, the corresponding system hardware being shown photographically in figures 2.9 and 2.10.

2.4.1 Experimental System Hardware

The experimental system incorporates the following components:

1) Fluidic Vortex Rate Sensor

The fluidic vortex rate sensor utilized (Aviation Electric Type 1600 RS01; linearity ± 1% to 150 degs./sec.; noise threshold limit 0.05 deg./sec. for 1 Hz bandpass; flow rate 2.3 scfm at 5 psi) incorporates a 5" diameter slotted coupling ring and two 0.060" O.D. pick-off pitot tubes mounted tangentially to the swirl flow component in the sensor outlet duct as shown in figure 2.11. The rate sensor frequency response is given by the manufacturer as shown in figure 2.12 and the sensor blocked load static gain has been experimentally determined at 5 psi supply pressure as given in figure 2.13. The observed sensor output signal null offset results probably from small flexing or shifting in the pick-off drain assembly.

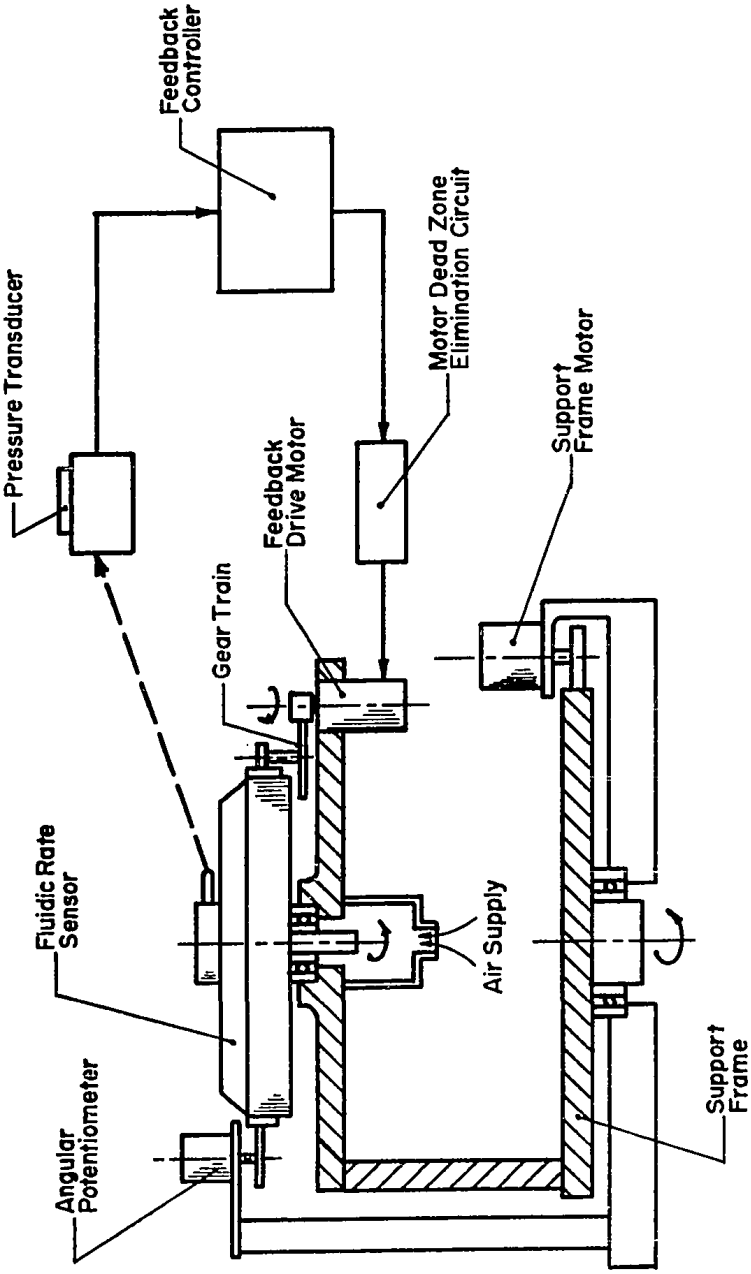

FIGURE 2.8 EXPERIMENTAL HEADING REFERENCE SYSTEM SCHEMATIC

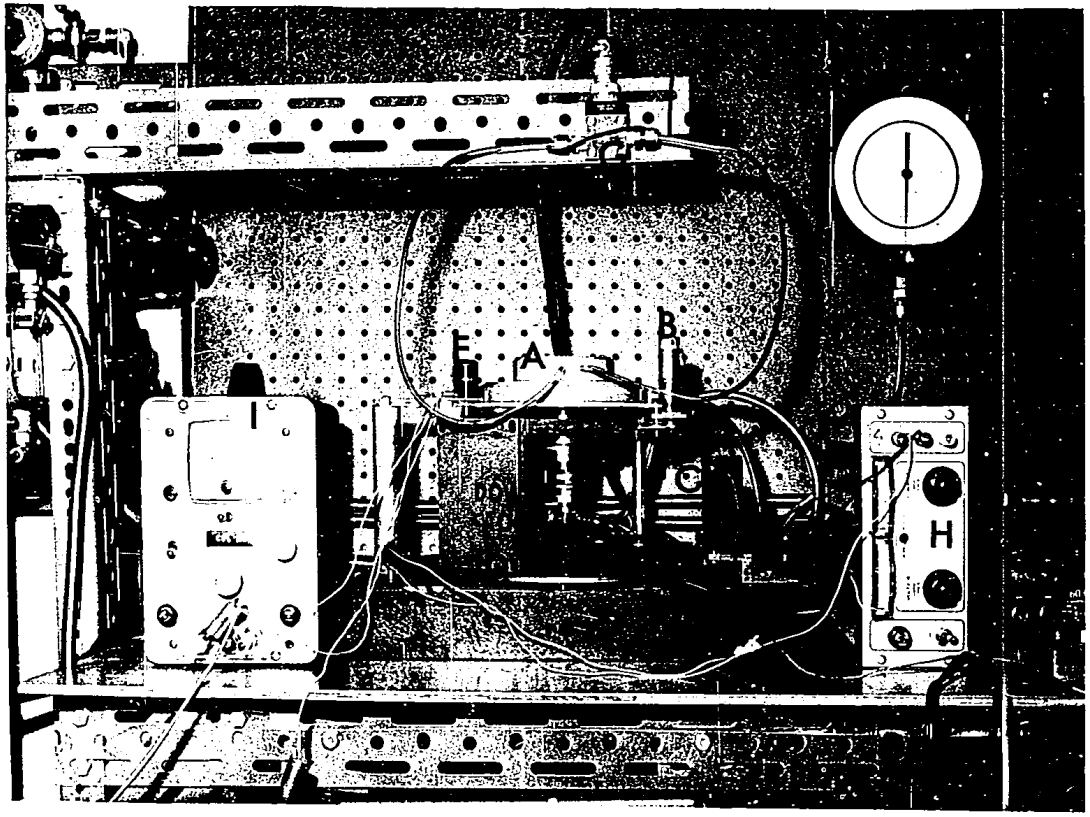

FIGURE 2.9 EXPERIMENTAL HEADING REFERENCE SYSTEM MECHANICAL ASSEMBLY

A_Fluidic Rate Sensor, B_Feedback Drive Motor, C_Support Frame Drive Motor, D_Rotary Support Frame, E_Angular Position Potentiometer, F_Air Supply, G_Differential Pressure Transducer, H_Support Frame Drive Motor Power Supply, I_Angular Position Potentiometer Power Supply.

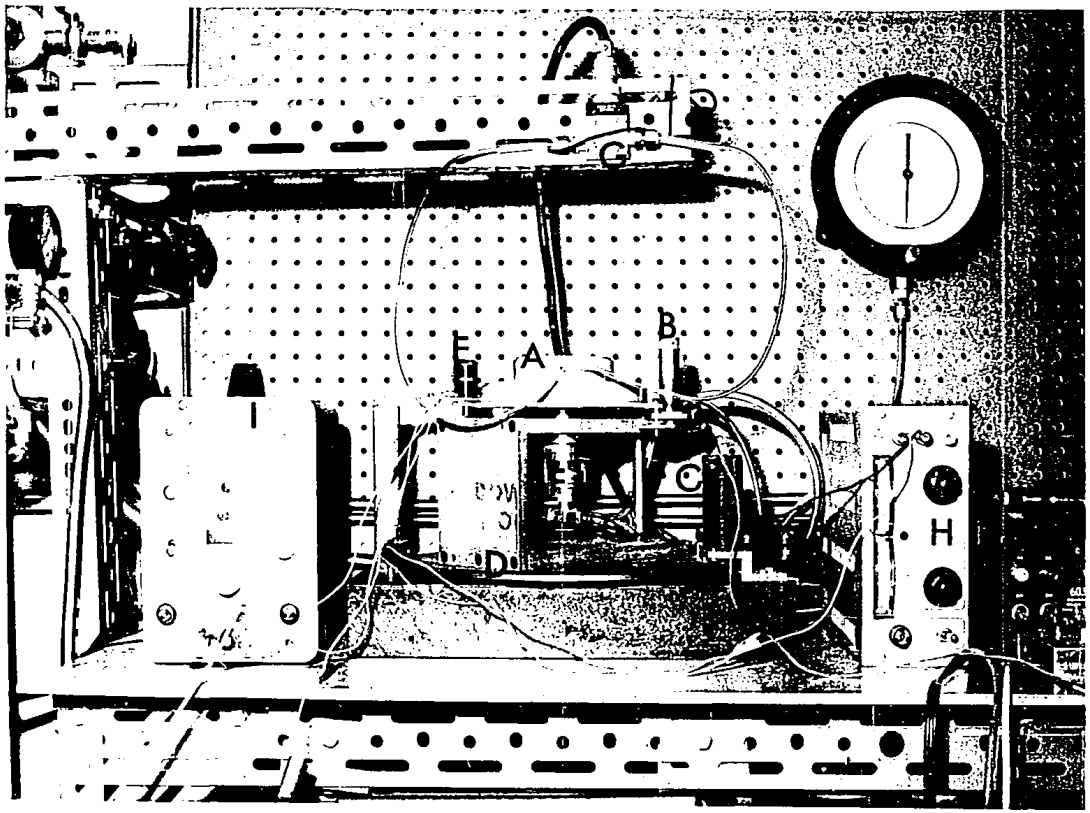

FIGURE 2.9 EXPERIMENTAL HEADING REFERENCE SYSTEM MECHANICAL ASSEMBLY

A_Fluidic Rate Sensor, B_Feedback Drive Motor, C_Support Frame Drive Motor,
D_Rotary Support Frame, E_Angular Position Potentiometer, F_Air Supply,
G_Differential Pressure Transducer, H_Support Frame Drive Motor Power Supply,
I_Angular Position Potentiometer Power Supply.

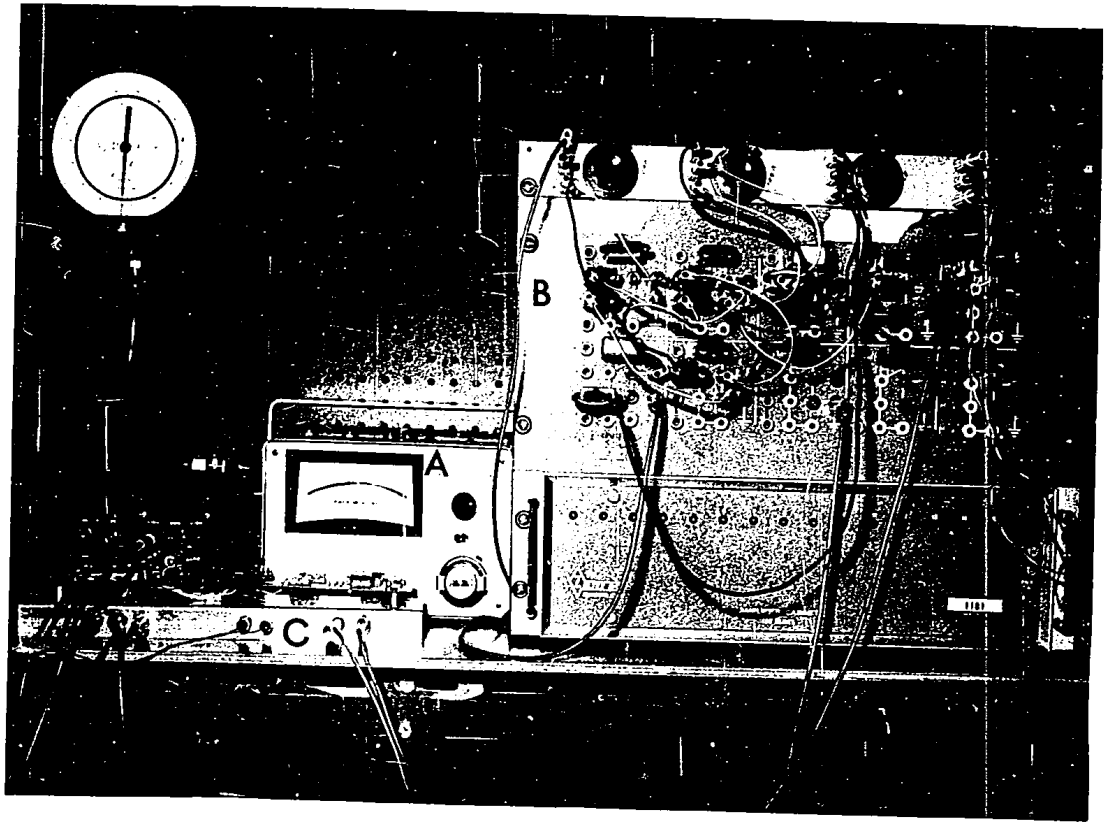

FIGURE 2.10 EXPERIMENTAL HEADING REFERENCE SYSTEM FEEDBACK LOOP

A-Pressure Transducer Indicator, B-Feedback Controller,
C-Feedback Drive Motor Dead Zone Elimination Circuit,
D-Feedback Drive Motor Power Supply.

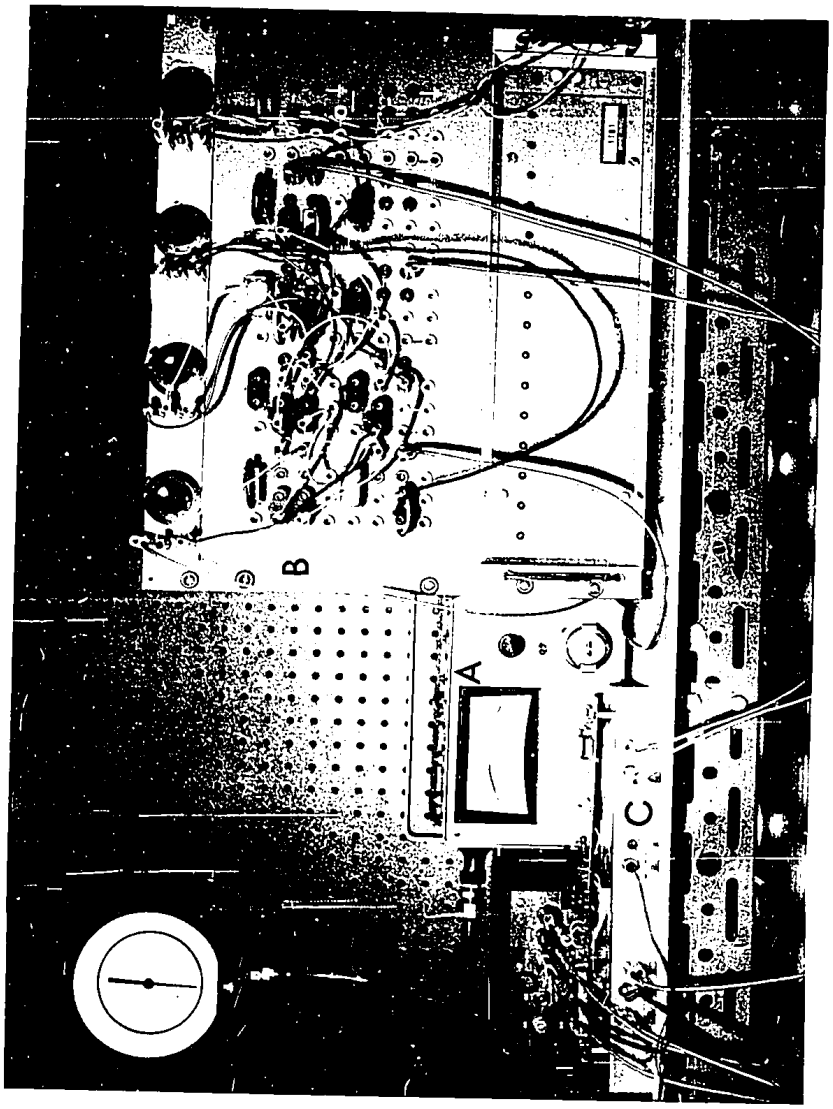

FIGURE 2.10 EXPERIMENTAL HEADING REFERENCE SYSTEM FEEDBACK LOOP

A_Pressure Transducer Indicator, B_Feedback Controller,
C_Feedback Drive Motor Dead Zone Elimination Circuit,
D_Feedback Drive Motor Power Supply.

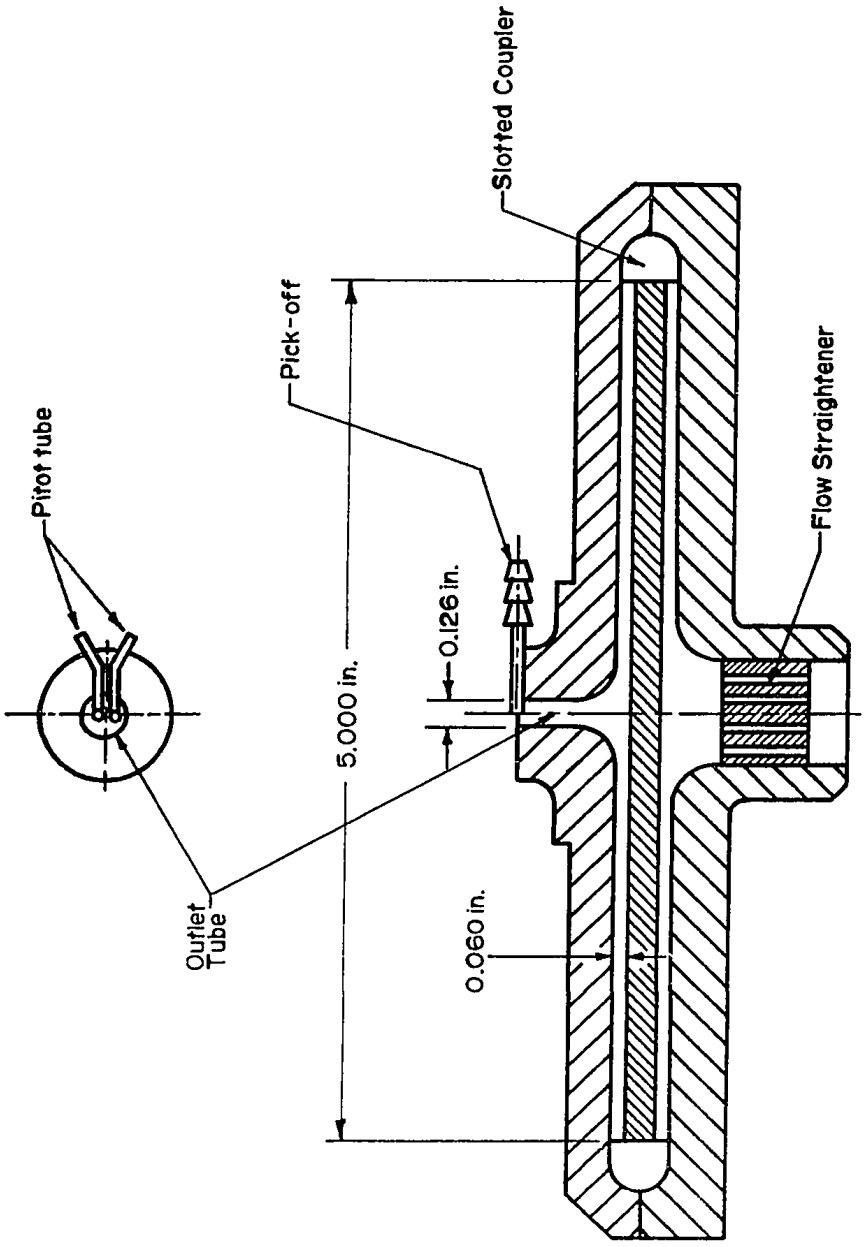

FIGURE 2.11 FLUIDIC RATE SENSOR

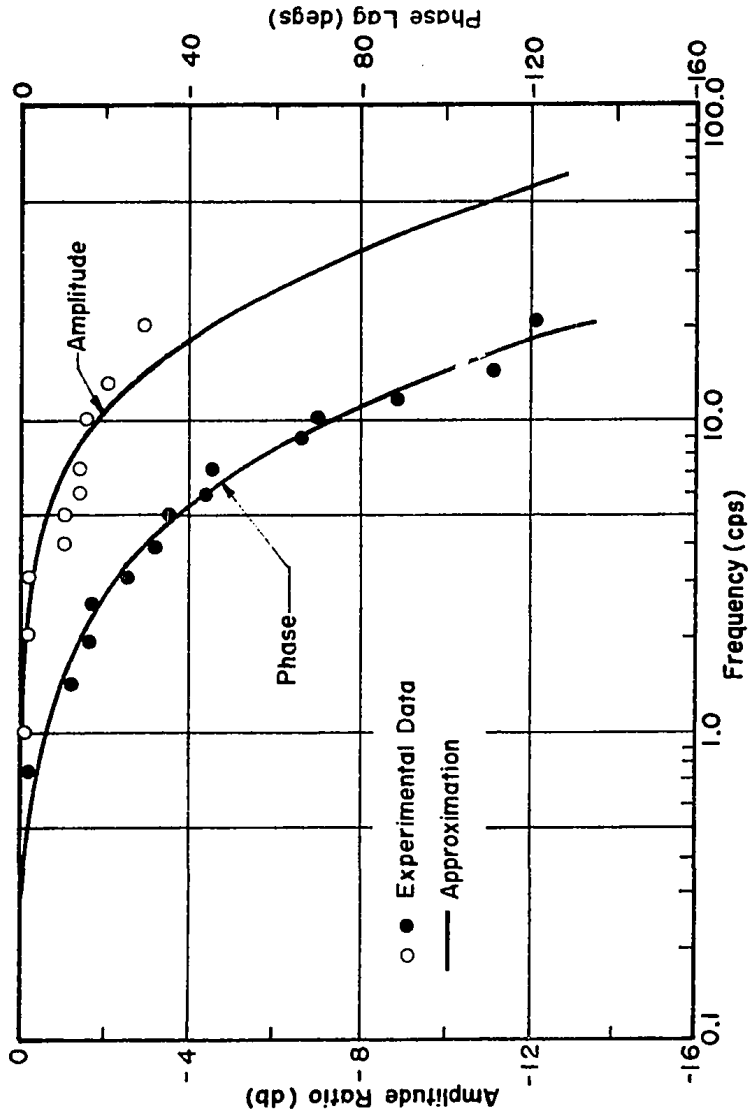

FIGURE 2.12 FLUIDIC RATE SENSOR FREQUENCY RESPONSE

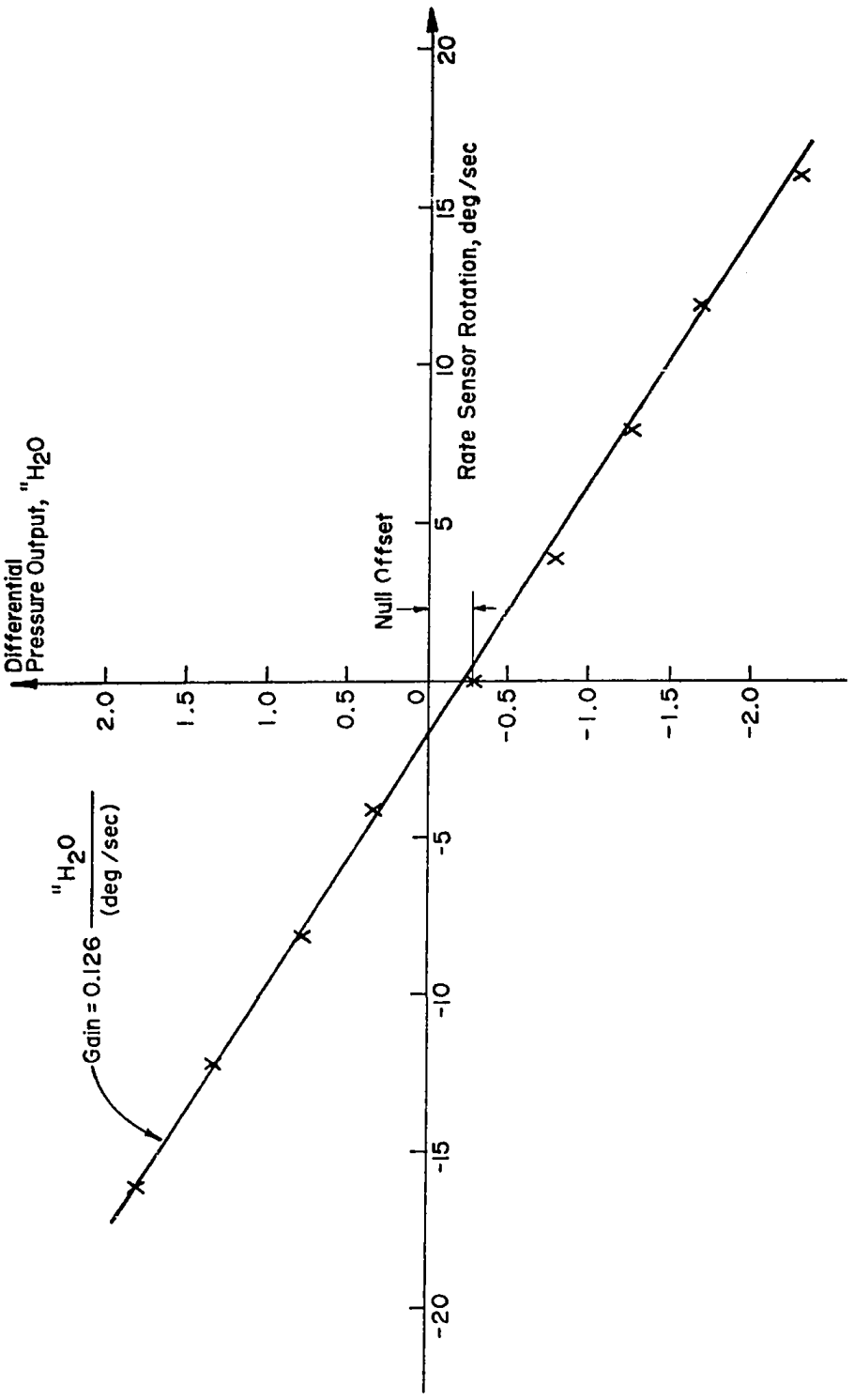

FIGURE 2.13 FLUIDIC RATE SENSOR GAIN CHARACTERISTICS

2) Pressure Transducer

A high sensitivity variable reluctance differential pressure transducer (Pace Eng. Model CD10; ± 1.0 psi; ± 0.5% linearity; 1 KHz response) provides the pneumatic/electrical conversion.

3) Feedback Drive Motor

A D.C. permanent magnet planetary gearmotor has been utilized to drive the rate sensor (Globe Industries Type 168A149; 27 volts D.C.; 0.080 amps. maximum no load current; 0.48 amps. nominal stall current; 1 to 33.28 speed reduction ratio; 450 rpm maximum no load speed).

The experimentally determined output/input operating characteristic of the D.C. drive motor shown in figure 2.14 indicated a dead zone which results from commutator brush friction. An electronic circuit has been specifically designed as illustrated in figure 2.15 to eliminate the motor dead zone. The resulting drive motor output/input operating characteristic is given in figure 2.16.

4) Angular position potentiometer

A continuous rotation potentiometer (New England

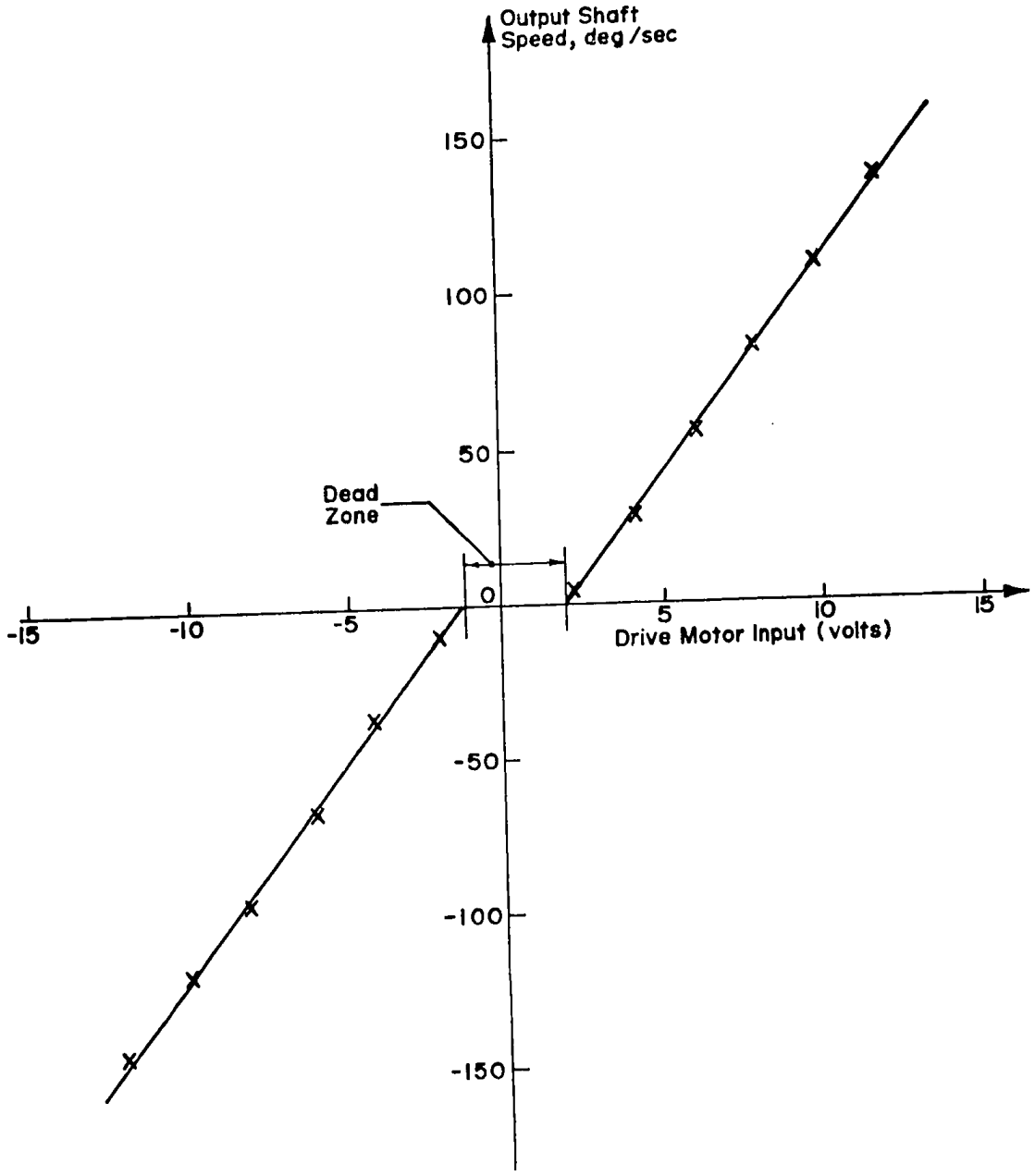

FIGURE 2.14 DRIVE MOTOR OPERATING CHARACTERISTICS

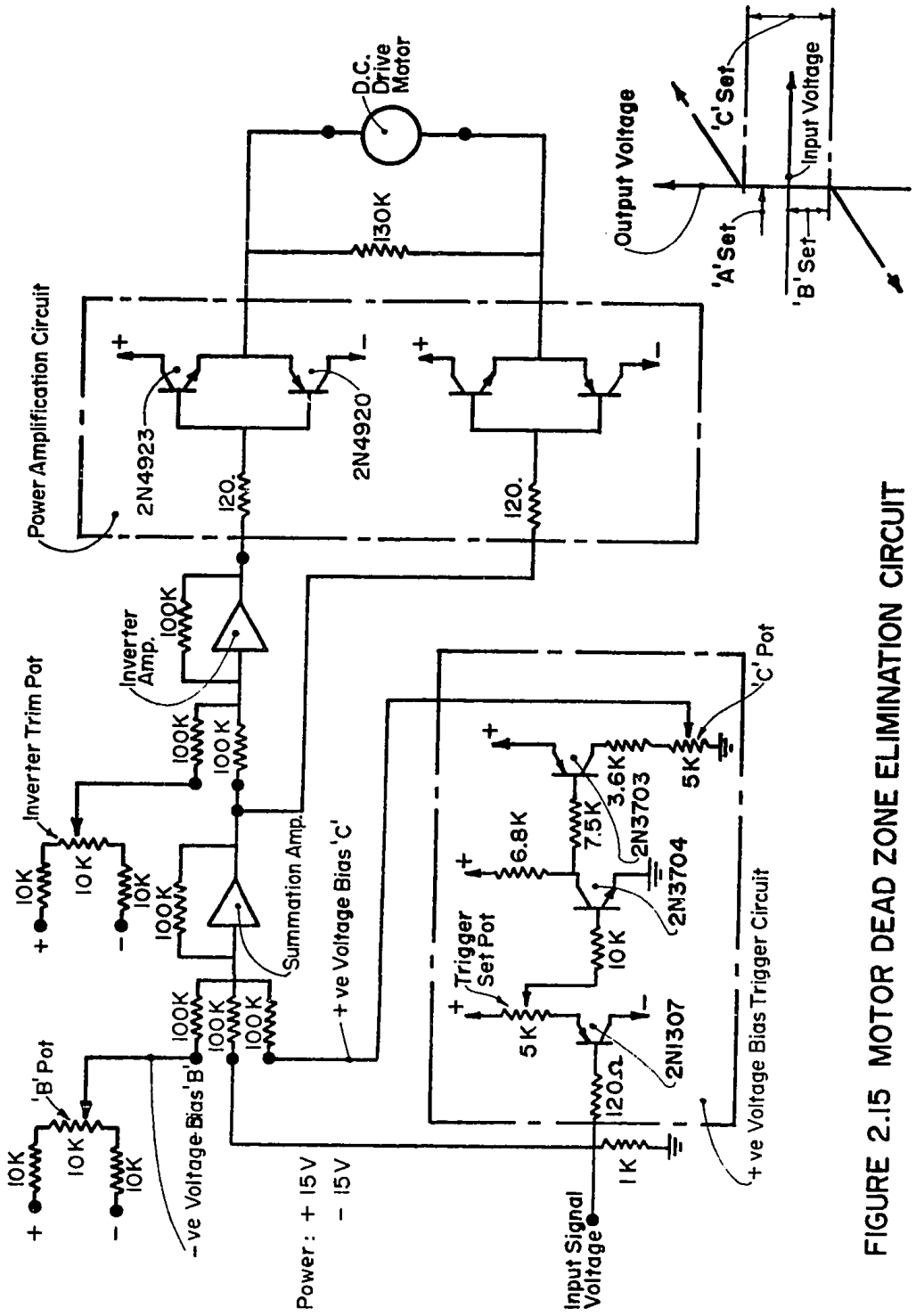

FIGURE 2.15 MOTOR DEAD ZONE ELIMINATION CIRCUIT

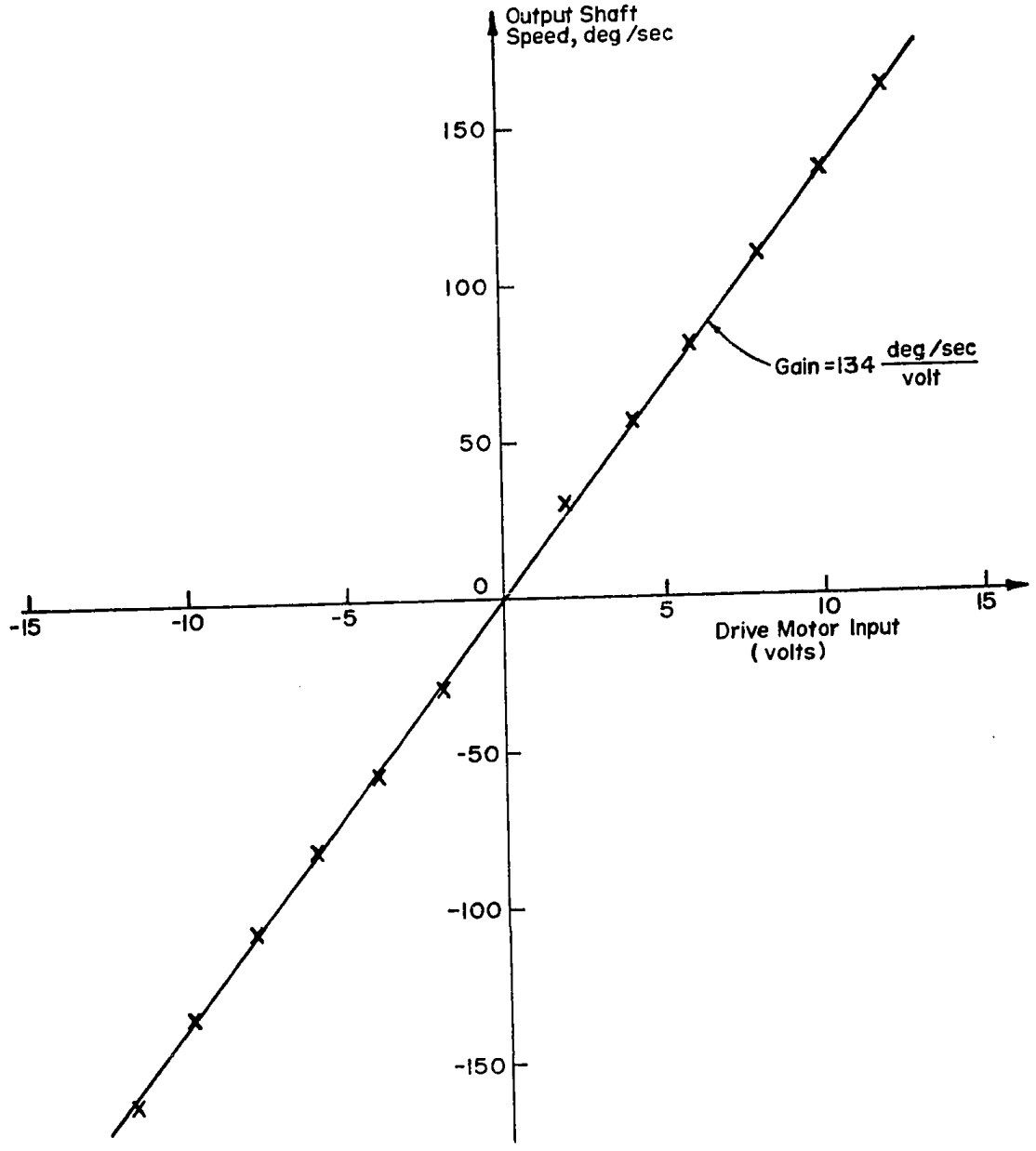

FIGURE 2.16 DRIVE MOTOR OPERATING CHARACTERISTICS WITH DEAD ZONE ELIMINATION CIRCUIT

Instrument Co. Type 78PS146, 10 KΩ resistance, 50 mV. noise, 340^{o} function angle) has been used to detect the sensor angular position.

5) Mechanical Gear Drives

Two pass spring-loaded anti-backlash gearing between the drive motor and the fluidic rate sensor with an overall gear ratio of 1 to 56.8 and single pass anti-backlash gearing between the fluidic rate sensor and the angular potentiometer have been utilized to give a potentiometer scale factor of approximately 50.0 degs. of rate sensor relative rotation per total applied potentiometer voltage.

6) Support Frame Motor

A D.C. permanent magnet gearmotor has been utilized to rotate the rate sensor support frame through a 48:1 speed reduction friction drive (G.E. 27 volts D.C., 110 rpm no load speed).

7) Controllers

The feedback controllers are electronically implemented through an operational amplifier cabinet

(Zeltex Inc. Series 120; ± 110V. operating voltage) which could be externally patched to obtain the desired controller function. Figure 2.17 illustrates the hardware implementation of the proportional-integral-derivative controller, where it will be noted that an external bias trim circuit has been introduced in the buffer amplifier to eliminate any system steady-state bias. Such bias may result from the fluidic rate sensor output signal null offset and/or extraneous steady-state voltages internally generated within the electrical circuits.

2.4.2 Experimental System Gain Analysis

The experimental system component gains are:

— Rate sensor gain = 0.126 in.H_2O/deg/sec (see figure 2.13)

— Pressure transducer gain = 1.0 volt/in.H_2O

— Feedback D.C. drive motor gain including the coupled motor dead zone elimination circuit and the 56.8:1 gear ratio between the motor and the rate sensor = 134/56.8 = 2.35 (deg/sec)/volt (see figure 2.16).

To facilitate the adjustment of the controller parameters, a gain of 3.49 has been set into the buffer amplifier such that the overall system gain excluding the controller is equal to unity, i.e.

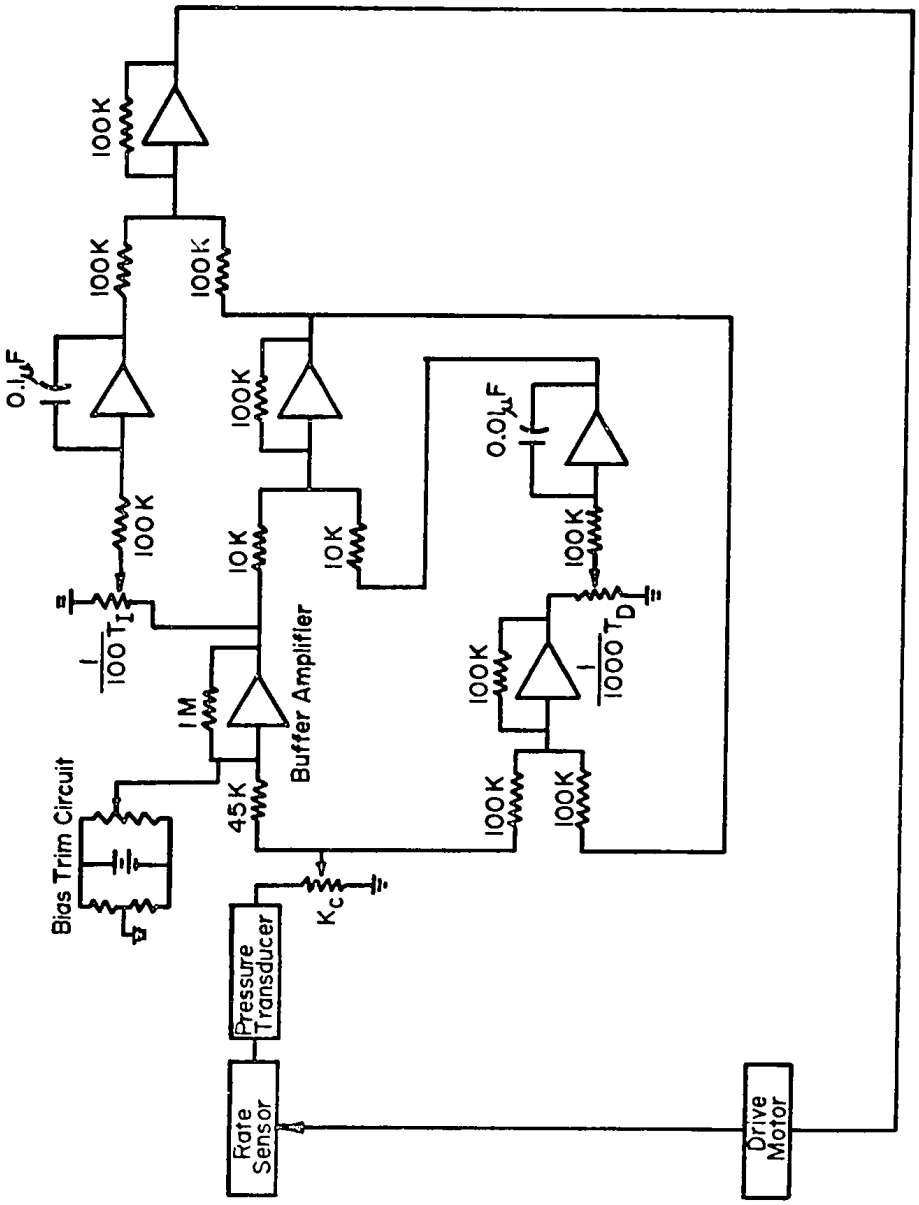

FIGURE 2.17 HARDWARE IMPLEMENTATION OF PROPORTIONAL-INTEGRAL-DERIVATIVE CONTROLLER

$$\text{Overall system gain (excluding the controller)} = 0.126\frac{\text{in.}H_2O}{\text{deg/sec}} \times 1\frac{\text{volt}}{\text{in.}H_2O} \times 2.35\frac{\text{deg/sec}}{\text{volt}} \times 3.49$$

$$= 1.0$$

2.4.3 Experimental System Time Responses

The performance of the heading reference system is experimentally evaluated by measuring the heading angle transient of the rate sensor with the angular potentiometer in response to a step angular rate input applied to the support frame through the application of a voltage step to the frame motor drive.

Typical experimental system heading transient response performance for a 10.0 degs./sec. step rate input as recorded by a X-Y plotter is shown in figures 2.18a,b, 2.19a,b and 2.20a,b respectively for the PID, PI and I controller for both optimum and arbitrary controller parameter settings. The Y-axis sensitivity was limited by the plotter response capability.

Experimental results are also plotted together with the corresponding theoretical responses in figures 2.21a,b, 2.22a,b and 2.23a,b to facilitate direct comparison. It is seen that the experimental responses exhibit approximate correlation with the theoretical predictions,

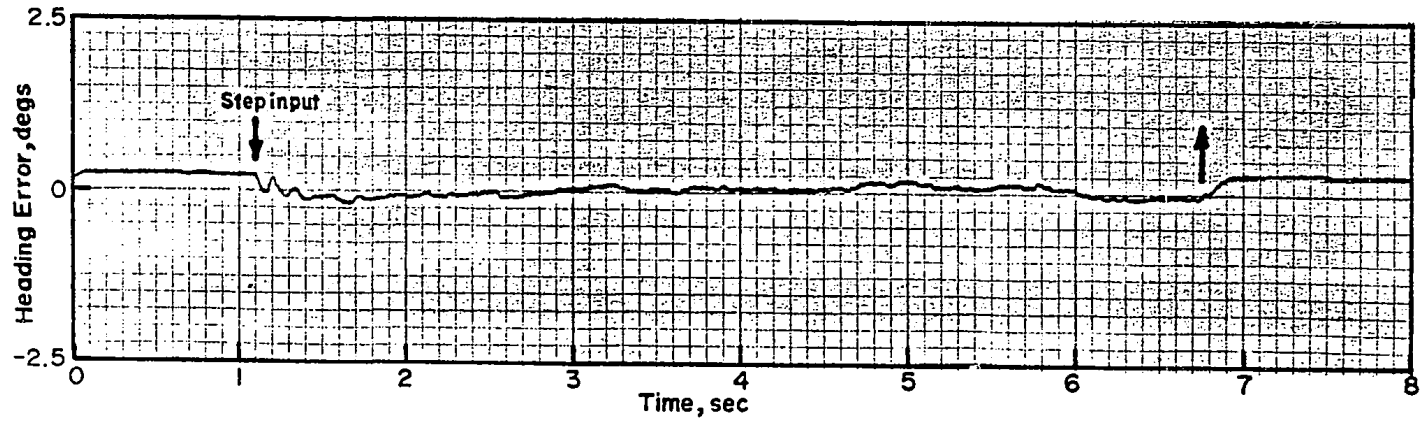

(a) $K_c = 2.0, T_I = 0.0273$ sec, $T_D = 0.0068$ sec (Optimum Setting)

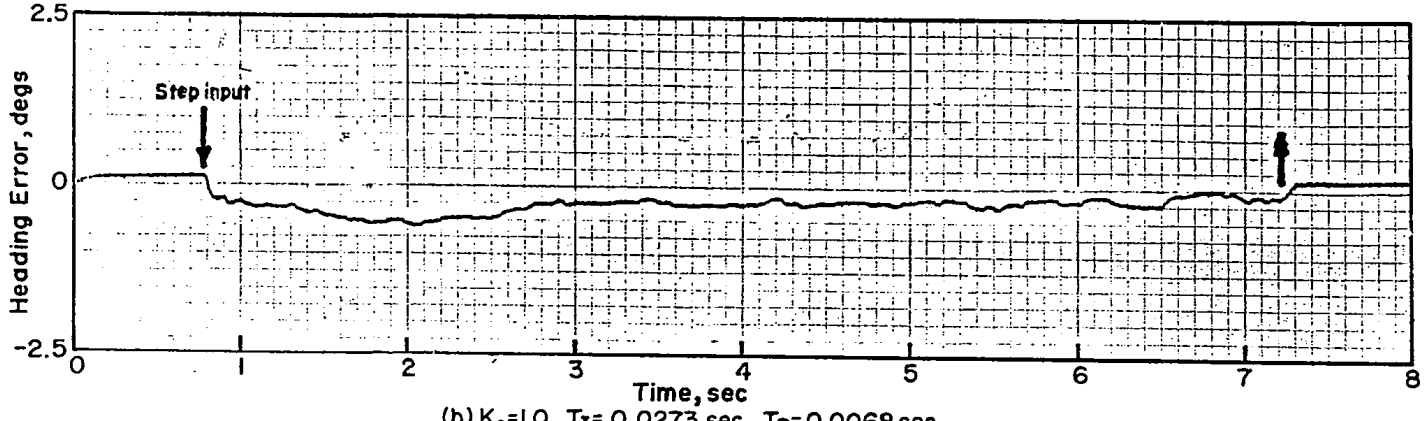

(b) $K_c = 1.0, T_I = 0.0273$ sec, $T_D = 0.0068$ sec

FIGURE 2.18 EXPERIMENTAL SYSTEM RESPONSES TO A STEP RATE INPUT OF 10.0 degs/sec (PID Controller)

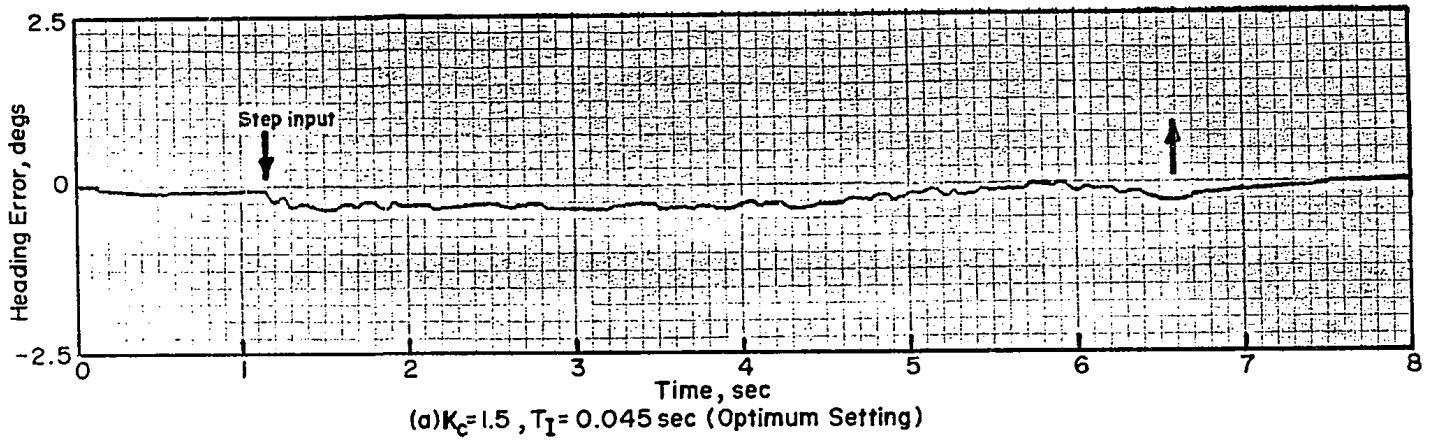

(a) $K_c = 1.5$, $T_I = 0.045$ sec (Optimum Setting)

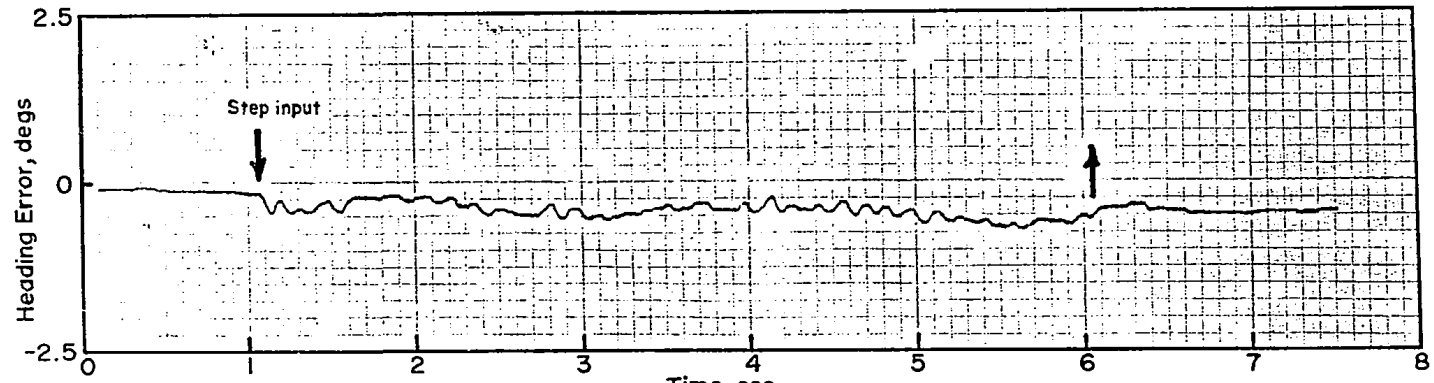

(b) K = 1.5 , T = 0.025 sec

FIGURE 2.19 EXPERIMENTAL SYSTEM RESPONSES TO A STEP RATE INPUT OF 10.0 degs/sec (PI Controller)

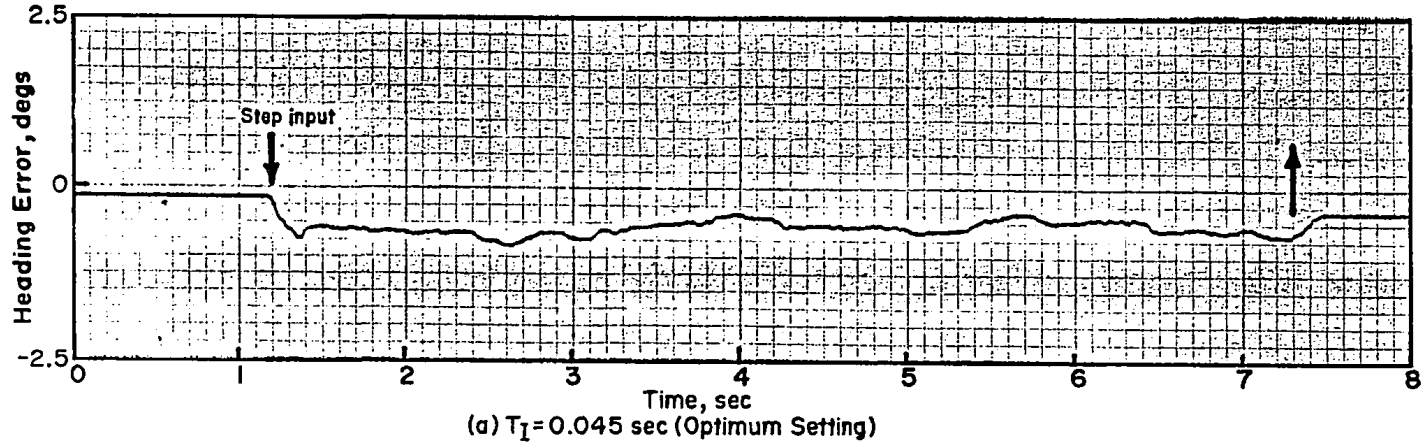

(a) $T_I = 0.045$ sec (Optimum Setting)

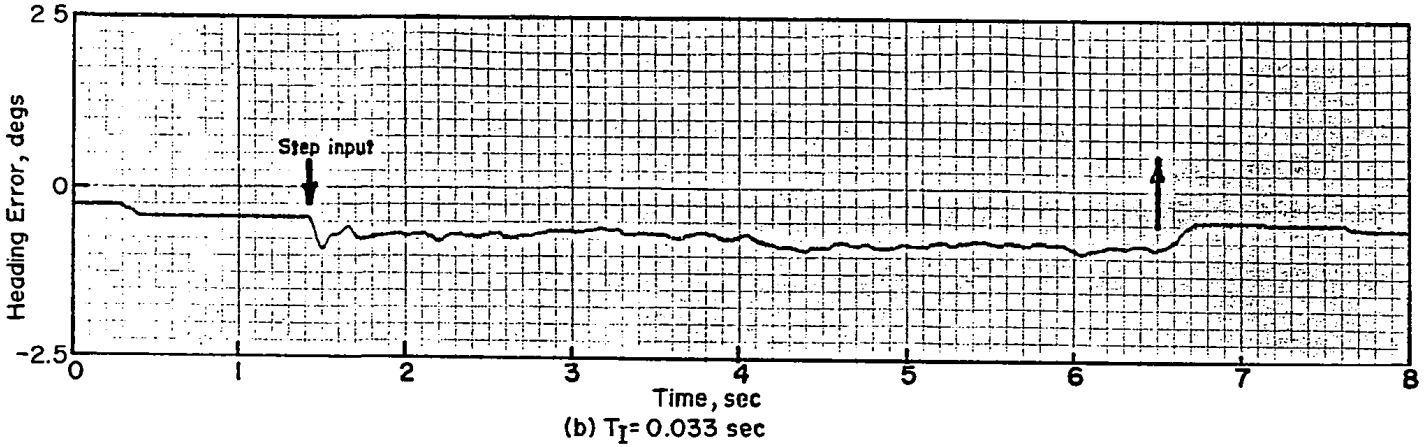

(b) $T_I = 0.033$ sec

FIGURE 2.20 EXPERIMENTAL SYSTEM RESPONSES TO A STEP RATE INPUT OF 10.0 degs/sec (Integral Controller)

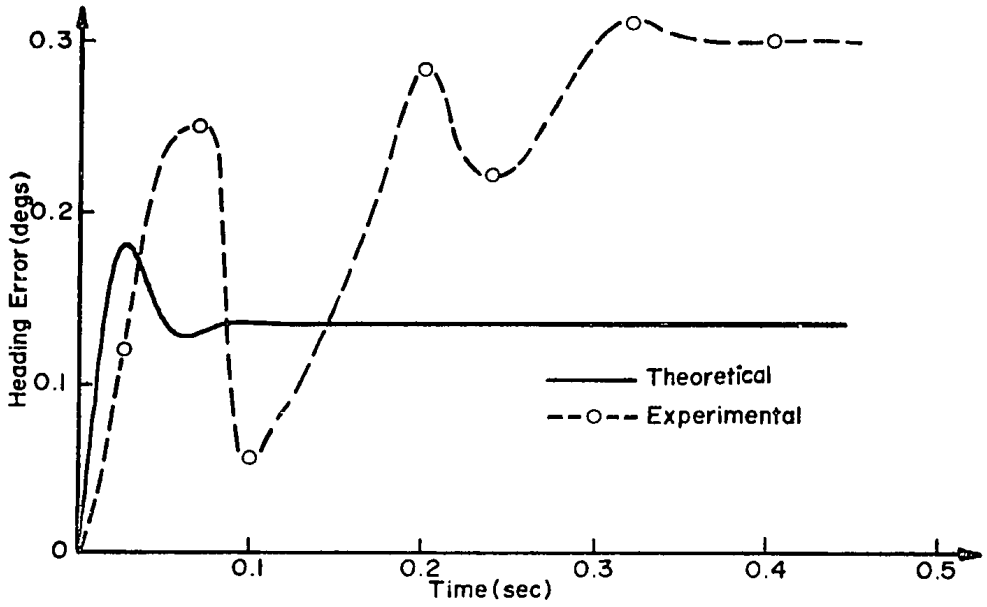

(a) $K_c = 2.0$, $T_I = 0.0273$ sec, $T_D = 0.0068$ sec
(Optimum Setting)

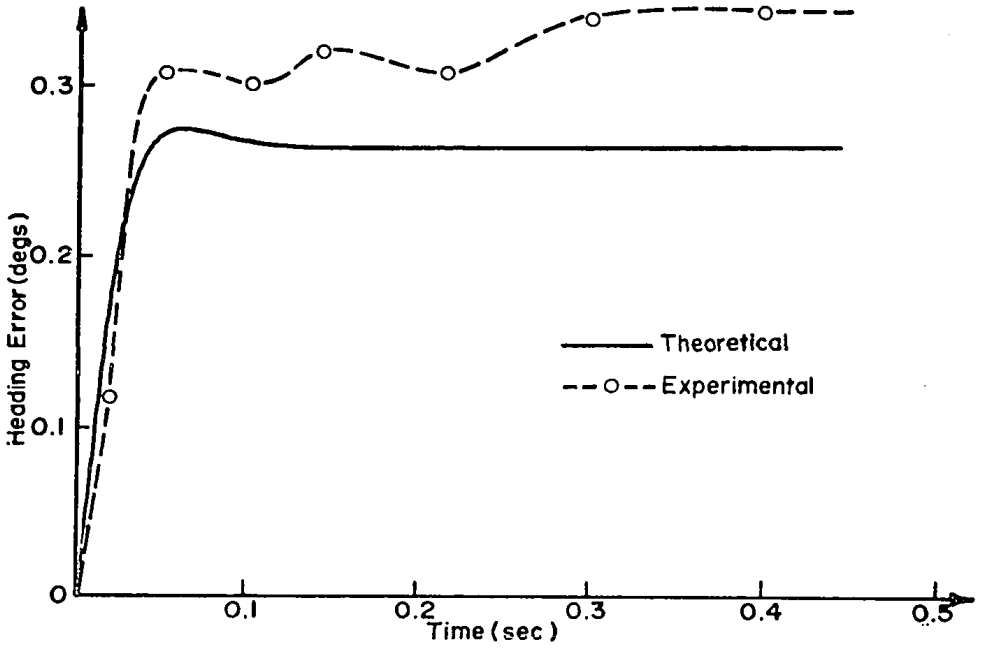

(b) $K_c = 1.0$, $T_I = 0.0273$ sec, $T_D = 0.0068$ sec

FIGURE 2.21 COMPARISON OF THEORETICAL AND EXPERIMENTAL SYSTEM RESPONSES (PID Controller)

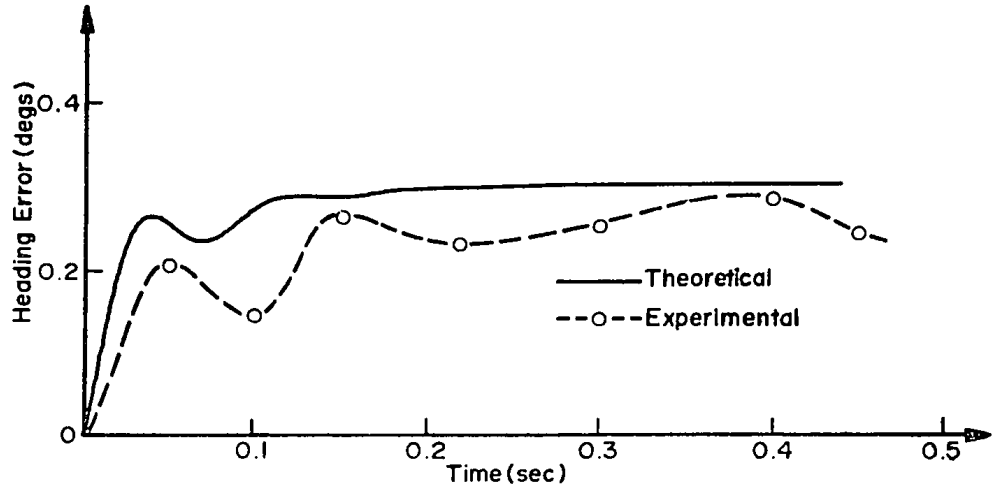

(a) $K_c = 1.5$, $T_I = 0.045$ sec
(Optimum Setting)

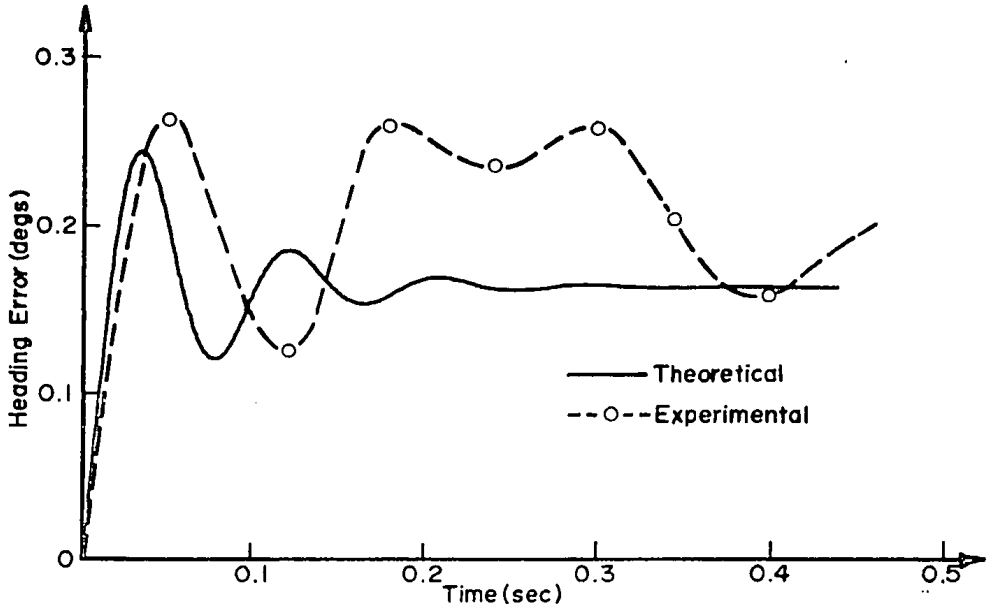

(b) $K_c = 1.5$, $T_I = 0.025$ sec

FIGURE 2.22 COMPARISON OF THEORETICAL AND EXPERIMENTAL SYSTEM RESPONSES (PI Controller)

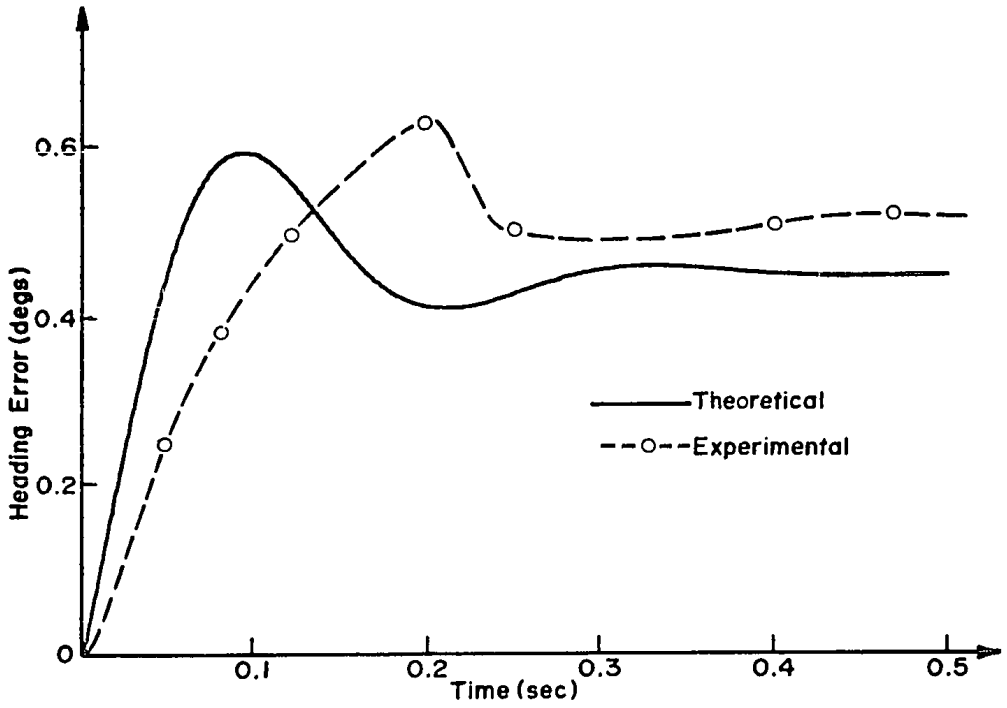

(a) $T_I = 0.045$ sec (Optimum Setting)

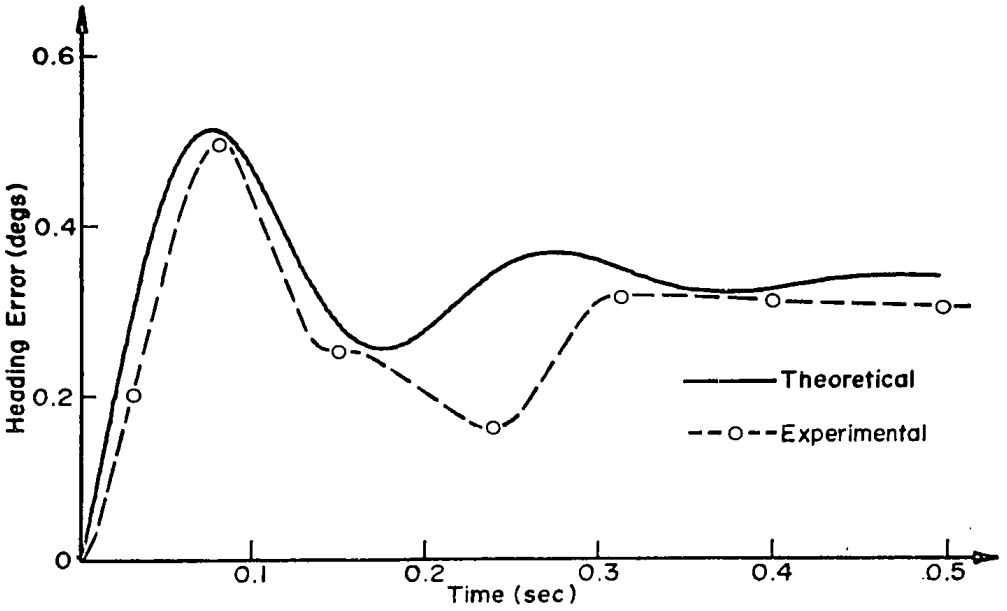

(b) $T_I = 0.033$ sec

FIGURE 2.23 COMPARISON OF THEORETICAL AND EXPERIMENTAL SYSTEM RESPONSES (Integral Controller)

the observed random deviations in heading being attributed to rate sensor noise, mechanical drive system gear backlash, and heading detected potentiometer resolution. The slower experimental transient is attributed to the less than ideal experimental step rate input which is discussed in more detail in the next chapter.

2.5 Alternative for Fluidic Implementation of System Feedback Loop

A specified feedback linear controller function for the heading reference system could be implemented fluidically using high gain operational amplifiers (Reference 38) in combination with passive fluidic resistors and capacitors. Commonly used proportional, differential and integral fluidic circuits are shown with the associated transfer functions in references 30 and 31. Such fluidic implementation of the system feedback loop would necessitate the use of a mechanical rotary actuator compatible with the controller output fluidic signal. A convenient actuator combining the features of relative simplicity and fluidic signal compatibility as proposed in reference 39 is a reversible impulse turbine geared to the rate sensor and driven directly by the momentum of the feedback controller output signal.

The incorporation of a turbine drive, where viscous friction effects may be rendered negligible relative to the inertia effects by appropriate mechanical design refinement, facilitates the simple implementation of the integral controller function as shown in figure 2.24. Herein, the substantial polar moment of inertia associated with high sensivity rate sensor configurations is utilized to implement the integration function, the transfer function of the turbine drive plus the rate sensor inertia load (J) coupled by gear ratio (N) being given by:

$$\frac{\Theta_o(s)}{\Delta P_t(s)} = \frac{1}{s} \frac{G_t}{(J/g)s} \qquad (2.13)$$

where the drive turbine input pressure differential to output torque gain is given by G_t.

The heading error transfer function of the reference system with turbine drive, as derived from the system block diagram shown in figure 2.25, will be:

$$\frac{\Theta_e(s)}{\Theta_i(s)} = \frac{1}{1 + \frac{e^{-0.01s}}{1+0.011s} \frac{1}{T_I s}} \qquad (2.14)$$

where the integration time constant is given by:

$$T_I = \frac{(J/g)}{G_1 . K_c . G_t . N} \qquad (2.15)$$

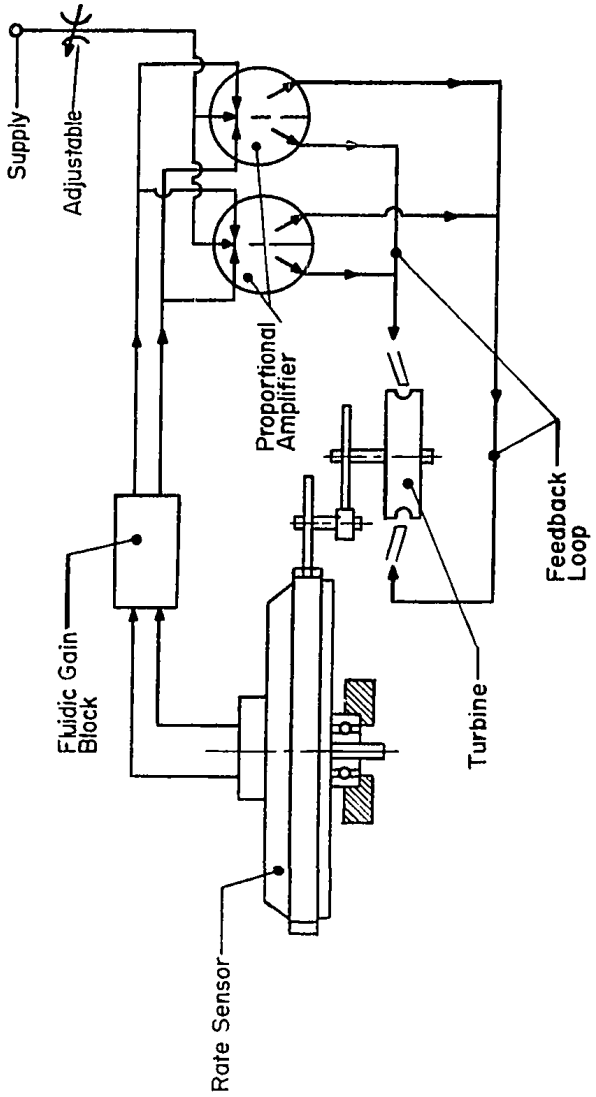

FIGURE 2.24 WHOLLY FLUIDIC HEADING REFERENCE SYSTEM

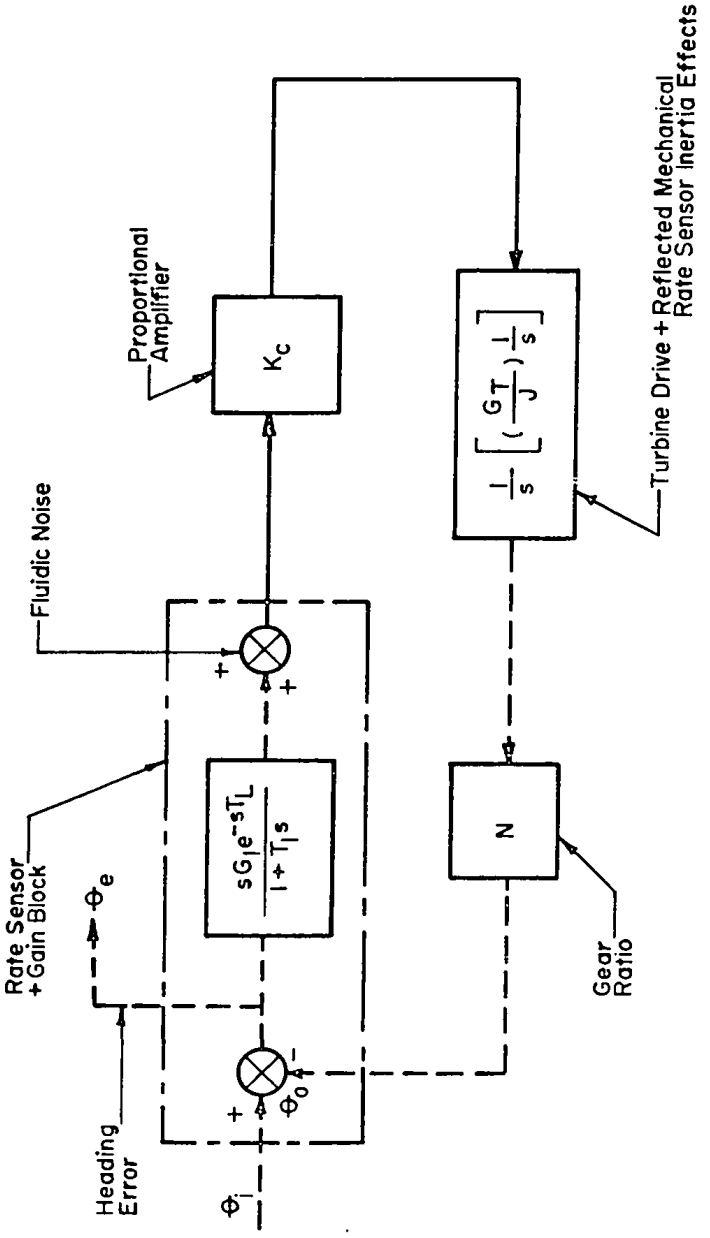

FIGURE 2.25 WHOLLY FLUIDIC HEADING SYSTEM BLOCK DIAGRAM

Accordingly, an optimized integration time constant (T_I) may be attained by suitable mass distribution in the mechanical design of the fluidic rate sensor, coupled with judicious selection of the system gain factors (G_1 and G_t). Reference 39 reported the performance potential of the heading reference system with turbine drive, wherein a 1.0" diameter curved vane impulse turbine wheel driven by two opposed nozzles of approximately 0.018" diameter was postulated.

The above approach would appear to be one of the most attractive methods of achieving a wholly fluidic heading reference system with adequate transient response combined with acceptable steady-state heading error. Actual implementation of such system would require further study of the mechanical design parameters and of fluidic signal impedance matching to realistically evaluate practical system performance. This study is suggested for a future research project.

CHAPTER 3

SYSTEM HEADING ERROR MINIMIZATION

3.1 General

The Ziegler-Nichols rules for determination of optimum controller parameter settings previously described are based on a somewhat arbitrary performance criterion (i.e., a compromise of gain and phase margin) as derived from the performance of typical industrial process control systems. This method has been utilized as a first estimate to evaluate the heading reference system feasibility. The obtained results, while demonstrating feasibility with regard to acceptable system transient response, indicate that the Ziegler-Nichols rules could not be considered as the ultimate optimum criteria, particularily with regard to the system with the proportional-integral controller. One can effectively see by examining the system heading responses shown in figure 2.6 that the response with optimized "heading rate" parameter settings is definitely not optimum with regard to "heading". This is due to the Ziegler-Nichols optimum criteria being derived to obtain a good compromise between amplitude overshoot and oscillation period of the "heading rate deviation" response to a step rate input, while the optimization parameter in the system is the

"heading deviation" which is the time-integral of the rate deviation response.

As mentioned in the previous chapter, there exists in the literature a number of derivations of criteria which define the optimum settings for linear controllers that have been developed on a more rigorous theoretical basis than that of the Ziegler-Nichols approach. However, some of the derivations can only apply to systems without pure time delay (References 37, 40), while others are only applicable to systems with a first-order lag and a pure time delay subjected to a load change (References 34, 35, 36). Neither of the above conditions are satisfied in the case of the hybrid fluidic heading reference system where:

— the vortex rate sensor transfer function in its most simplified form contains a first-order lag plus a pure time delay and the feedback drive motor is represented by another first-order lag.

— the system is always subjected to a set-point rather than a load change, i.e., an angular rate input.

Thus, there is a need for developing new criteria which would provide the optimum settings for the controllers based on a defined performance requirement appropriate to the heading reference system as derived in the subsequent sections.

3.2 Performance Index and Choice of Controllers

It is obvious that the best heading reference system will be the one which, when subjected to an angular input change, will result in a minimum heading error within a minimum transient time. The system step input transient response performance obtained previously indicates that with controller parameter settings given by Ziegler-Nichols criteria the system will attain steady-state in a relatively short time, i.e., 0.15 second with PID controller and 0.25 second with PI controller (see figures 2.5 and 2.6). This suggests that, for analysis simplification purpose, a "minimum steady-state heading error" (i.e., a minimum time-integral of heading "rate error") alone could be considered to be an adequate performance index.

In addition, superfluous analysis effort can be avoided in the developing of an optimization criterion for the heading system by choosing one of the three controller types considered in the previous chapter, on the basis of ease of hardware implementation, electronically or fluidically compatible with an acceptable system performance. A theoretical analysis had been undertaken by G. Nielson (Reference 41) to evaluate and compare the three principal linear control methods on a quantitative basis in order to determine their relative advantages and disadvantages. In

this analysis, a normalized performance index, which was defined as the ratio of minimized time-integral controlled system error by time-integral uncontrolled system error, had been used as comparison basis for some typical systems consisting of first-order lags and a pure time delay. Accordingly, a decreasing normalized index value means an increasing improvement in response. It is shown by this investigation that an integral control is relatively slow while a proportional-integral-derivative control may improve by up to 20% the normalized performance index value of a proportional-integral control, provided that an ideal derivative function can be implemented. It is suggested in reference 41 that it is seldom worthwhile, due to the limitations of practical derivative control implementation and system noise effects, to use more complicated controller functions than that of the proportional-integral type. Fluidic implementation of the derivative function exhibits much the same limitations as in the electronically implementation case with the additional disadvantage of relatively poor amplitude dynamic range as limited by noise generation. Additionally, the substantial noise generated by the rate sensor (Reference 45) would tend to reverse any beneficial controller derivative action in improving the heading system response. Accordingly, only the proportional-integral controller function is considered for feedback compensation in the optimization analysis for the heading reference system.

3.3 Heading Error Minimization

3.3.1 Theoretical Heading Error for a Step Rate Input

The heading reference system with a proportional-integral controller can be represented by the block diagram as shown in figure 3.1, where angular rate variables are used to simplify mathematical analysis. Accordingly, the system steady-state heading error is given by:

$$\Theta_e = \int_0^\infty \omega_e(t)dt \tag{3.1}$$

For convenience, let

$$K_1 = G_1 K_c G_2 \quad \text{and} \quad K_2 = \frac{1}{T_I}$$

By introducing the following Laplace auxiliary variable

$$q = T_L s$$

the angular rate error for a step rate input of ω_i deg./sec. will be given by (see Appendix A)

$$\omega_e(s) = \frac{T_L \omega_i}{q}\left[\frac{1}{1 + \frac{K_1 T_L^2 (K_2 T_L + q)e^{-q}}{q(T_L + T_1 q)(T_L + T_2 q)}}\right] \tag{3.2}$$

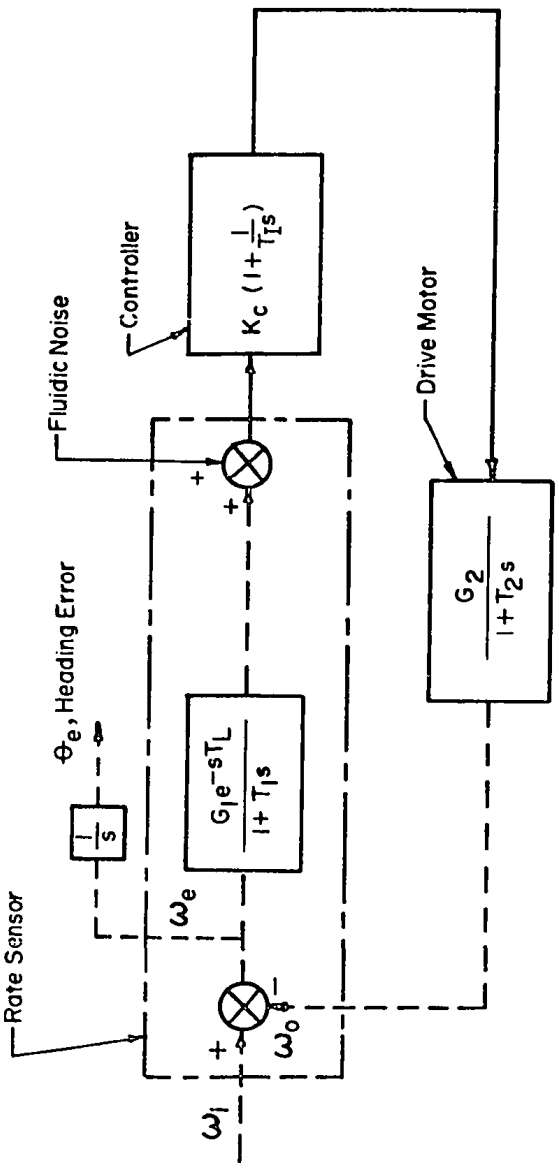

FIGURE 3.1 HEADING REFERENCE SYSTEM BLOCK DIAGRAM WITH PI CONTROLLER

According to Laplace transform theory (Reference 42)

$$\int_0^{\infty} \omega_e(t)dt = \omega_e(s) \Big|_{\infty}^{0} \tag{3.3}$$

Substituting equations (3.2) and (3.3) in equation (3.1)

$$\Theta_e = \frac{T_1\omega_i}{q} \left[\frac{1}{1 + \frac{K_1T_L^2(K_2T_L+q)e^{-q}}{q(T_L+T_1q)(T_L+T_2q)}} \right] \Bigg|_{\infty}^{0}$$

$$= T_L\omega_i \left[\frac{1}{q + \frac{K_1T_L^2(K_2T_L+q)e^{-q}}{(T_L+T_1q)(T_L+T_2q)}} \right] \Bigg|_{\infty}^{0}$$

which gives:

$$\Theta_e = \frac{\omega_i}{K_1K_2} \tag{3.4}$$

Equation (3.4) indicates that the defined performance criterion of heading error (Θ_e) is minimum when $K_1K_2 = \infty$. However, the stability limit associated with the rate sensor time delay in the closed loop system will impose a finite maximum value on the system gain (K_1K_2). Thus, it is necessary to investigate the system stability conditions.

3.3.2 Stability Analysis

The phase-shift associated with the pure time delay in the closed loop system as given by

$$\Phi = -360.f.T_L \text{ degs.}$$

will obviously introduce instability into the system at some finite loop gain (K_1K_2).

In order to determine the system stability conditions, consider equation (3.2) which could be rewritten as follows:

$$\omega_e(s) = T_L\omega_i \left[\frac{(T_L+T_1q)(T_L+T_2q)}{q(T_L+T_1q)(T_L+T_2q)+K_1T_L^2(K_2T_L+q)e^{-q}} \right]$$

Rearranging the terms gives the equation:

$$\omega_e(s) = T_L\omega_i \left[\frac{q^2+\frac{T_1+T_2}{T_1T_2}T_Lq+\frac{T_L^2}{T_1T_2}}{q^3+\frac{T_1+T_2}{T_1+T_2}T_Lq^2+\frac{T_L^2}{T_1T_2}q+\frac{K_1T_L^2}{T_1T_2}(K_2T_L+q)e^{-q}} \right] \qquad (3.5)$$

Introducing the following dimensionless quantities:

$$A = \frac{K_1 T_L^2}{T_1 T_2}$$

$$B = K_2 T_L$$

$$C = \frac{T_1 + T_2}{T_1 T_2} T_L \qquad (3.6)$$

$$D = \frac{T_L^2}{T_1 T_2}$$

equation (3.5) becomes:

$$\omega_e(s) = T_L \omega_i \left[\frac{q^2+Cq+D}{q^3+Cq^2+Dq+A(B+q)e^{-q}} \right] \qquad (3.7)$$

Using the inverse Laplace transform, the rate error response in time domain is given by:

$$\frac{\omega_e(\tau)}{\omega_i} = \frac{1}{2\pi i} \int_{-i\infty}^{+i\infty} \frac{q^2+Cq+D}{q^3+Cq^2+Dq+A(B+q)e^{-q}} e^{-q\tau} d\tau \qquad (3.8)$$

where $\tau = (t/T_L)$ is the corresponding variable in time domain of the auxiliary variable $q = T_L s$ in Laplace domain.

The roots of the integrand denominator in equation

(3.8) which is hereafter called "characteristic equation", will be of the form:

$$q_n = -\delta_n + i\Omega_n$$

accompanied by its conjugates of the form:

$$\bar{q}_n = -\delta_n - i\Omega_n$$

Provided that the stability condition which will be determined in this section is satisfied, then when:

— $\Omega_n = 0$ and $\delta_n \neq 0$ the characteristic equation contains only real poles, which signifies a system overdamped response

— $\delta_n = 0$ and $\Omega_n \neq 0$ the characteristic equation contains only imaginary poles, which signifies a system sustained oscillatory response

— $\Omega_n \neq 0$ and $\delta_n \neq 0$ the characteristic equation contains complex poles, which signifies a system underdamped response

— $\Omega_1=\Omega_2=\Omega_3 = 0$ and $\delta_1=\delta_2=\delta_3 \neq 0$ the characteristic equation contains a triple real pole, which signifies a system critical damped response.

As will be shown later, the ratio of the real part of the characteristic equation's root over its imaginary part (δ_n/Ω_n) will characterize system response damping ratio and it will be considered as the system primary independent variable during the heading error minimization procedure. A smaller value of (δ_n/Ω_n) will imply a more oscillatory system response.

Since e^{-q_n} is a periodical function, i.e.

$$e^{-q_n} = e^{-(-\delta_n+i\Omega_n)} = e^{\delta_n}(\cos\Omega_n - i\sin\Omega_n)$$

the characteristic equation has an infinity of roots.

According to the residue theorem, equation (3.8) could be rewritten as follows:

$$\frac{\omega_e(\tau)}{\omega_i} = \sum_{n=o}^{\infty} \left[\text{Res.}(q_n) + \text{Res.}(\bar{q}_n) \right] \qquad (3.9)$$

The residues of q_n and $\bar{q}_n$ are determined using Laurent's series theory and l'Hospital's rules as shown in Appendix A to be:

$$\text{Res.}(q_n) + \text{Res.}(\bar{q}_n) = X_n e^{q_n\tau} + \bar{X}_n e^{\bar{q}_n\tau} \qquad (3.10)$$

where $X_n = f(q_n)$ and $\bar{X}_n = f(\bar{q}_n)$

Substituting the complex representations for q_n and $\bar{q}_n$ and trigonometrically manipulating the terms, equation (3.10) becomes:

$$\text{Res.}(q_n)+\text{Res.}(\bar{q}_n) = \left|X_n\right| e^{-\delta_n \tau} \cos(\Omega_n \tau - \phi_n) \qquad (3.11)$$

where $\left|X_n\right| = f_n(\delta_n, \Omega_n)$ and $\phi_n = g_n(\delta_n, \Omega_n)$ as given in Appendix A.

By combining equations (3.9) and (3.11) we obtain the following time domain rate error response:

$$\frac{\omega_e(\tau)}{\omega_i} = \sum_{n=0}^{\infty} \left|X_n\right| e^{-\delta_n \tau} \cos(\Omega_n \tau - \phi_n) \qquad (3.12)$$

Equation (3.12) indicates that the system is stable only for positive values of δ_n.

Further, since the response of $\omega_e(\tau)$ is approximated by its first and obviously dominant component, equation (3.12) becomes:

$$\frac{\omega_e(\tau)}{\omega_i} = \left|X_o\right| e^{-\delta_o \tau} \cos(\Omega_o \tau - \phi_o) \qquad (3.13)$$

The typical form of the system rate error response

given by equation (3.13) is shown in figure 3.2.

At the response peaks (i.e. points $\tau_1, \tau_2, \tau_3 \ldots$ etc...on figure 3.2) we obtain the following relationship:

$$\frac{d\left[\frac{\omega_e(\tau)}{\omega_i}\right]}{d\tau} = \frac{d\left[\left|X_o\right| e^{-\delta_o \tau} \cos(\Omega_o \tau - \phi_o)\right]}{d\tau} = 0$$

which gives:

$$-\delta_o \left|X_o\right| e^{-\delta_o \tau} \cos(\Omega_o \tau - \phi_o) - \left|X_o\right| e^{-\delta_o \tau} \Omega_o \sin(\Omega_o \tau - \phi_o) = 0$$

or:

$$\tan(\Omega_o \tau - \phi_o) = -\frac{\delta_o}{\Omega_o}$$

The times corresponding to these peaks are then given by:

$$\Omega_o \tau = -\arctan\frac{\delta_o}{\Omega_o} + \phi_o + k\pi \qquad (3.14)$$

Let 'M' be the ratio of two successive absolute amplitude values (i.e., ratio of a_2/a_1, $a_3/a_2 \ldots$ etc ... on figure 3.2) 'M' will be given by combining equations (3.13) and (3.14):

$$M = \left| \frac{\left|X_o\right| e^{-\frac{\delta_o}{\Omega_o}\left(-\arctan\frac{\delta_o}{\Omega_o} + \phi_o + (k+1)\pi\right)} \cos\left[-\arctan\frac{\delta_o}{\Omega_o} + (k+1)\pi\right]}{\left|X_o\right| e^{-\frac{\delta_o}{\Omega_o}\left(-\arctan\frac{\delta_o}{\Omega_o} + \phi_o + k\pi\right)} \cos\left[-\arctan\frac{\delta_o}{\Omega_o} + k\pi\right]} \right| \qquad (3.15)$$

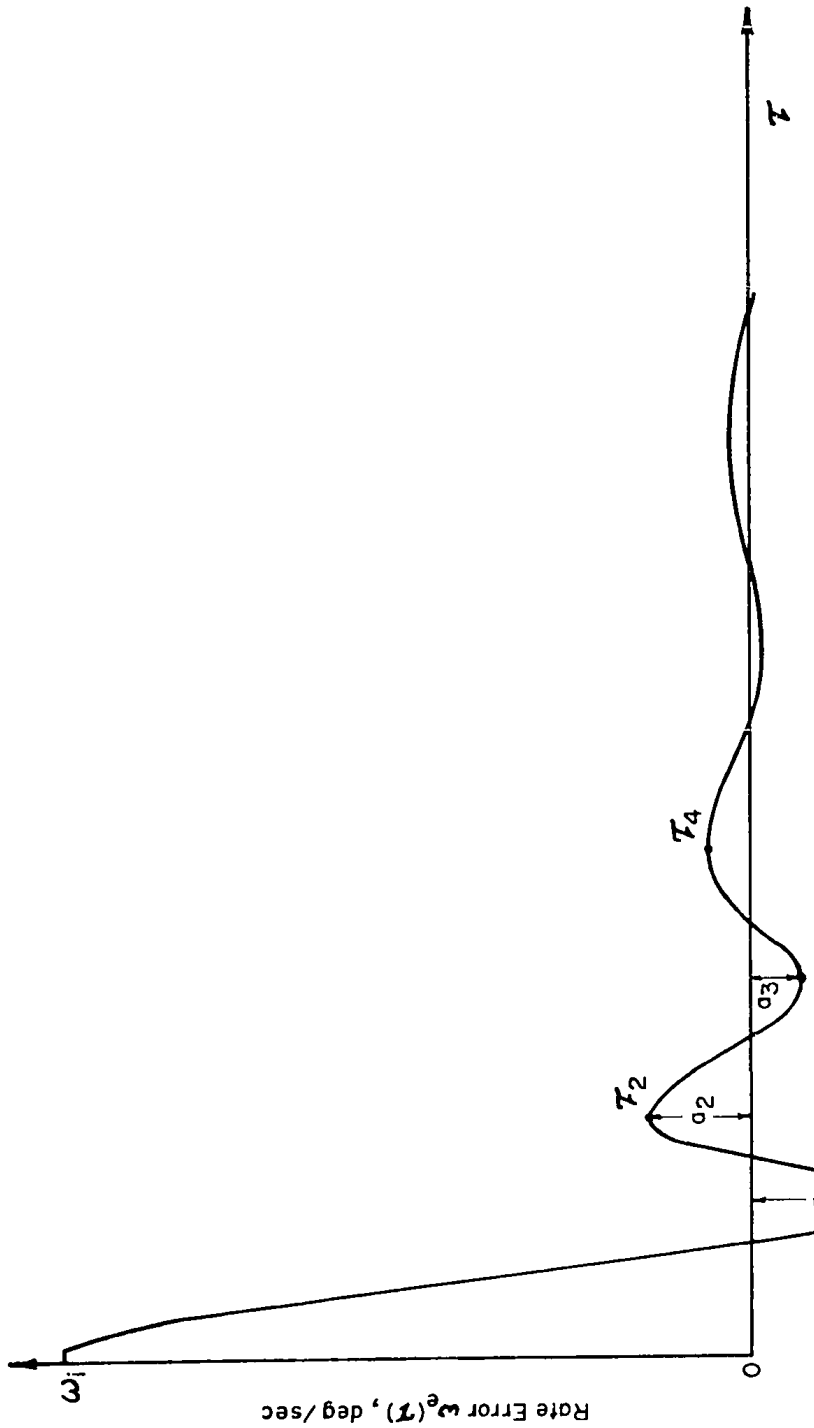

FIGURE 3.2 TYPICAL HEADING RATE ERROR RESPONSE

But:

$$\cos\left[-\arctan\frac{\delta_o}{\Omega_o} + (k+1)\pi\right] = -\cos\left[-\arctan\frac{\delta_o}{\Omega_o} + k\pi\right]$$

Hence, equation (3.15) reduces to:

$$M = e^{-\frac{\delta_o}{\Omega_o}\pi} \tag{3.16}$$

Equation (3.16) indicates that the ratio of two successive amplitudes depends on the ratio of the real part of the characteristic equation's root (δ_o) over its imaginary part (Ω_o), and accordingly, the system amplitude response damping will be a unique function of the "damping ratio" (δ_o/Ω_o). Figure 3.3 plots M as function of (δ_o/Ω_o) on semi-logarithm coordinates.

3.3.3 Minimization Procedure

Substituting the dimensionless quantities defined by equation (3.6) into the steady-state heading error as given by equation (3.4):

$$\Theta_e = \frac{\omega_i}{K_1 K_2} = \frac{\omega_i T_L^3}{T_1 T_2}\left[\frac{1}{AB}\right] \tag{3.17}$$

Equation (3.17) indicates that, while respecting the stability requirement described previously, (AB) should

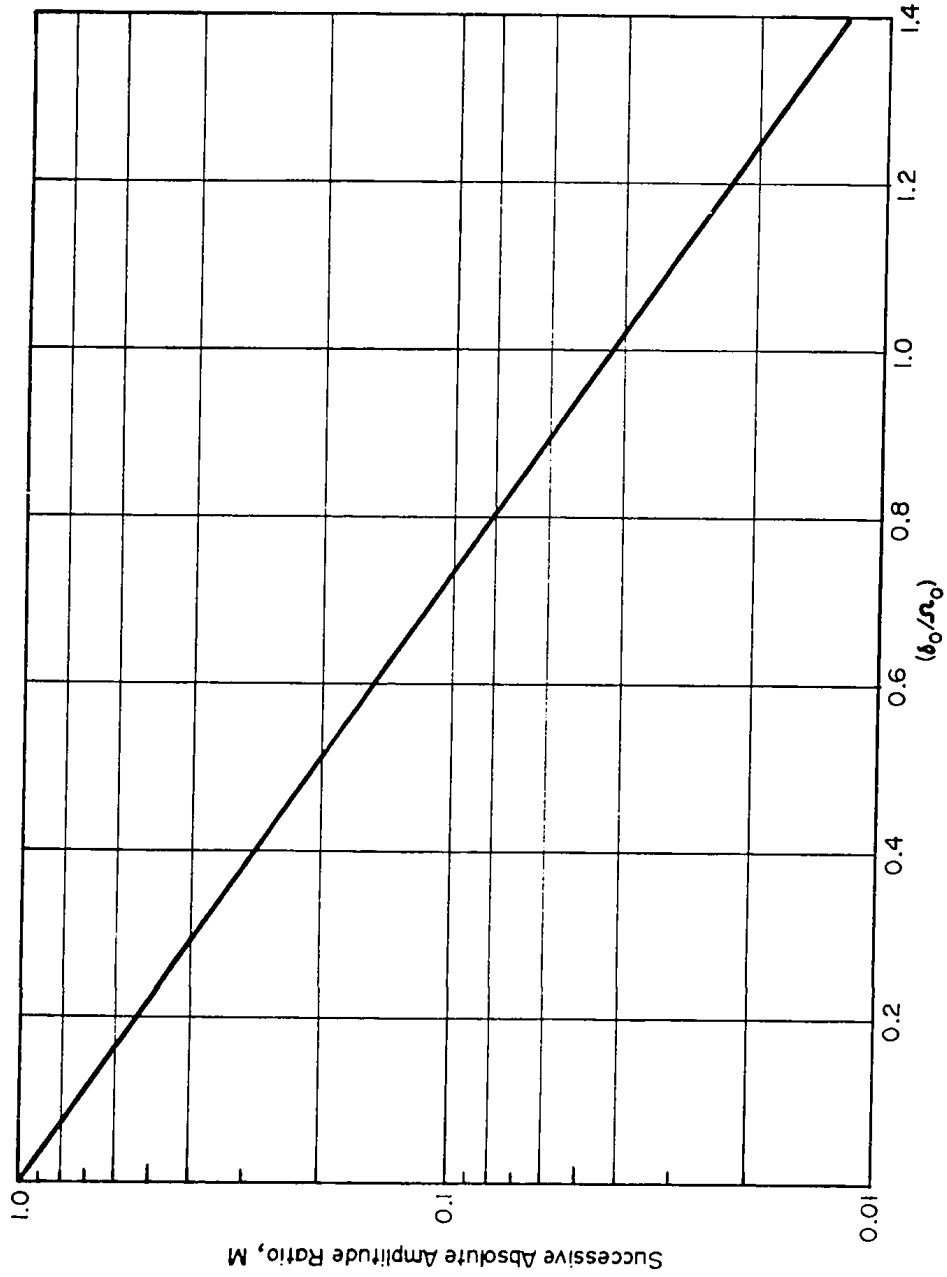

FIGURE 3.3 PLOT OF SUCCESSIVE AMPLITUDE RATIO VS (δ_o/Ω_o)

be maximized to attain a minimum heading error (Θ_e).

This means that, for a specified response damping ratio (i.e., (δ_o/Ω_o) = constant), one should find a root of the following transcendental characteristic equation:

$$q^3+Cq^2+Dq+A(B+q)e^{-q} = 0 \qquad (3.18)$$

which has a negative real part and gives a maximum (AB).

Let $q = -\delta + i\Omega$ be a root of equation (3.18). After substitution of this value of (q) into equation (3.18) and performing some complex algebra manipulations (Appendix A), the resulting real and imaginary parts are equalized to zero to maintain:

$$-\delta^3+3\Omega^2\delta+C(\delta^2-\Omega^2)-D\delta+ABe^{\delta}\cos\Omega+Ae^{\delta}(\Omega\sin\Omega-\delta\cos\Omega)=0 \qquad (3.19)$$

$$-\Omega^3+3\delta^2\Omega-2C\delta\Omega+D\Omega-ABe^{\delta}\sin\Omega+Ae^{\delta}(\delta\sin\Omega+\Omega\cos\Omega)=0 \qquad (3.20)$$

Solving equations (3.19) and (3.20) to obtain (AB) as shown in Appendix A:

$$AB = \left[\begin{array}{l}\left[\Omega^3\left(3\frac{\delta^2}{\Omega^2}-1\right)-2\Omega^2C\left(\frac{\delta}{\Omega}\right)+\Omega D\right]\left(\sin\Omega-\frac{\delta}{\Omega}\cos\Omega\right) \\ -\left[\Omega^3\left(3\frac{\delta}{\Omega}-\frac{\delta^3}{\Omega^3}\right)+\Omega^2C\left(\frac{\delta^2}{\Omega^2}-1\right)-\Omega D\left(\frac{\delta}{\Omega}\right)\right]\left(\frac{\delta}{\Omega}\sin\Omega+\cos\Omega\right)\end{array}\right] e^{-\left(\frac{\delta}{\Omega}\right)\Omega}$$

Since (δ/Ω) is constant for a specified response damping ratio, it is sufficient to differentiate equation (3.21) with respect to (Ω) and let the derivative equal zero to get a value of (Ω) which gives a maximum (AB).

After extensive mathematical manipulations as described in Appendix A, the required value of (Ω) for a maximum (AB) may be shown to be given by the roots of the equation:

$$\tan\Omega = - \frac{\Omega^3(3\frac{\delta^2}{\Omega^2} - 1) - 2\Omega^2(C+3)(\frac{\delta}{\Omega}) + \Omega(2C+D)}{\Omega^3\{\frac{\delta}{\Omega}\}(3-\frac{\delta^2}{\Omega^2}) + \Omega^2(C+3)(\frac{\delta^2}{\Omega^2} - 1) - \Omega(\frac{\delta}{\Omega})(2C+D) + D} \qquad (3.22)$$

The following observations can be made regarding the solution of equation (3.22):

i) $\Omega = 0$ is a trivial root which will be excluded in the subsequent analysis since the root is meaningless.

ii) Since a discontinuity might occur in the right hand side of equation (3.22) and approximate values of equation roots are not known in advance, a graphical solution of this equation would appear to be preferred to a numerical solution which might be divergent.

iii) Since tan Ω is a periodical function, equation (3.22) contains an infinite number of roots. However, only the one with the smallest positive value, which being probably situated

between $\Omega = 0$ and $\Omega = \pi/2$, will be considered since it represents the response basic and dominant component.

iv) Since δ should be always positive due to system stability requirement, the right hand side of equation (3.22) is symmetrical with respect to coordinate origin. Since tan Ω is also symmetrical with respect to the origin, there will be a negative root corresponding to each positive root, both with the same absolute value. This verifies the well-known fact that a complex root always appears as a conjugate pair.

Figure 3.4 illustrates some typical graphical solutions of equation (3.22) with the experimental heading system parameter numerical values of $T_1 = 0.011$ sec., $T_2 = 0.020$ sec. and $T_L = 0.010$ sec., where (δ/Ω) was considered as the independent variable. The corresponding variation of system heading error (θ_e) with respect to angular frequency (Ω) is shown in figure 3.5, the minimum heading error occuring at the roots defined in figure 3.4.

Once the required root (Ω) is obtained, (AB) may be determined from equation (3.21) rearranged as follows:

$$AB = \left[\begin{array}{l} \left(\frac{\delta^2}{\Omega^2}+1\right)\left[\Omega^3\left(\frac{\delta^2}{\Omega^2}-1\right)-\Omega^2 C\left(\frac{\delta}{\Omega}\right)+\Omega D\right]\sin\Omega \\ \quad +\left(\frac{\delta^2}{\Omega^2}+1\right)\left[-2\Omega^3\left(\frac{\delta}{\Omega}\right)+\Omega^2 C\right]\cos\Omega \end{array} \right] e^{-\left(\frac{\delta}{\Omega}\right)\Omega} \qquad (3.23)$$

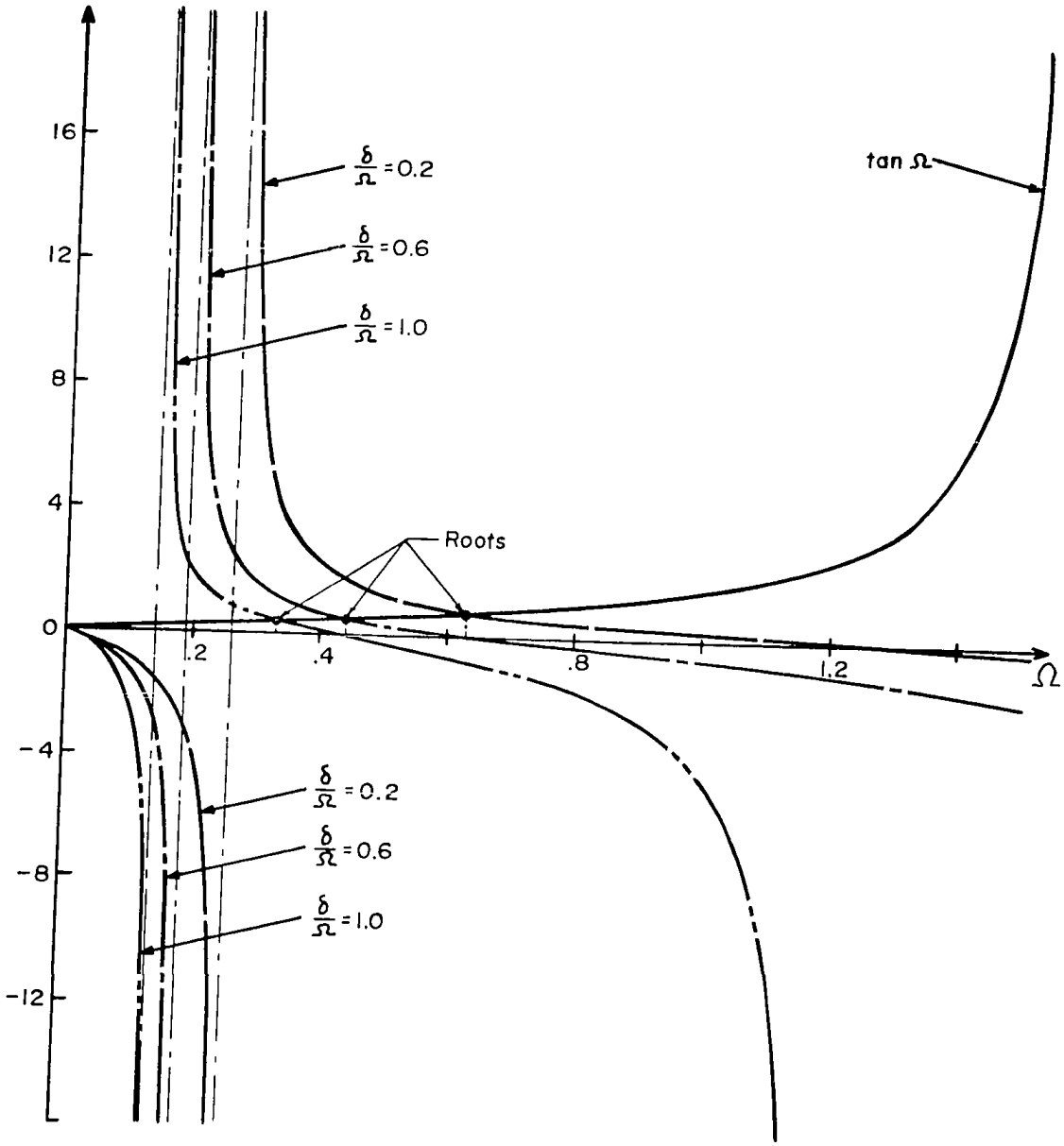

FIGURE 3.4 GRAPHICAL SOLUTION OF EQUATION (3.22)

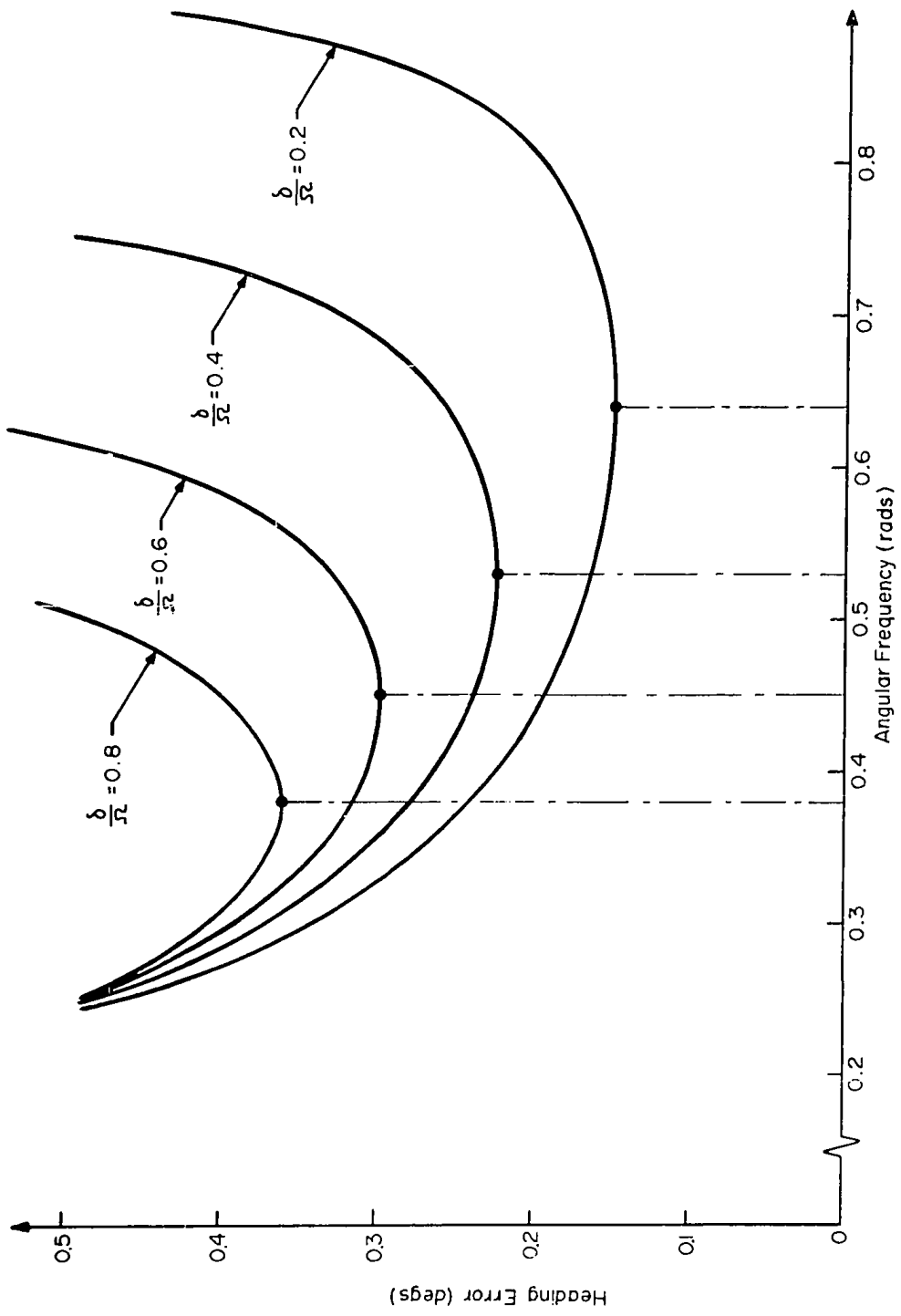

FIGURE 3.5 VARIATION OF HEADING ERROR (Θ_e) WITH RESPECT TO ANGULAR FREQUENCY (Ω), ω_i = 10.0 degs/sec

Subsequently (A) may be obtained by simultaneously solving equations (3.19) and (3.20) (see Appendix A)

$$A = -\left[\begin{array}{l}\left[\Omega^2\left(3\frac{\delta^2}{\Omega^2}-1\right)-2\Omega C\left(\frac{\delta}{\Omega}\right)+D\right]\cos\Omega \\ +\left[\Omega^2\left(\frac{\delta}{\Omega}\right)\left(3-\frac{\delta^2}{\Omega^2}\right)+\Omega C\left(\frac{\delta^2}{\Omega^2}-1\right)-D\left(\frac{\delta}{\Omega}\right)\right]\sin\Omega\end{array}\right] e^{-\left(\frac{\delta}{\Omega}\right)\Omega} \tag{3.24}$$

Finally, the controller parameter setting which gives a minimum heading error is determined by:

$$K_1 = \frac{T_1 T_2}{T_L^2} A \quad \text{and} \quad K_2 = \frac{B}{T_L} \tag{3.25}$$

3.4 System Heading Responses in Time Domain

3.4.1 Simulated System Responses to a Step Rate Input

A hybrid simulation of the actual heading system was carried out using the same simulation technique described in chapter 2 to verify the optimization criterion derived in section 3.3.

a) System with Manufacturer Specified Rate Sensor Transfer Function

Rate sensor transfer function equation (2.5) with associated parameter numerical values as specified by the manufacturer (Reference 10) was initially used for the

system simulation study. Typical optimum heading time responses to a 10.0 degs./sec. step rate input are shown in figures 3.6a to 3.6d where, with (δ/Ω) as parameter, a set of optimum values of (K_1) and (K_2) are determined following the procedure described in section 3.3.3. These figures also show the heading error step input responses for other than optimum sets of (K_1) and (K_2) magnitudes as determined by directly solving equations (3.23), (3.24) and (3.25) for values of (Ω) other than the root of the predicted optimum equation (3.22). These numerical results verify the derived minimized heading error criterion

b) System with More Accurate Rate Sensor Transfer Function

Recent investigations of the fluidic rate sensor dynamic response (References 43, 44) have indicated that a more realistic function than that specified by the manufacturer will be of the form:

$$\frac{\Delta P(s)}{\Theta_i(s)} = \frac{G_1 . s . \psi_n^2 . e^{-T_L s}}{s^2 + 2\zeta\psi_n s + \psi_n} \qquad (3.26)$$

Describing the rate sensor transfer function by equation (3.26), the heading system theoretical steady-state heading error will still be given by (see Appendix A):

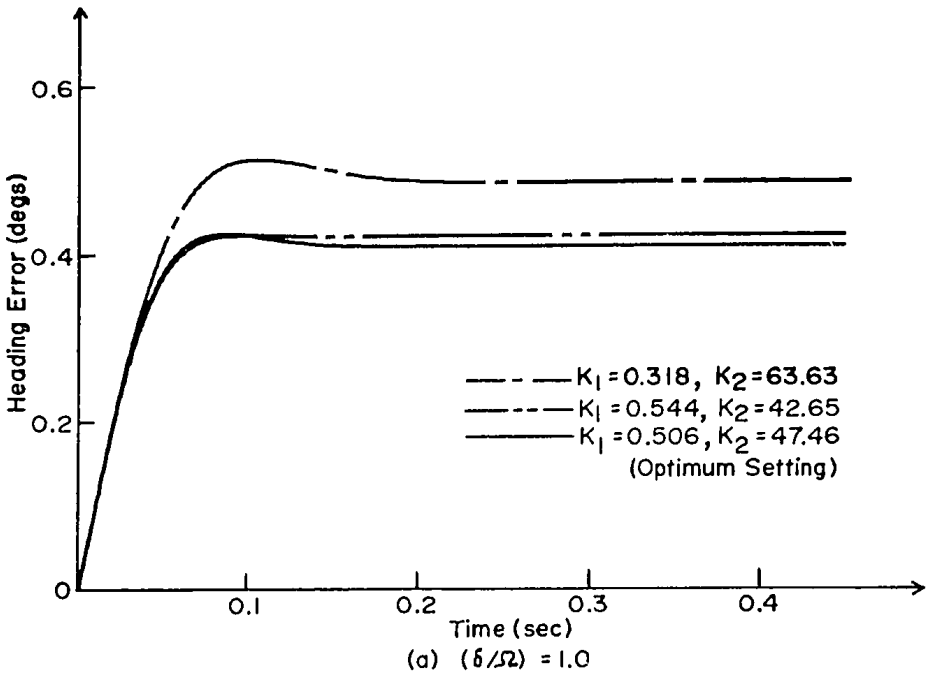

(a) $(\delta/\Omega) = 1.0$

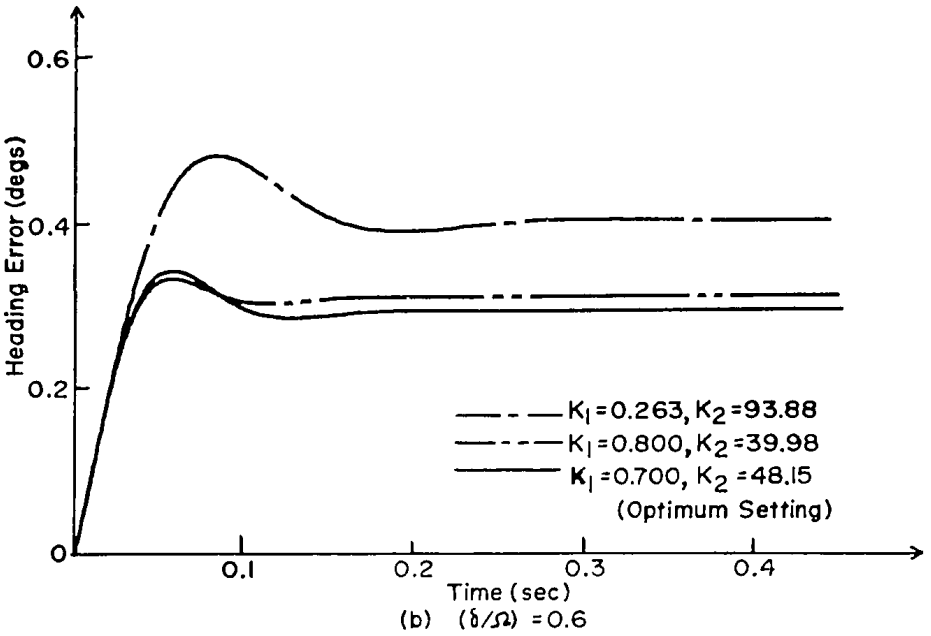

(b) $(\delta/\Omega) = 0.6$

FIGURE 3.6 SYSTEM RESPONSES TO A STEP RATE INPUT OF 10 degs/sec

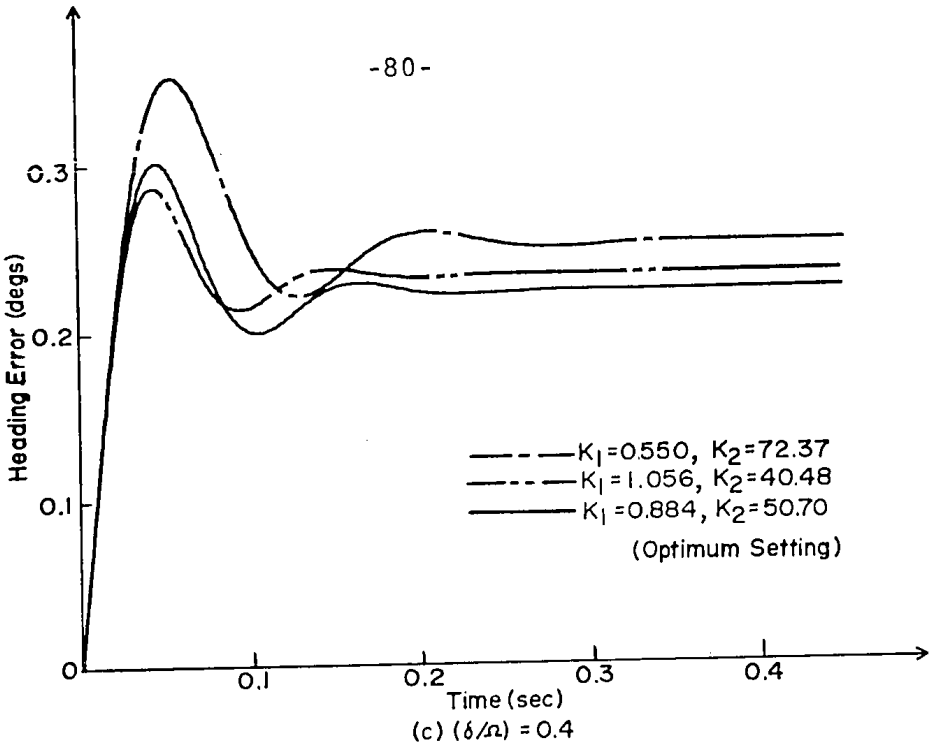

(c) $(\delta/\Omega) = 0.4$

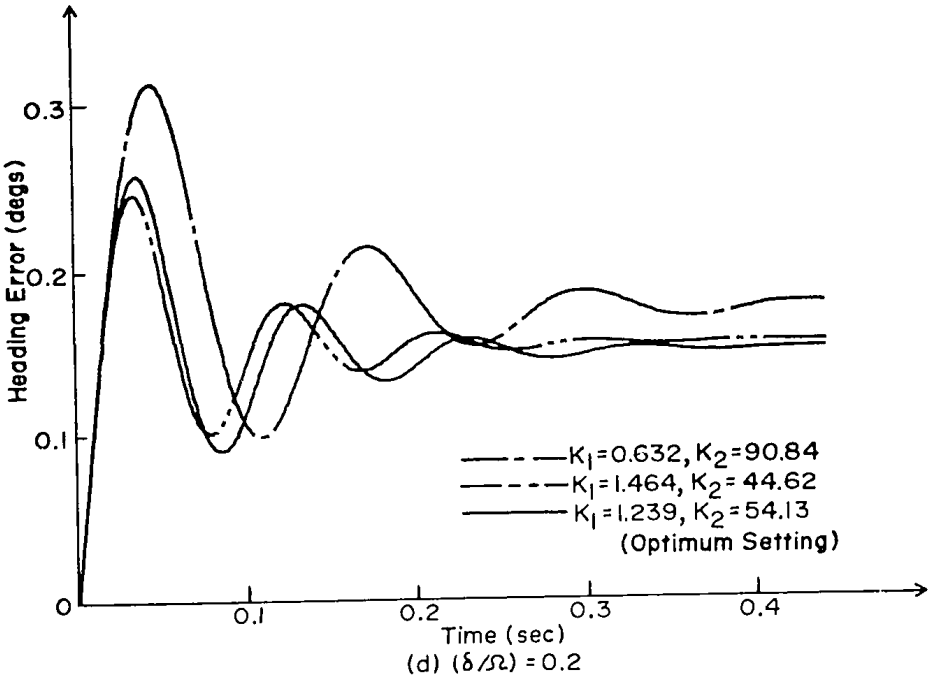

(d) $(\delta/\Omega) = 0.2$

FIGURE 3.6 SYSTEM RESPONSES TO A STEP RATE INPUT OF 10 degs/sec

$$\Theta_e = \frac{\omega_i}{K_1 K_2} \qquad (3.4)$$

A mathematical analysis to minimize the system heading error when the rate sensor is described by equation (3.26) is much more complicated than in the previous case where the rate sensor was represented by a first-order lag plus a pure time delay. The more accurate sensor representation results in the characteristic equation becoming a fourth-order transcendental equation due to the introduction of the second-order lag in the sensor transfer function. It is thereby proposed to investigate the simulated system response using the optimum parameter settings derived in section 3.3.3 for the manufacturer's specified rate sensor transfer function of the form $e^{-T_L s}/(1+T_1 s)$ in order to estimate the degree of dependency of the optimization criterion upon the rate sensor transfer function form.

Typical system heading error responses to a 10.0 degs./sec. step rate input are shown in figures 3.7a to 3.7d, where rate sensor transfer function parameters defined by equation (3.26) are estimated from the experimental rate sensor step input response at the nominal sensor supply pressure of 5.0 psi to be (Reference 44):

$$\psi_n = 44.2 \text{ Hz}$$

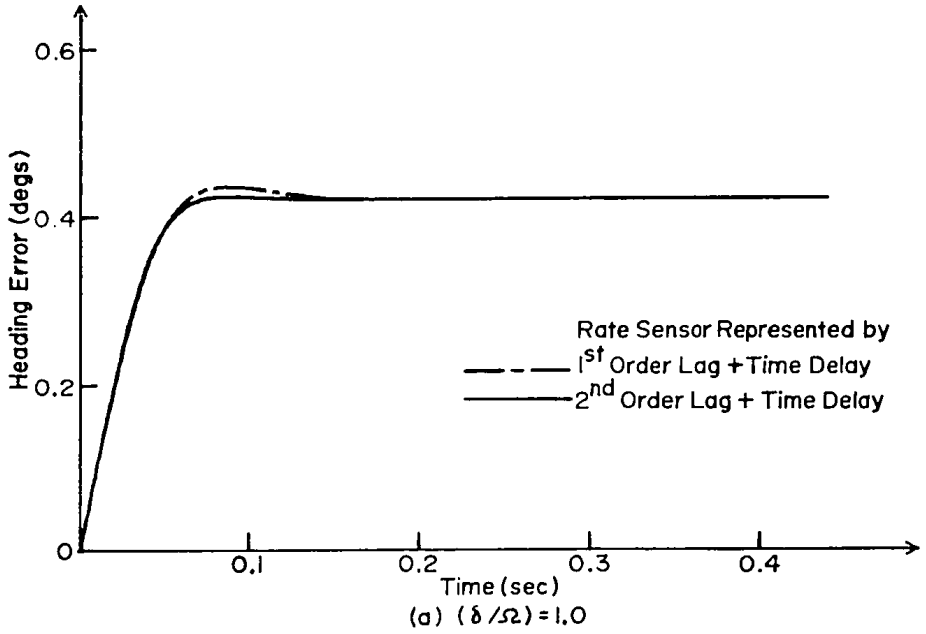

(a) $(\delta/\Omega) = 1.0$

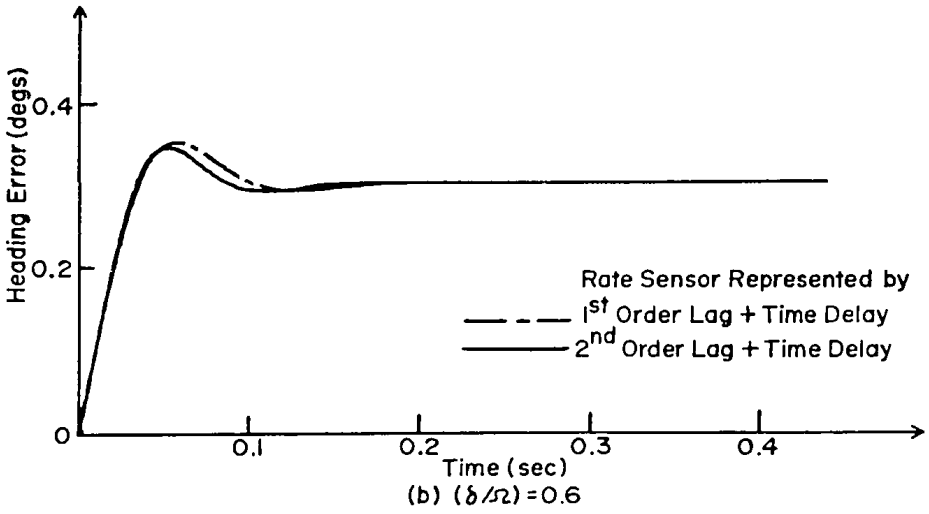

(b) $(\delta/\Omega) = 0.6$

FIGURE 3.7 OPTIMUM SYSTEM RESPONSES TO A STEP RATE INPUT OF 10 degs/sec

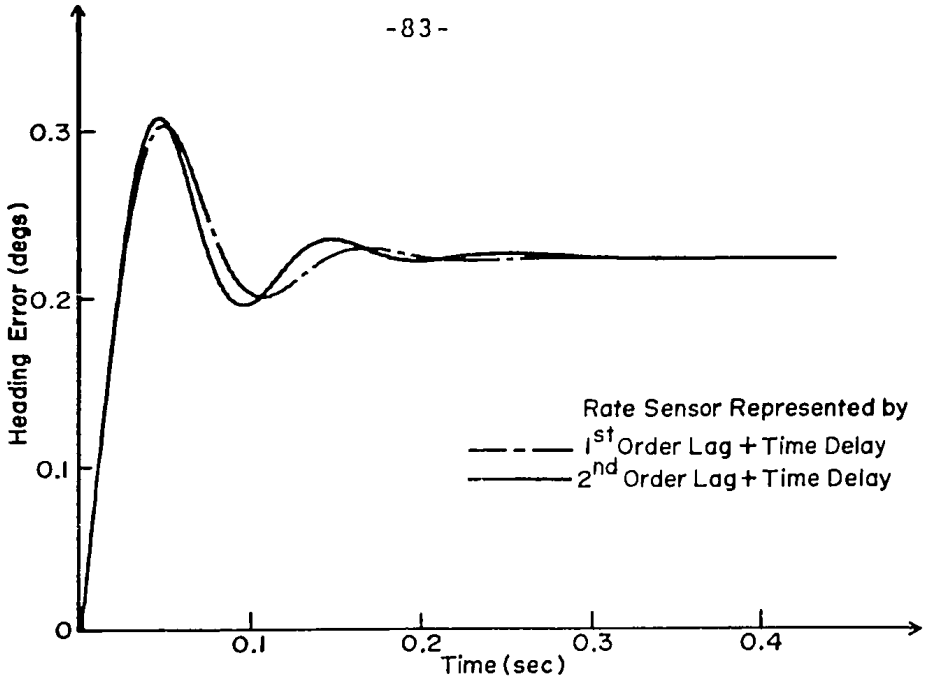

(c) $(\delta/\Omega) = 0.4$

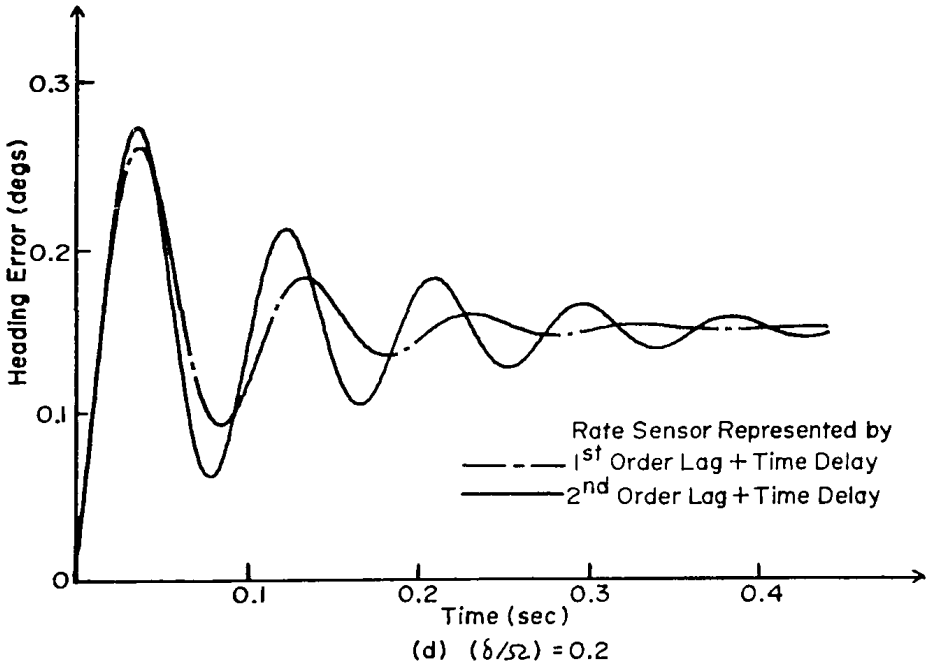

(d) $(\delta/\Omega) = 0.2$

FIGURE 3.7 OPTIMUM SYSTEM RESPONSES TO A STEP RATE INPUT OF 10 degs/sec

$\zeta = 0.8$

$T_L = 0.014$ sec.

Superimposed on the same figures are the minimized heading error responses of system with original rate sensor transfer function. It is evident that, except near the stability limit, the system behavior remains very much the same for both rate sensor transfer function representations. This indicates that a first-order lag plus a pure time delay provides an acceptable representation of the rate sensor dynamics for purposes of heading system performance prediction.

3.4.2 Simulated System Responses to a More Realistic Input

In terms of actual application of the system to provide a heading reference in a land vehicle, a step input of rate as used in the prior system simulation studies would not appear to be realistic in that this input corresponds to an infinite rate of change of vehicle direction at the instant of the step initiation. A more realistic angular rate input would be a ramp followed by a constant rate which corresponds to a vehicle directional heading variation given by a parabolic function merging with a ramp function at the

input rate break point as shown in figure 3.8. The duration of the rate input ramp will be a function of the driver reaction characteristics as related to the particular vehicle polar inertia about its turning axis. Additionally, the use of such an input in the system simulation study will facilitate direct comparison between theoretical results and data obtained from the experimental set-up where the system input was generated by switching on the high torque support frame motor driving the high inertia rotary mounted support frame and coupled rate sensor as shown in figure 2.9.

Typical time domain heading responses to a rate input ramp of 100.0 degs./sec.^{2} slope with 0.1 sec. duration and saturated at 10.0 degs./sec. are shown in figures 3.9a to 3.9d, for both optimum and non-optimum values of (K_1) and (K_2). To facilitate direct comparison, system responses for the two different types of input considered (i.e., ideal step and ramp plus saturation rate inputs) with same controller parameter settings are plotted together in figures 3.10a to 3.10d.

The following points regarding the results for differing rate input types are noted below:

— The minimized heading error criterion is valid for

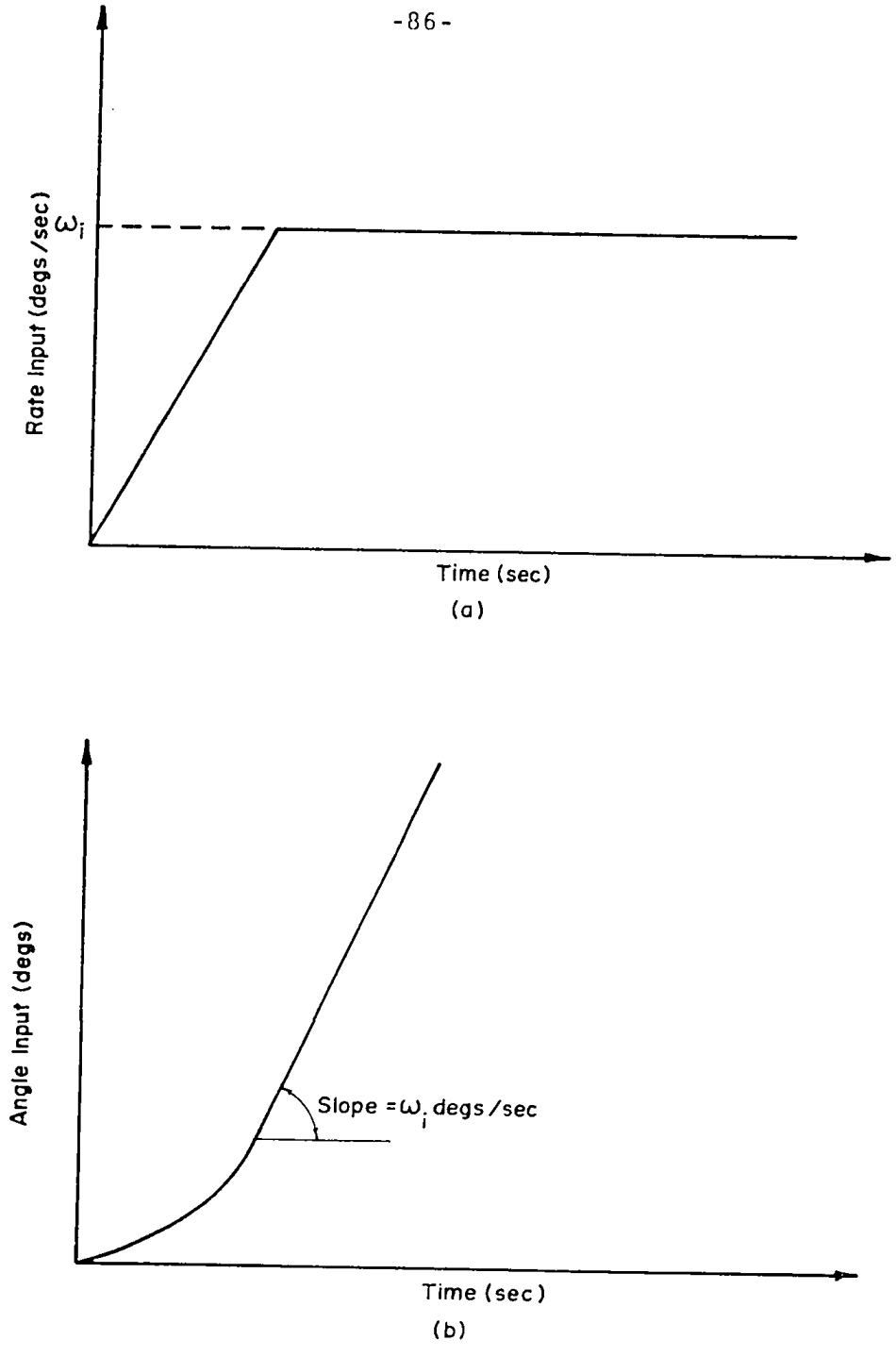

FIGURE 3.8 MORE REALISTIC SYSTEM INPUT

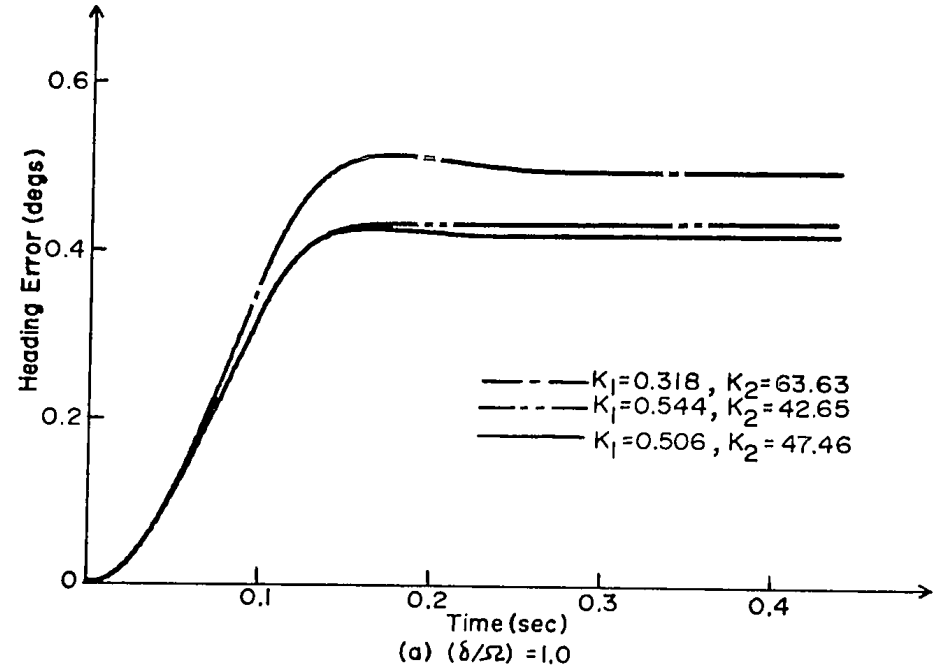

(a) $(\delta/\Omega) = 1.0$

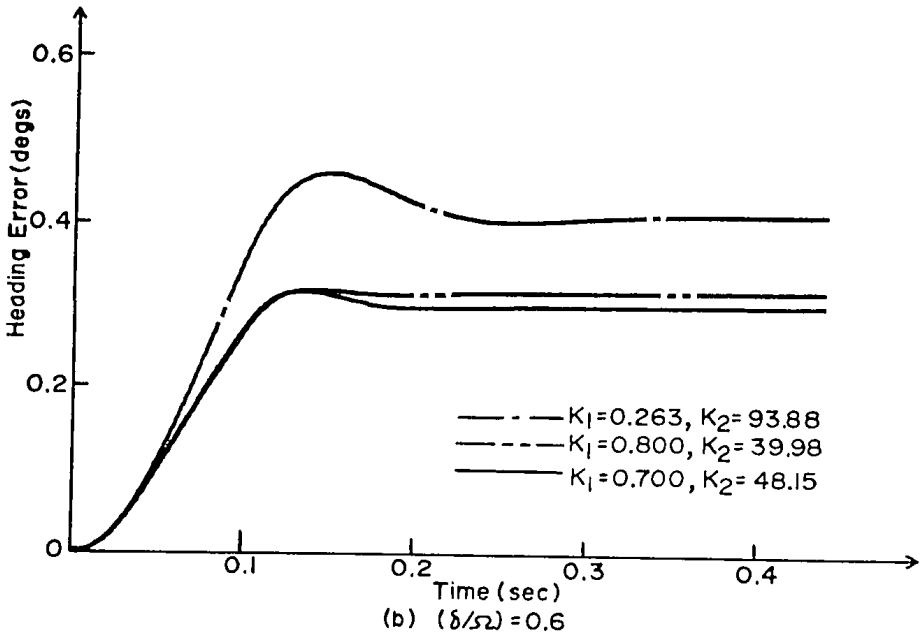

(b) $(\delta/\Omega) = 0.6$

FIGURE 3.9 SYSTEM RESPONSES TO A RAMP + SATURATION RATE INPUT

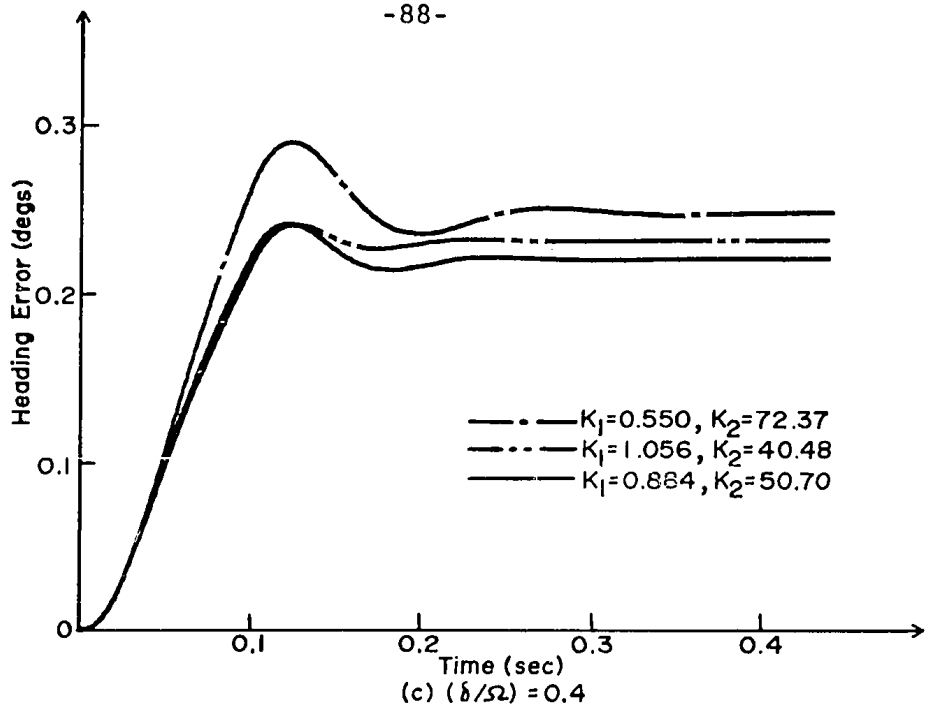

(c) $(\delta/\Omega) = 0.4$

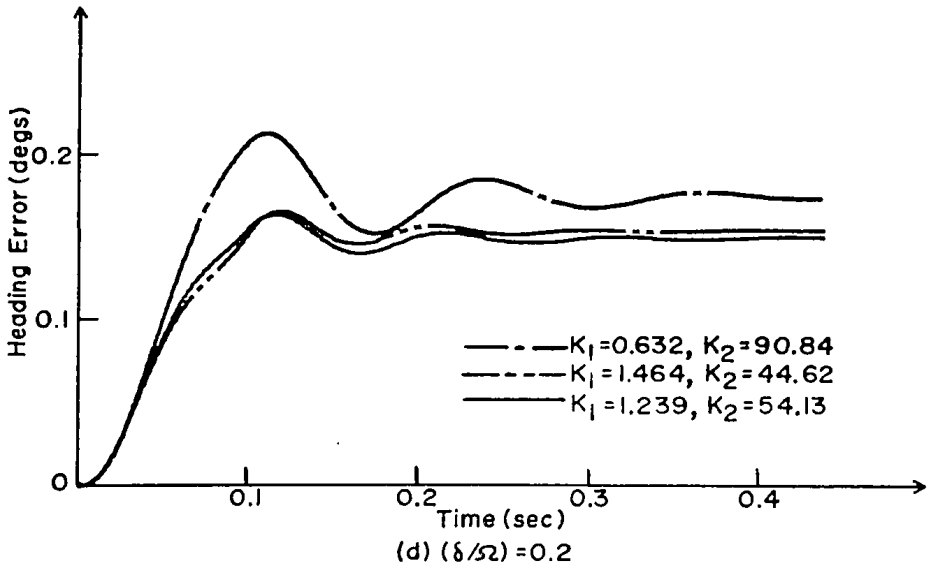

(d) $(\delta/\Omega) = 0.2$

FIGURE 3.9 SYSTEM RESPONSES TO A RAMP + SATURATION RATE INPUT

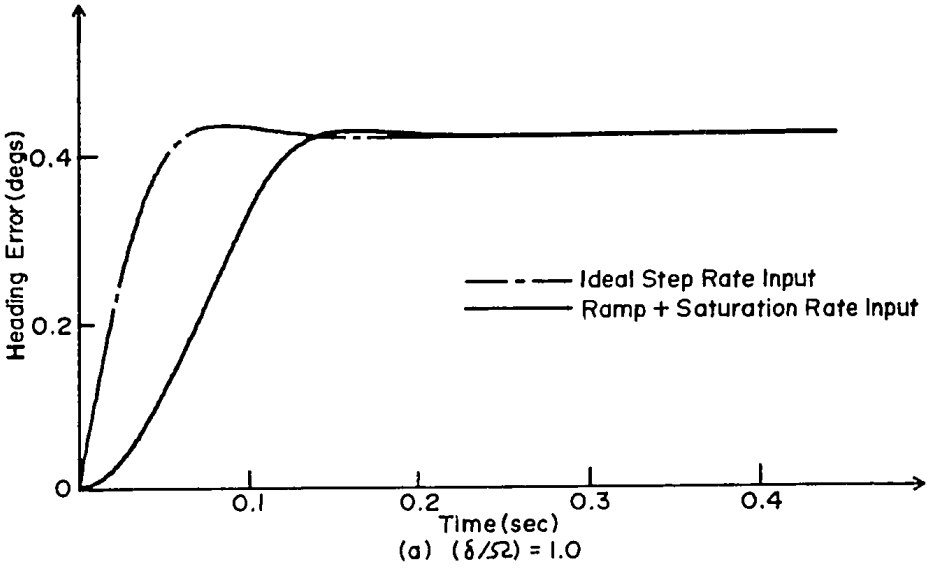

(a) $(\delta/\Omega) = 1.0$

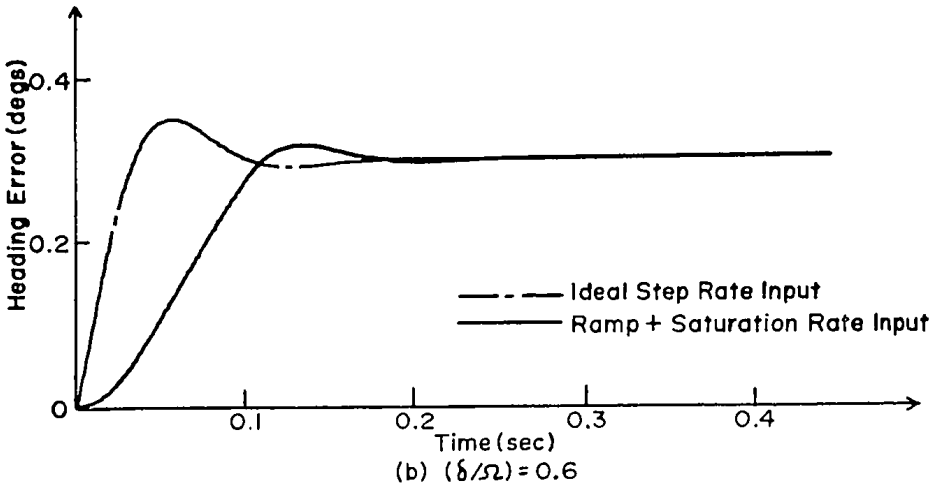

(b) $(\delta/\Omega) = 0.6$

FIGURE 3.10 OPTIMUM SYSTEM RESPONSES TO DIFFERENT RATE INPUTS

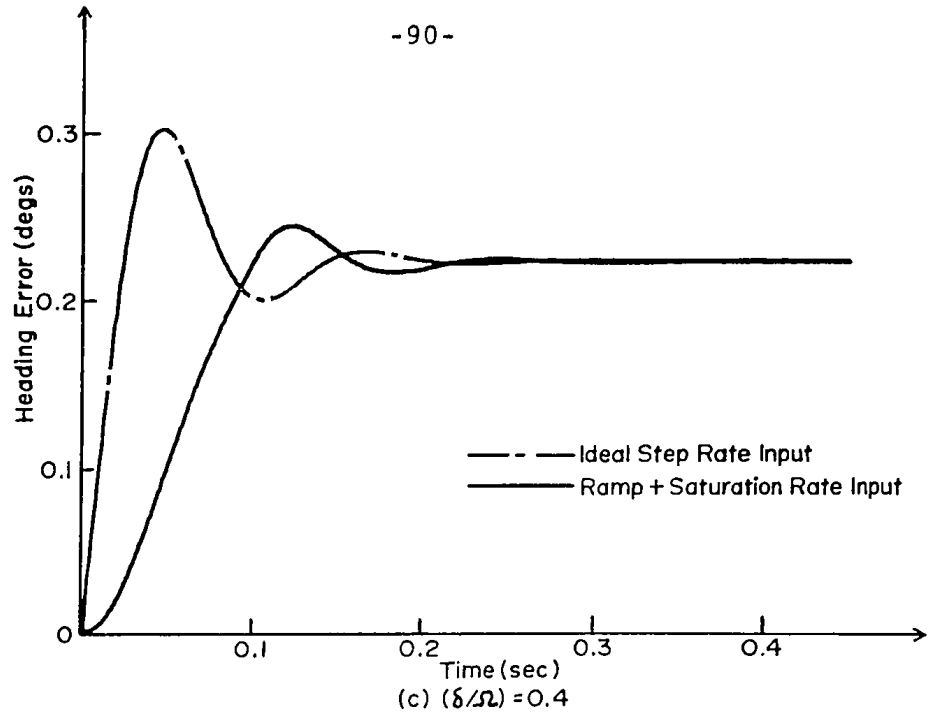

(c) $(\delta/\Omega) = 0.4$

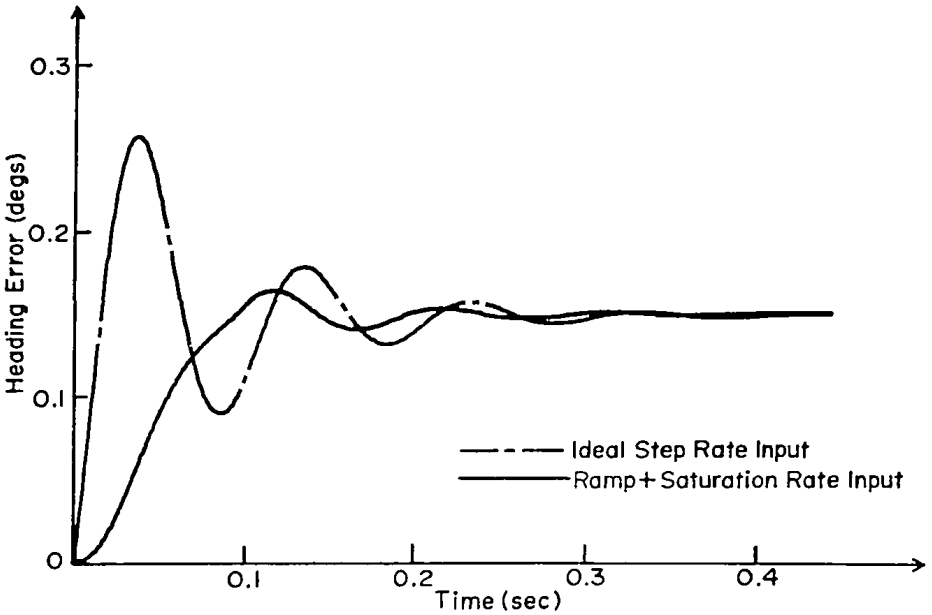

(d) $(\delta/\Omega) = 0.2$

FIGURE 3.10 OPTIMUM SYSTEM RESPONSES TO DIFFERENT RATE INPUTS

both types of rate inputs as expected in that the criterion is based on the minimization of system steady-state heading error.

— The system transient response is slower with a ramp plus saturation rate input which is to be expected due to the initially slower change of rate input as compared with the step rate input.

— It is evident that the system steady-state minimum heading error decreases with decreasing damping ratio (δ/Ω). This ratio, however, is limited by the system transient response overshoot. Since the system transient response is more damped for a ramp plus saturation rate input, a relatively small damping ratio (δ/Ω) is acceptable in practice as a ramp plus saturation rate input is the more accurate representation of real system operation.

3.4.3 Experimental System Performance

Experimental system performance tests were carried out, using the same experimental set-up as described in chapter 2, to verify the optimization criterion theoretically developed. As mentioned before, the experimental system input was provided by a support frame rotation through the application of a voltage step to the motor drive shown in

figure 2.9. It is evident that the system input will attain a constant rate only after a finite transient time resulting from motor drive time constant and associated support frame polar inertia. A typical experimental support frame angular input is shown in figure 3.11a. The support frame angular rotation was detected by the angular potentiometer coupling to the rate sensor with the system feedback loop disconnected. The angular potentiometer output signal was recorded by a memory scope which has been triggered approximately 30 milliseconds before the application of the supply voltage to the support frame motor drive. The accuracy with which the assumed ramp plus saturation rate input (i.e., parabolic plus ramp angle input) used for the simulated system study represents the experimental system input is indicated in figure 3.11b where both inputs are shown superimposed.

Experimental system heading transient response performance for an angular input shown in figure 3.11 with optimum and non-optimum controller parameter settings are shown in figures 3.12a, b to 3.15a, b. Since the rate sensor "output noise amplitude/input rotational rate" ratio decreases with increasing input rotational rate (output noise exhibits only a weak dependency upon rotational rate, reference 45), a rate input of higher magnitude was applied to the system with intention of reducing the rate sensor noise

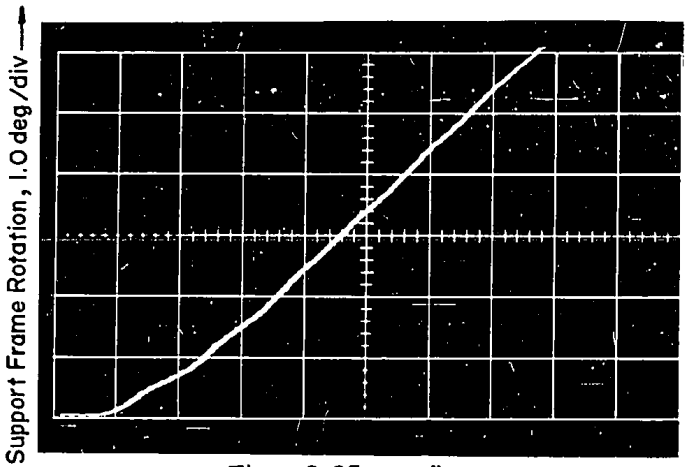

(a) Experimental Input

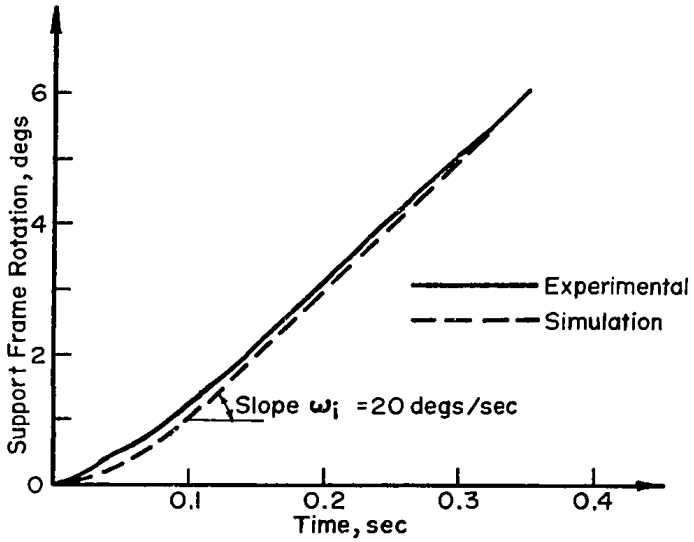

(b) Comparison of Simulated and Experimental Inputs

FIGURE 3.11 SYSTEM ANGULAR INPUT

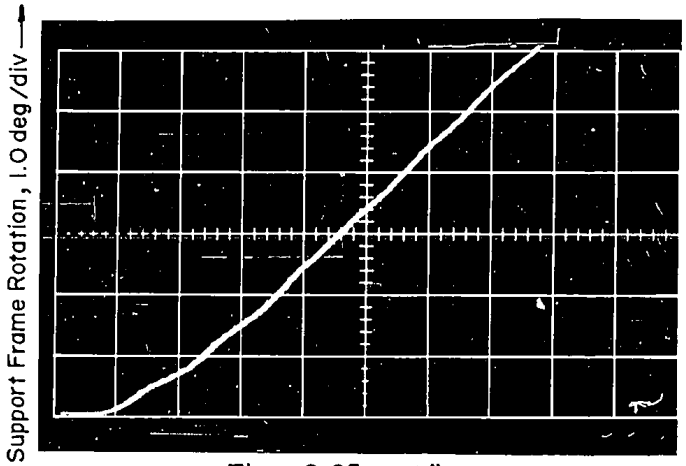

(a) Experimental Input

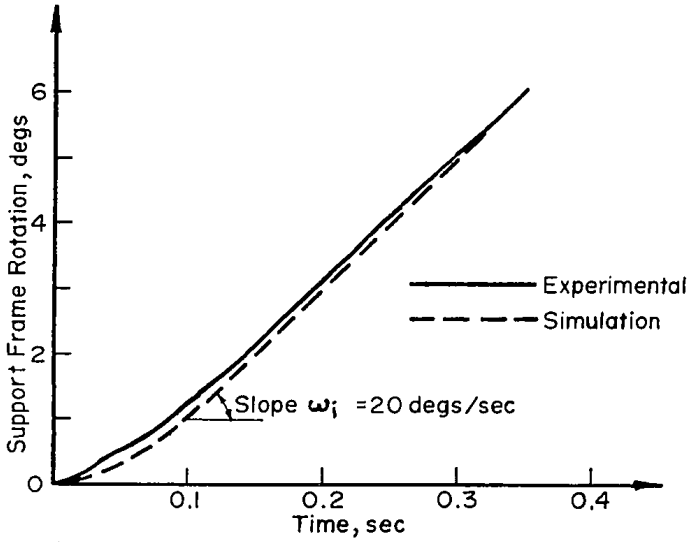

(b) Comparison of Simulated and Experimental Inputs

FIGURE 3.11 SYSTEM ANGULAR INPUT

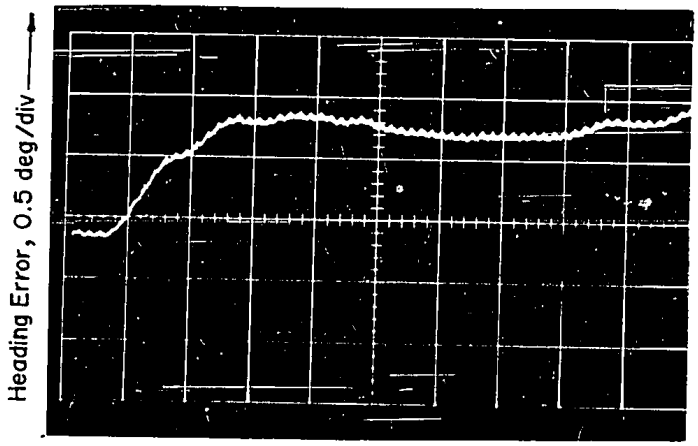

(a) $K_1 = 0.318$, $K_2 = 63.63$

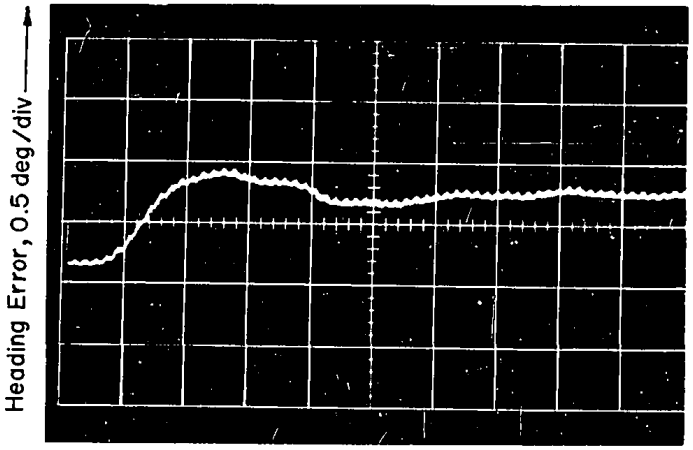

(b) $K_1 = 0.506$, $K_2 = 47.46$ (Optimum Setting)

FIGURE 3.12 EXPERIMENTAL HEADING RESPONSES TO A STEP RATE INPUT OF 20 degs/sec , $(\delta/\Omega) = 1.0$

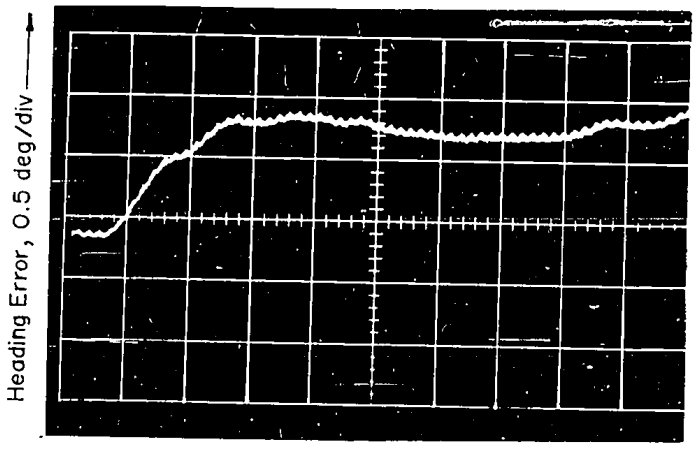

(a) $K_1 = 0.318$, $K_2 = 63.63$

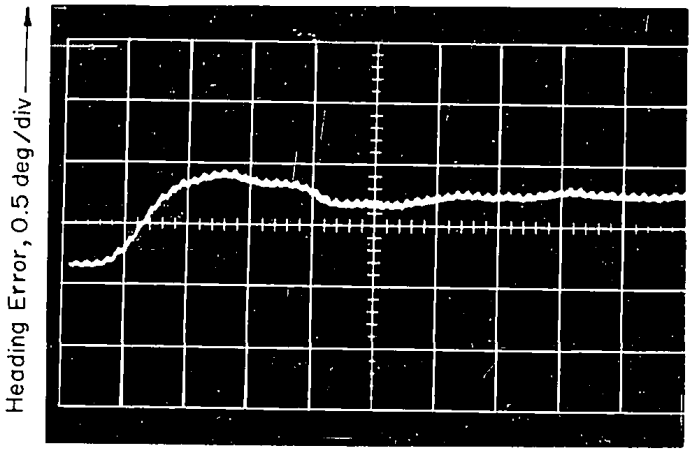

(b) $K_1 = 0.506$, $K_2 = 47.46$ (Optimum Setting)

FIGURE 3.12 EXPERIMENTAL HEADING RESPONSES TO A STEP RATE INPUT OF 20 degs/sec, $(\delta/\Omega) = 1.0$

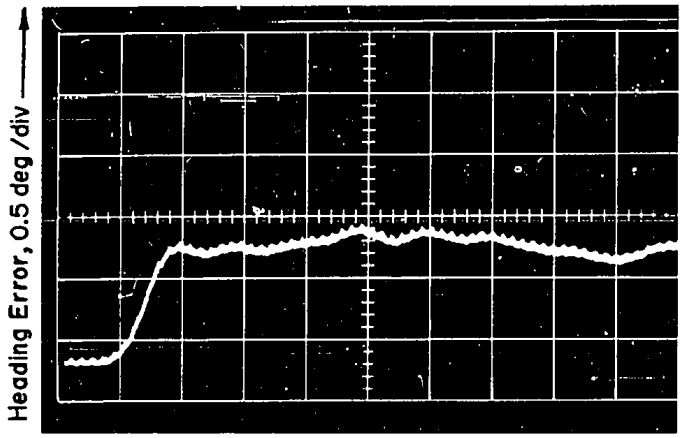

(a) $K_1 = 0.263$, $K_2 = 93.88$

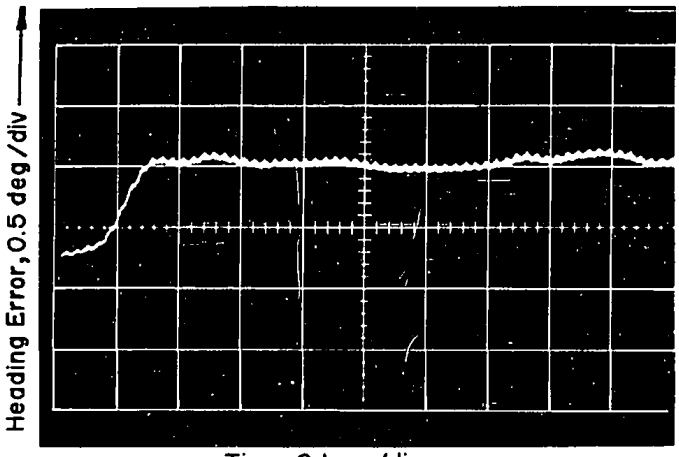

(b) $K_1 = 0.700$, $K_2 = 48.15$ (Optimum Setting)

FIGURE 3.13 EXPERIMENTAL HEADING RESPONSES TO A STEP RATE INPUT OF 20 degs/sec , (δ / Ω) = 0.6

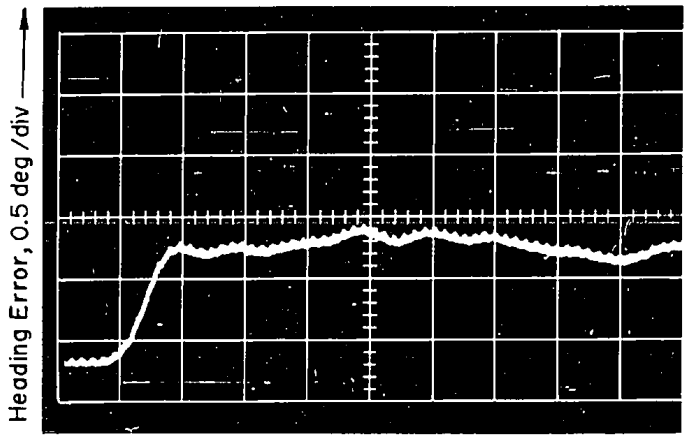

(a) $K_1 = 0.263$, $K_2 = 93.88$

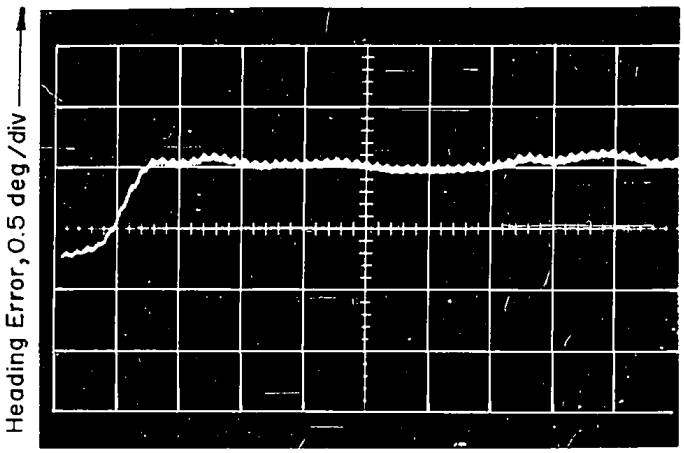

(b) $K_1 = 0.700$, $K_2 = 48.15$ (Optimum Setting)

FIGURE 3.13 EXPERIMENTAL HEADING RESPONSES TO A STEP RATE INPUT OF 20 degs/sec , $(\delta/\Omega) = 0$ S

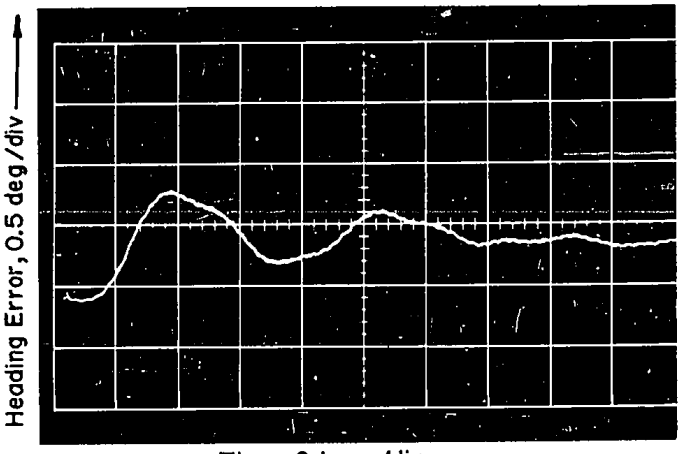

(a) $K_1 = 0.550, K_2 = 72.37$

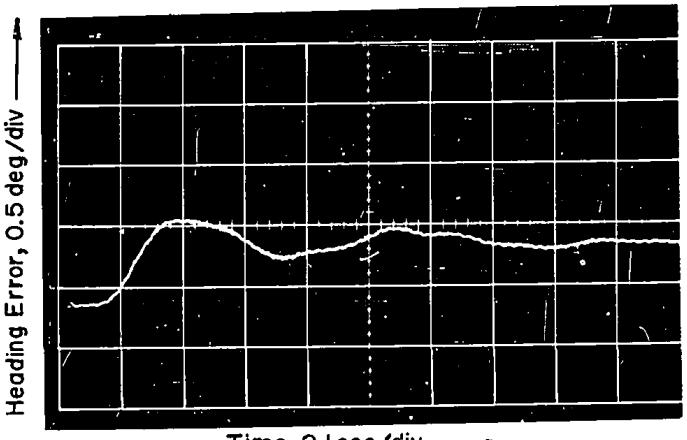

(b) $K_1 = 0.884, K_2 = 50.70$ (Optimum Setting)

FIGURE 3.14 EXPERIMENTAL HEADING RESPONSES TO A STEP RATE INPUT OF 20 degs/sec , $(\delta/\Omega) = 0.4$

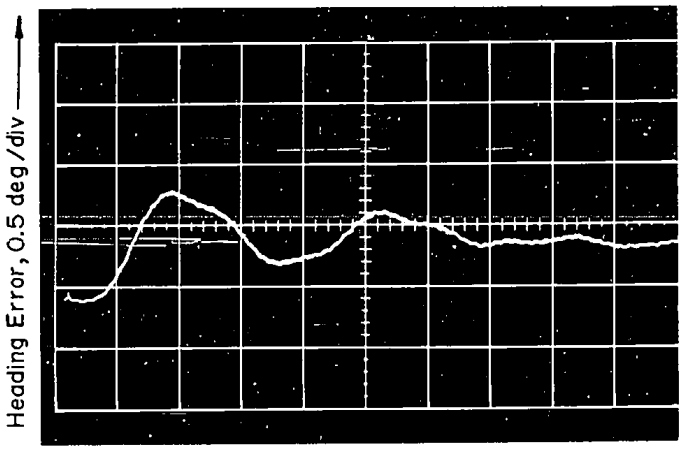

(a) $K_1 = 0.550, K_2 = 72.37$

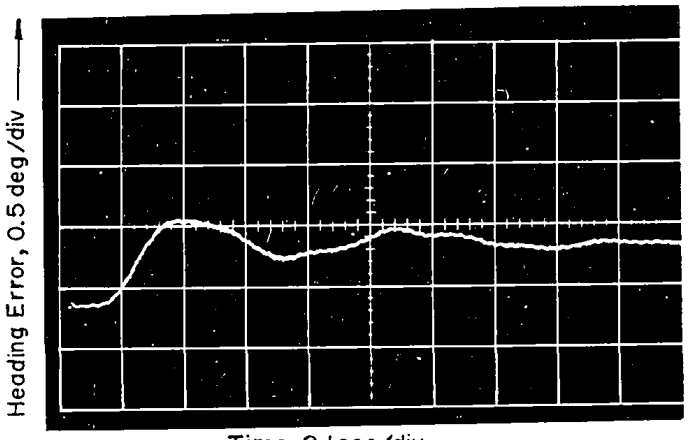

(b) $K_1 = 0.884, K_2 = 50.70$ (Optimum Setting)

FIGURE 3.14 EXPERIMENTAL HEADING RESPONSES TO A STEP RATE INPUT OF 20 degs/sec , $(\delta/\Omega) = 0.4$

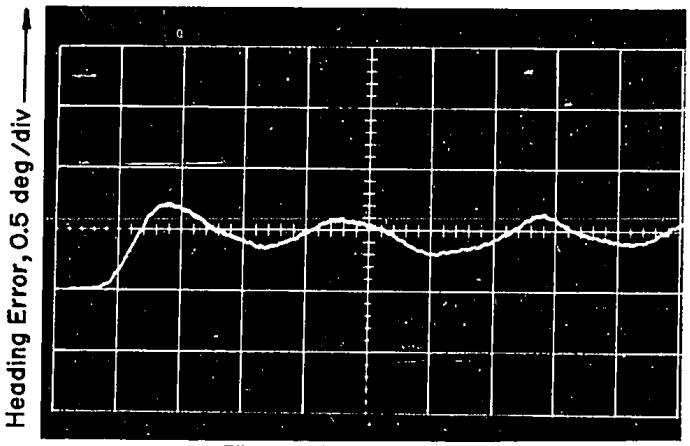

(a) $K_1 = 0.632$, $K_2 = 90.84$

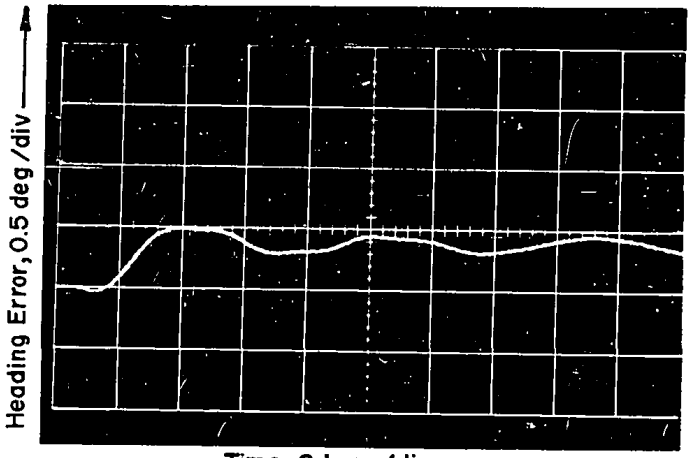

(b) $K_1 = 1.239$, $K_2 = 54.13$ (Optimum Setting)

FIGURE 3.15 EXPERIMENTAL HEADING RESPONSES TO A STEP RATE INPUT OF 20 degs/sec, $(\delta/\Omega) = 0.2$

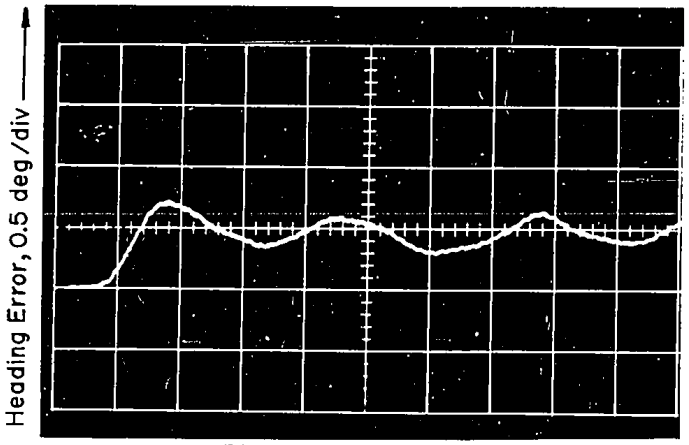

(a) $K_1 = 0.632, K_2 = 90.84$

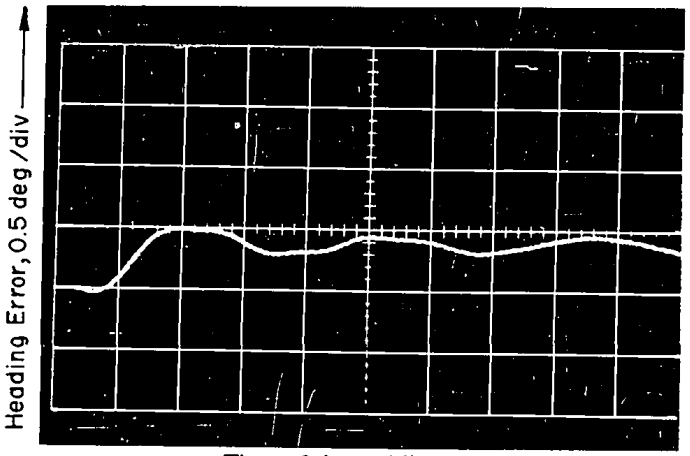

(b) $K_1 = 1.239, K_2 = 54.13$ (Optimum Setting)

FIGURE 3.15 EXPERIMENTAL HEADING RESPONSES TO A STEP RATE INPUT OF 20 degs/sec, $(\delta/\Omega) = 0.2$

induced heading random deviations observed in the 10.0 degs./sec. rate input results shown in figures 2.18 to 2.20. Figures 3.16a, b to 3.19a, b show the experimental responses together with corresponding theoretical responses to ideal step and ramp plus saturation rate input. It is seen that the experimental steady-state responses correlate reasonably with the theoretical predictions, while the experimental transients are somewhat more oscillatory. This may be attributed to the higher order dynamic behavior of the rate sensor as suggested by the results of figure 3.7. The optimization criterion is also verified by the experimental results, although the difference between optimum and non-optimum responses is less pronounced than the theoretical prediction shown in figures 3.6 and 3.9. This difference is attributed to experimental measurement instrumentation accuracy. Additionally, it is noted that the experimentally observed random deviations in heading responses with optimized controller parameter settings are reduced as compared with those obtained with Ziegler-Nichols optimum settings. This reduction results from the derived optimization criterion requiring a smaller proportional loop gain (K_1) and a greater controller integration gain (K_2) than the equivalent optimized gains estimated by the Ziegler-Nichols rules.

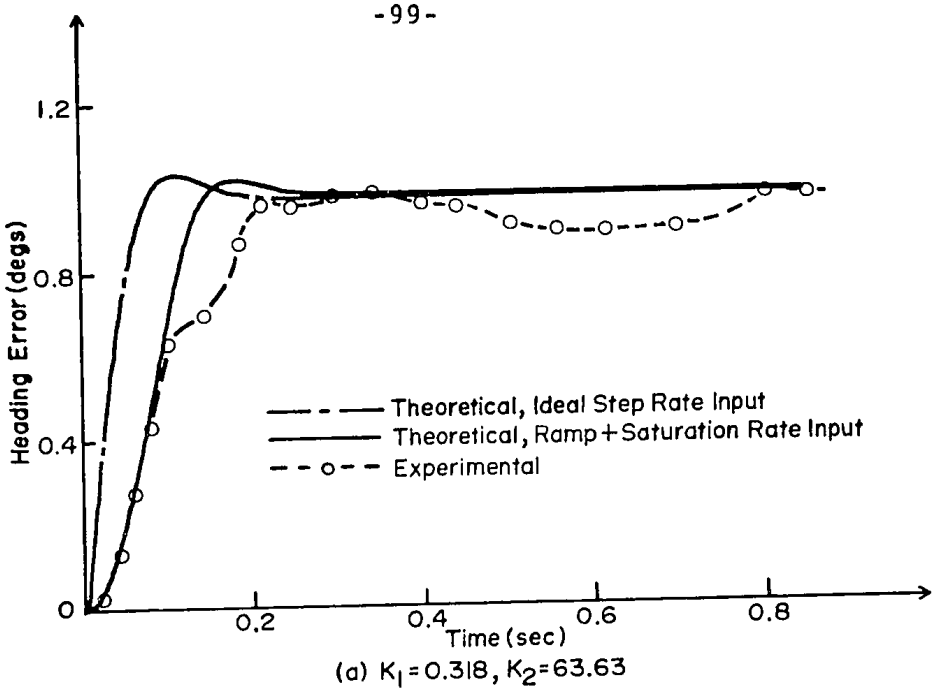

(a) $K_1 = 0.318$, $K_2 = 63.63$

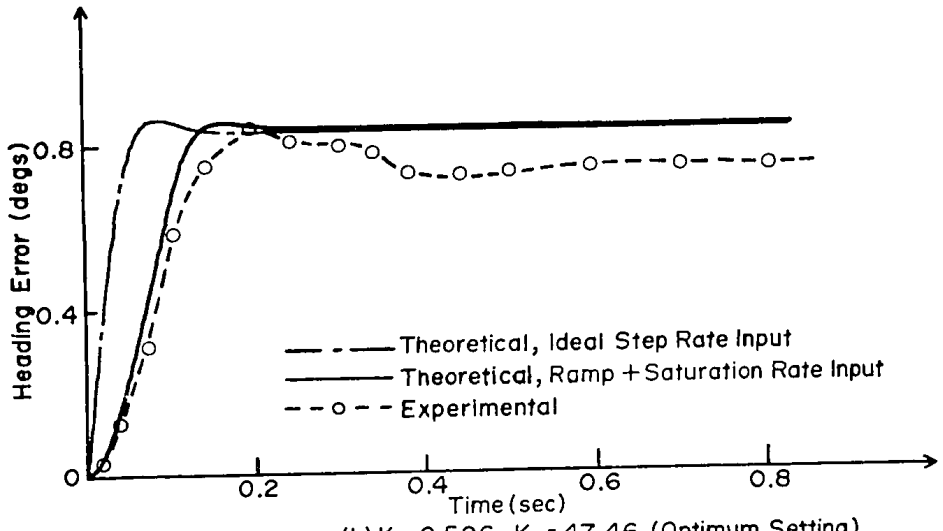

(b) $K_1 = 0.506$, $K_2 = 47.46$ (Optimum Setting)

FIGURE 3.16 COMPARISON OF THEORETICAL AND EXPERIMENTAL SYSTEM RESPONSES, $(\delta/\Omega) = 1.0$

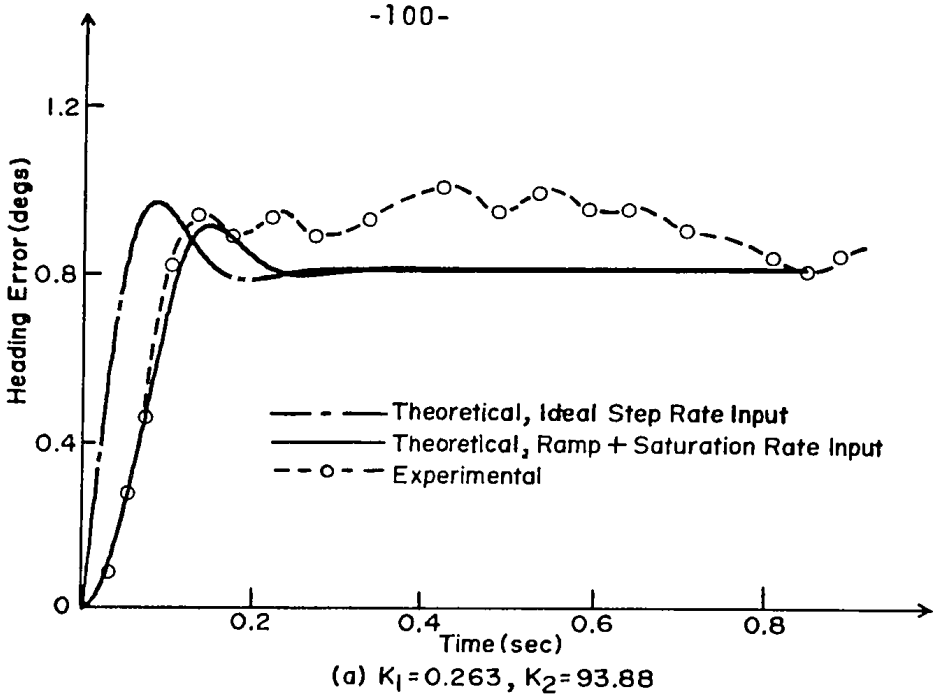

(a) $K_1 = 0.263$, $K_2 = 93.88$

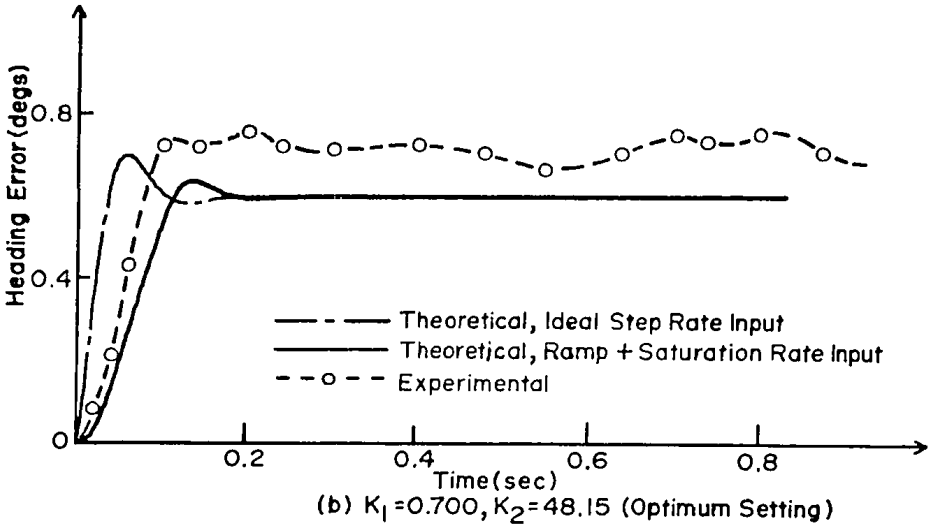

(b) $K_1 = 0.700$, $K_2 = 48.15$ (Optimum Setting)

FIGURE 3.17 COMPARISON OF THEORETICAL AND EXPERIMENTAL SYSTEM RESPONSES, $(\delta/\Omega) = 0.6$

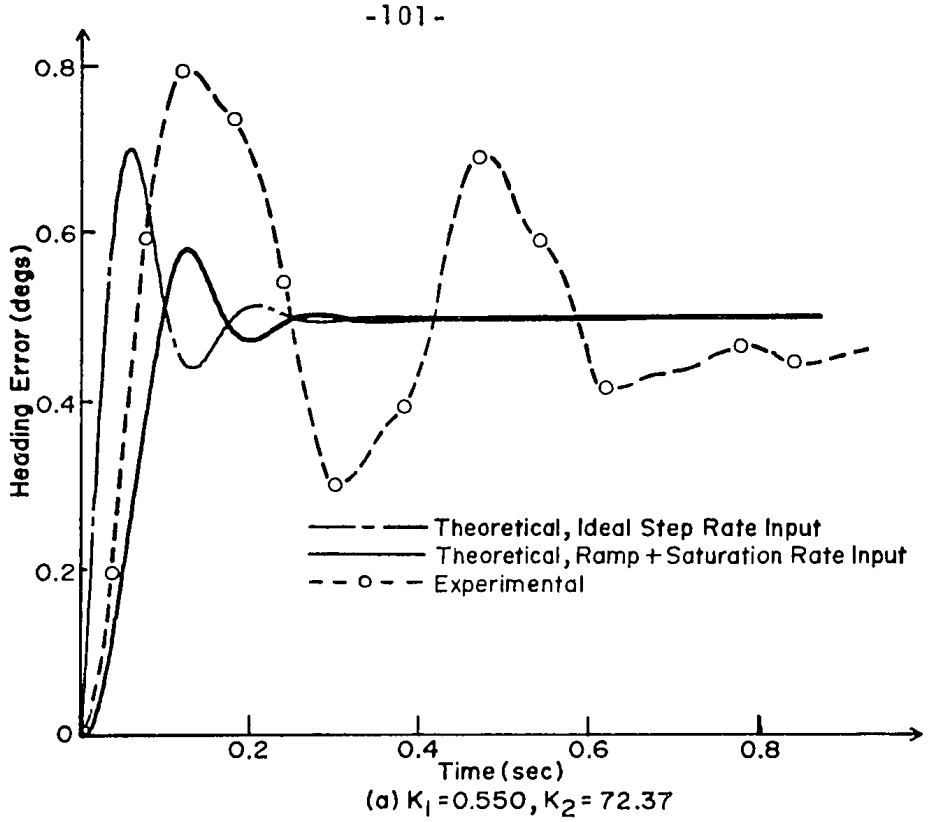

(a) $K_1 = 0.550$, $K_2 = 72.37$

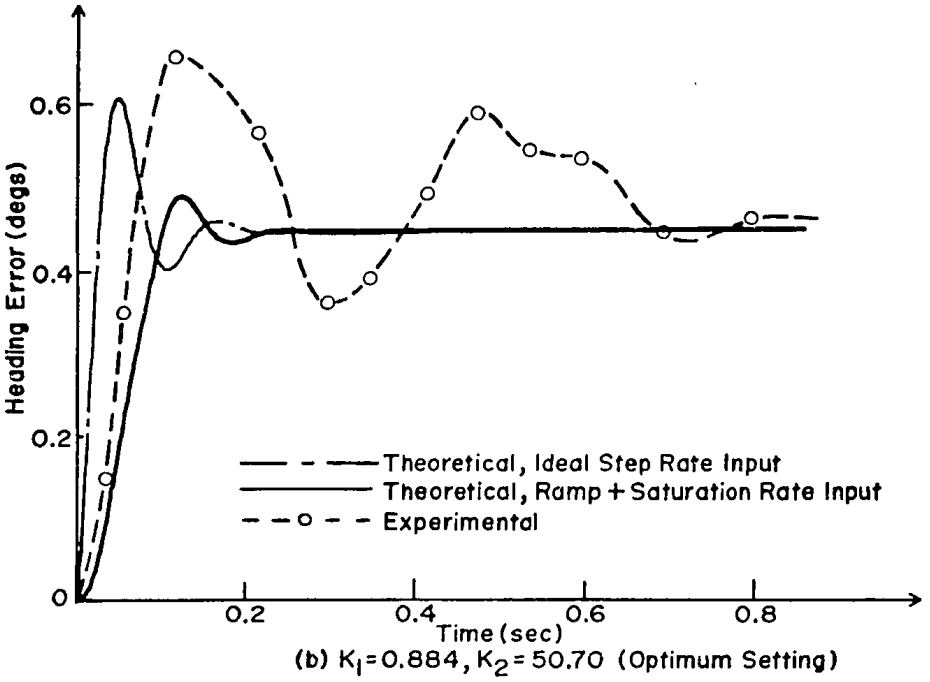

(b) $K_1 = 0.884$, $K_2 = 50.70$ (Optimum Setting)

FIGURE 3.18 COMPARISON OF THEORETICAL AND EXPERIMENTAL SYSTEM RESPONSES, $(\delta/\Omega) = 0.4$

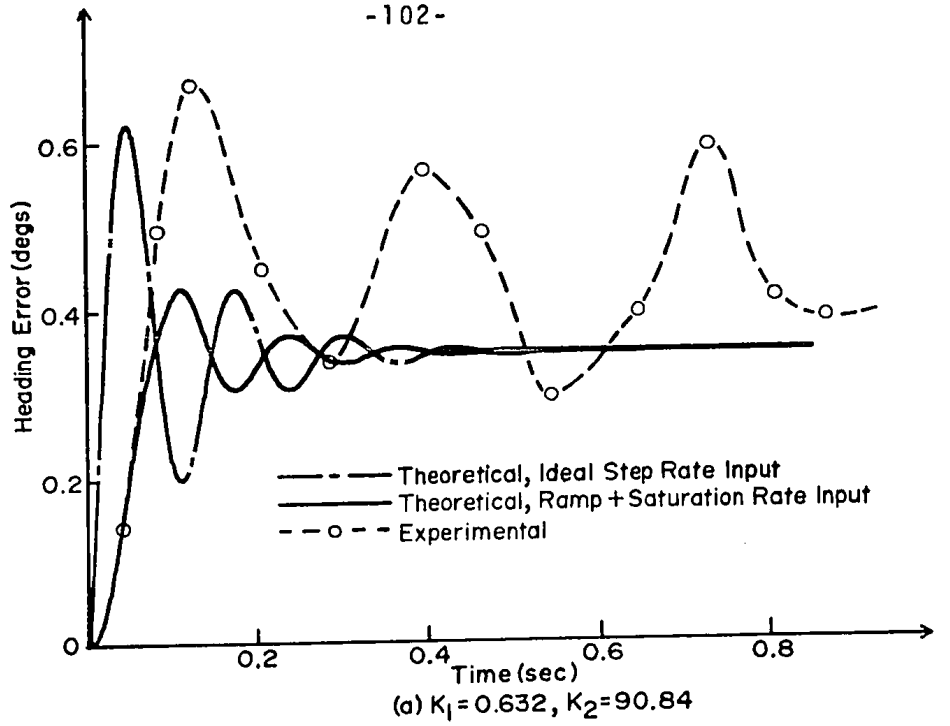

(a) $K_1 = 0.632$, $K_2 = 90.84$

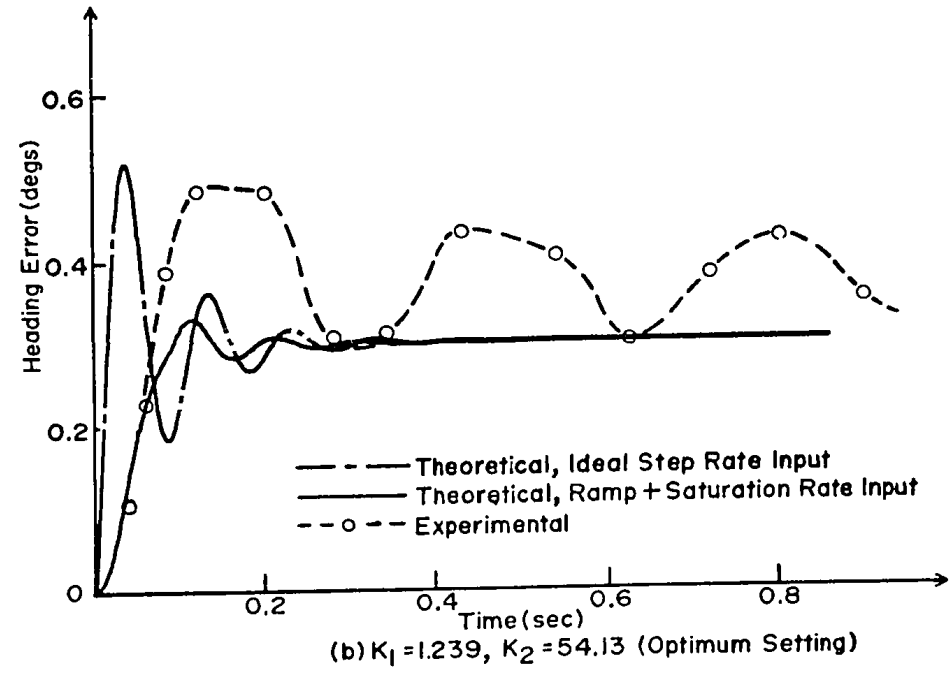

(b) $K_1 = 1.239$, $K_2 = 54.13$ (Optimum Setting)

FIGURE 3.19 COMPARISON OF THEORETICAL AND EXPERIMENTAL SYSTEM RESPONSES, $(\delta/\Omega) = 0.2$

3.5 System Frequency Responses

The system closed loop frequency response was theoretically determined using a digital computer with a complex variable arithmetic operations subroutine. This program generates the angular frequency within a specified range and calculates the magnitude and phase angle of the system from the appropriate closed loop transfer function representation. The frequency response of the system with the simplified rate sensor transfer function (equation 2.5) and with the more accurate rate sensor transfer function (equation 3.26) is shown in figures 3.20a, b for different step input optimized controller parameter values (K_1, K_2). The corresponding system closed loop transfer functions are given by equations (A.3) and (A.35).

The system frequency response, although of academic interest, will have limited practical significance in an actual vehicle heading reference system where an input heading signal frequency limit will exist representing the maximum rate of reversal of heading direction obtainable within vehicle manoeuvering safety limits. This frequency limit will be a function of the vehicle polar inertia about its turning axis coupled with the driver reaction characteristics. This input frequency would be anticipated to be relatively low (a maximum in the order of 1.0 rad./sec.)

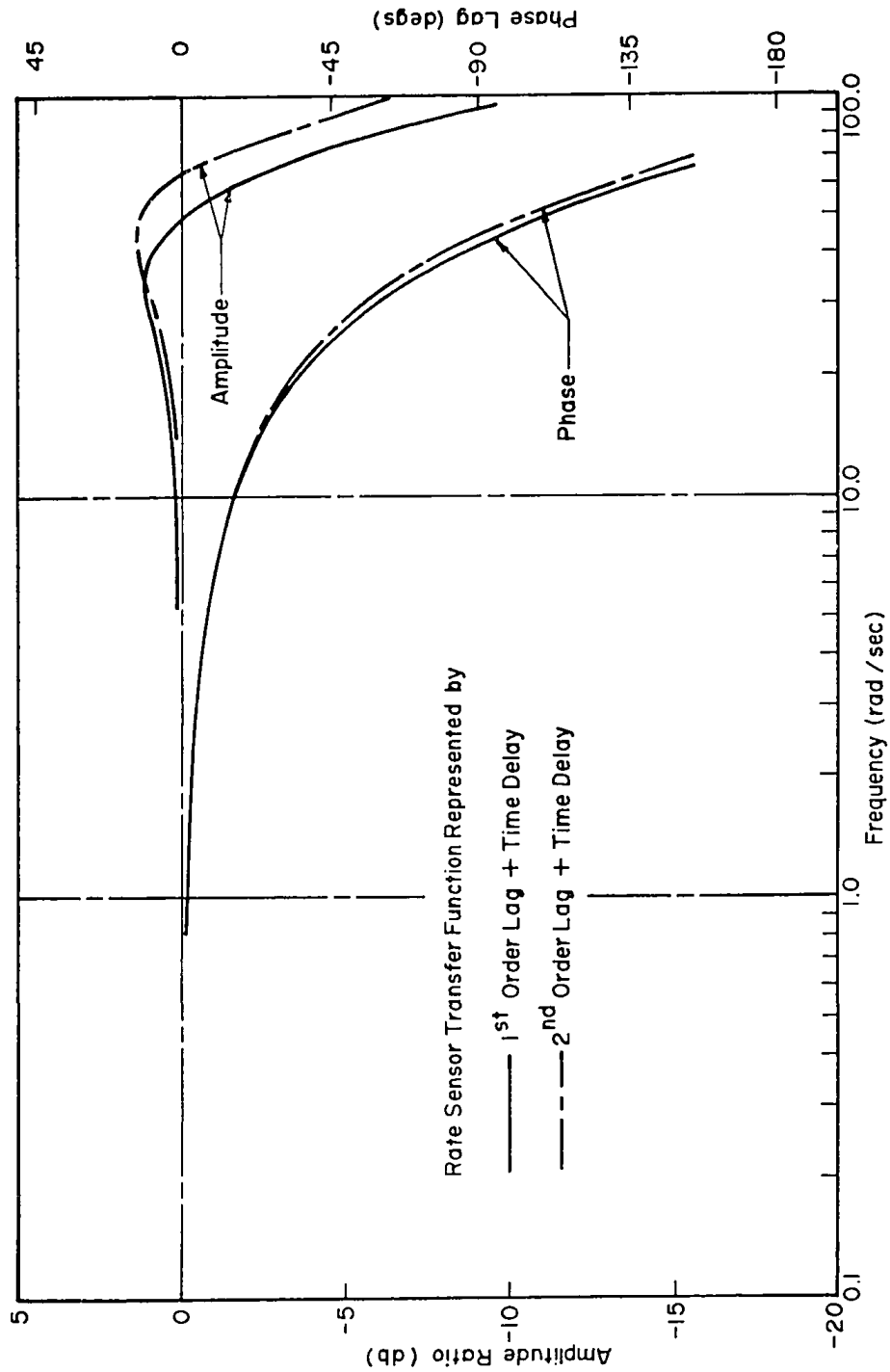

FIGURE 3.20a CLOSED LOOP SYSTEM FREQUENCY RESPONSE
($K_1 = 0.700$, $K_2 = 48.15$)

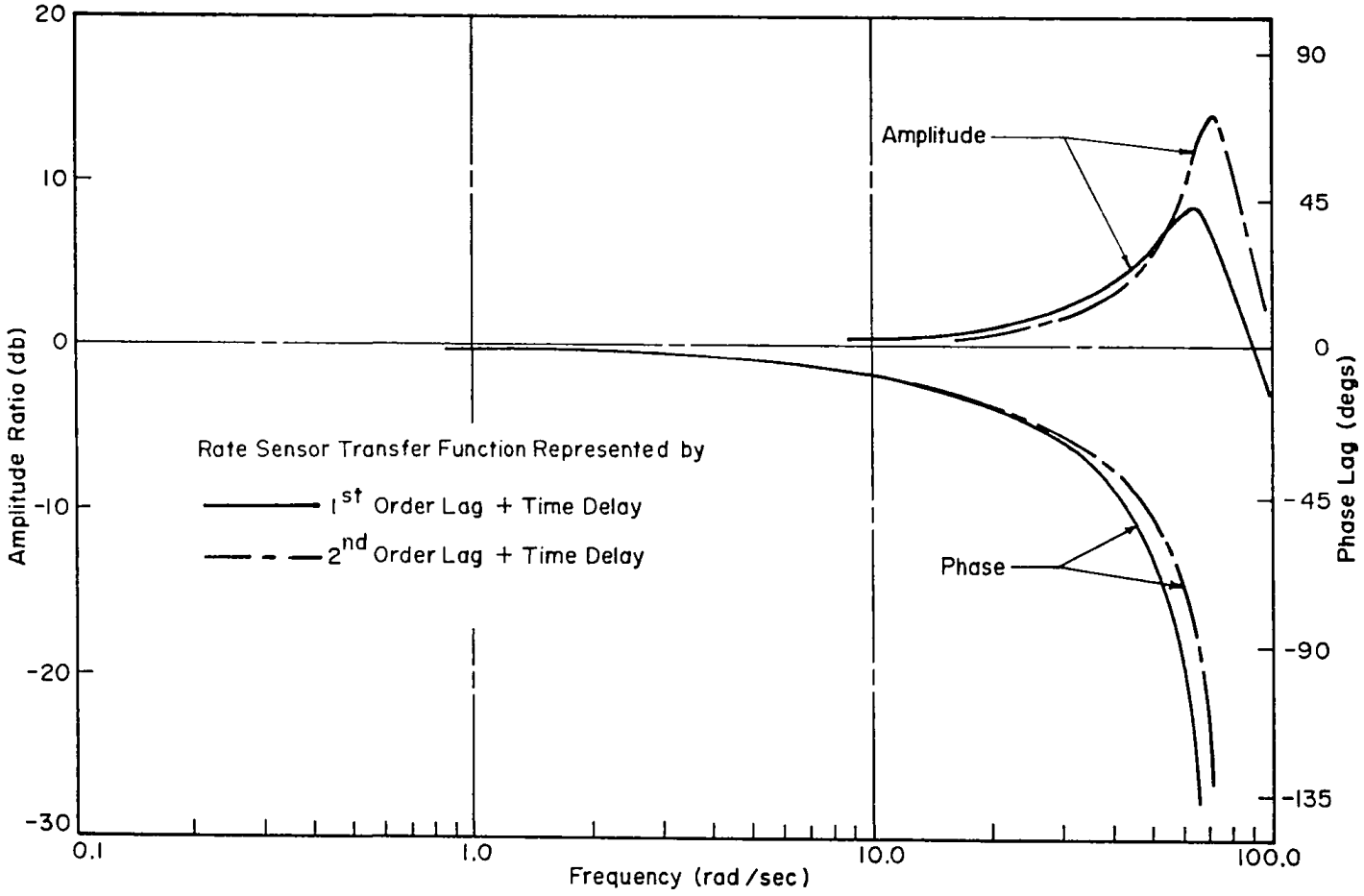

FIGURE 3.20b CLOSED LOOP SYSTEM FREQUENCY RESPONSE
($K_1 = 1.239$, $K_2 = 54.13$)

and the performance of the heading reference system could be predicted by approximating such a low frequency input by a series of ramp angular inputs such as previously investigated.

CHAPTER 4

SYSTEM PARAMETER ANALYSIS AND SIMPLIFIED CONTROLLER OPTIMUM SETTING EQUATIONS

4.1 General

The availability of system rate sensor, servomotor and coupling gear train hardware components has limited the system performance improvement to the adjustment of the feedback controller parameters. However, the apparent dependency of the optimum controller adjustment upon the system hardware transfer function parameters as shown by equations (3.23), (3.24) and (3.25) suggests that the system performance optimization dependency upon each of the hardware dependent parameters should be considered in order to obtain further system improvement.

The optimization procedure developed in the previous chapter for the heading reference system was general, and therefore could be applied to any control system with the same general type of transfer function representation. However, the determination of the optimum controller parameter setting for any given set of system hardware parameters by obtaining a numerical solution of the derived system optimization equations (3.22), (3.23) and (3.24) is

time consumming. The reduction of these equations to some simplified form acceptable for direct practical design purposesis considered in the subsequent analysis.

4.2 System Parameter Analysis

The system steady-state heading error previously derived is given by:

$$\Theta_e = \frac{\omega_i T_L^3}{T_1 T_2} \frac{1}{AB} \tag{3.17}$$

Since (AB) is a weak function of the system parameters as shown by equation (3.23), a mathematical approach to establish an explicit analytical dependency of the system heading error (θ_e) upon individual system parameter T_1, T_2 and T_L would be extremely difficult, if not unfeasible. An alternate numerical approach was undertaken by which any two of the three system parameters (T_1, T_2 and T_L) were kept constant and the heading error was numerically evaluated as a function of the third parameter. Since the heading error exhibits the same dependency upon T_1 and T_2, it is sufficient to analyze the effect of only one of the lag time constants on the system performance.

4.2.1 Dependency of the Minimum Heading Error upon T_L

The variation of the system minimum heading error ($\theta_e$min.) with respect to the pure time delay (T_L) was obtained by assigning a realistic range of values to T_1 and T_2 and subsequently solving successively the system optimum condition equations (3.22), (3.23), (3.24) and (3.25) for different values of T_L. The results are shown graphically in figure 4.1 for two selected system response damping ratios of (δ/Ω) = 0.6 and 0.2.

It is evident from these results that the minimum heading error ($\theta_e$min.) is directly proportional to the pure time delay (T_L) over the selected range. Therefore, any reduction of the time delay magnitude in the system would be expected to proportionally reduce the system steady-state minimum heading error.

4.2.2. Dependency of the Minimum Heading Error upon T_1 and T_2

The variation of the system minimum heading error ($\theta_e$min.) with respect to the time constant T_1 (or T_2) was obtained using the same technique as previously, but with T_L and T_2 (or T_1) kept constant and T_1 (or T_2) varied. The results are shown graphically in figure 4.2 for two

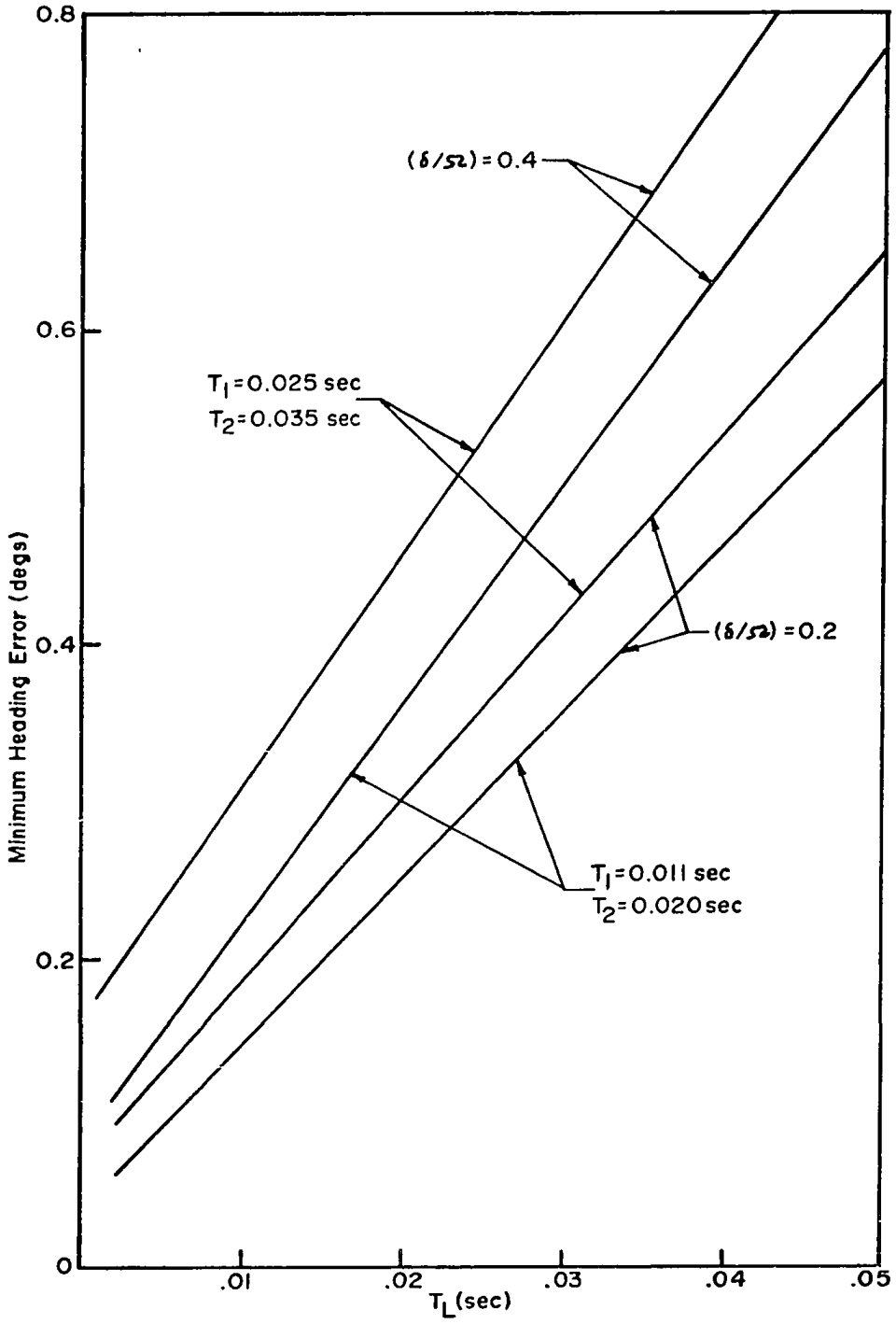

FIGURE 4.1 DEPENDENCY OF SYSTEM MINIMUM HEADING ERROR UPON TIME DELAY

selected system response damping ratios of (δ/Ω) = 0.2 and 0.4.

The minimum heading error exhibits a relatively weak dependency upon either of the system time constants T_1 or T_2. After a specific maximum value, the error decreases with increasing time constant magnitude. This signifies that a relatively larger time constant would result in a smaller steady-state minimum heading error, but obviously at the expense of system transient response time. Accordingly,the selection of the system time constants depends upon a compromise between the system transient and steady-state performance requirements.

Direct application of the above analysis to improve the heading reference system performance was not considered to be practically feasible, since:

i) With the available experimental rate sensor configuration, a significant reduction of the pure time delay (T_L) could be attained only by a substantial reduction of the supply pressure (Reference 44), but at the expense of significantly increased sensor time constant (T_1). Therefore, any improvement of the heading system performance obtaining by decreasing the pure time delay would be largely compensated by the effect of increasing sensor time constant.

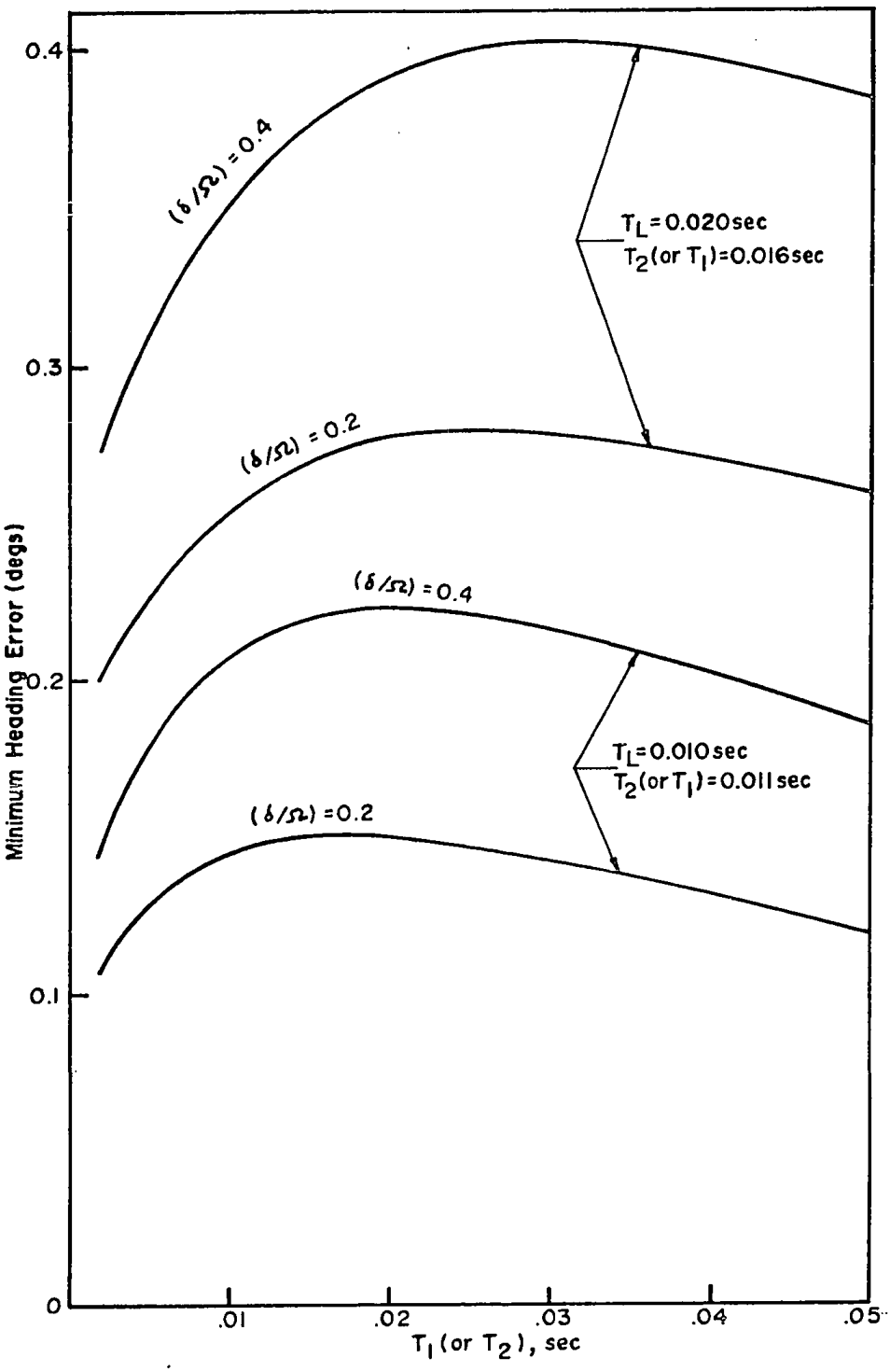

FIGURE 4.2 DEPENDENCY OF SYSTEM MINIMUM HEADING ERROR UPON SYSTEM TIME CONSTANTS

ii) An improvement of the system minimum heading error by decreasing the system time constants T_1 and T_2 (i.e., toward the left side of the maxima of the curves shown in figure 4.2) is not practically feasible, since the effective T_1 is largely compensated by the interdependent T_L for a given sensor configuration as per i) above and T_2 is limited by the drive motor characteristics and the associated coupled inertia load. The system steady-state minimum heading error could, however, be improved by increasing the feedback drive motor time constant T_2 (i.e., toward the right side of the maxima of the curves shown in figure 4.2) through the addition of suitable mass inertia on the rate sensor. But, as mentioned before, this heading error improvement would be obtainable at the expense of slower transient response. The validity of increasing T_2 would depend on the eventual application of the heading system.

However, this analysis provides a means by which one could estimate certain appropriate value ranges for the inherent parameters of a general control system represented by two first-order lags and a pure time delay, particularly when the system parameters could be independently adjusted and the system transient and steady-state performance requirements are specified.

4.3 Simplification of the System Optimum Condition Equations

As described in the preceding chapter, the optimum controller parameter setting is obtained by solving respectively equations (3.22), (3.23), (3.24) and (3.25). For convenience, these equations are rewritten below:

$$\tan\Omega = -\frac{\Omega^3\left(3\frac{\delta^2}{\Omega^2}-1\right)-2\Omega^2(C+3)\left(\frac{\delta}{\Omega}\right)+\Omega(2C+D)}{\Omega^3\left(\frac{\delta}{\Omega}\right)\left(3-\frac{\delta^2}{\Omega^2}\right)+\Omega^2(C+3)\left(\frac{\delta^2}{\Omega^2}-1\right)-\Omega\left(\frac{\delta}{\Omega}\right)(2C+D)+D} \qquad (3.22)$$

$$AB = \left[\begin{array}{l}\left(\frac{\delta^2}{\Omega^2}+1\right)\left[\Omega^3\left(\frac{\delta^2}{\Omega^2}-1\right)-\Omega^2C\left(\frac{\delta}{\Omega}\right)+\Omega D\right]\sin\Omega \\ \quad+\left(\frac{\delta^2}{\Omega^2}+1\right)\left[-2\Omega^3\left(\frac{\delta}{\Omega}\right)+\Omega^2C\right]\cos\Omega\end{array}\right] e^{-\left(\frac{\delta}{\Omega}\right)\Omega} \qquad (3.23)$$

$$A = -\left[\begin{array}{l}\left[\Omega^2\left(3\frac{\delta^2}{\Omega^2}-1\right)-2\Omega C\left(\frac{\delta}{\Omega}\right)+D\right]\cos\Omega \\ \quad+\left[\Omega^2\left(\frac{\delta}{\Omega}\right)\left(3-\frac{\delta^2}{\Omega^2}\right)+\Omega C\left(\frac{\delta^2}{\Omega^2}-1\right)-D\left(\frac{\delta}{\Omega}\right)\right]\sin\Omega\end{array}\right] e^{-\left(\frac{\delta}{\Omega}\right)\Omega} \qquad (3.24)$$

$$K_1 = \frac{T_1T_2}{T_L^2}A \qquad \text{and} \qquad K_2 = \frac{B}{T_L} \qquad (3.25)$$

It is evident that the computational difficulty consists principally in the solution of equation (3.22) for a root (Ω), a procedure which is time consumming for either graphical or numerical methods. Others quantities (i.e., AB, A, K_1 and K_2) are obtained through equations (3.23), (3.24) and (3.25) by direct algebraic calculations. Therefore, the computations involved in the optimization procedure would be largely simplified if the solution of equation (3.22) were no longer required.

Following this approach, the optimum equations were mathematically manipulated in an attempt to delete the 'Ω' terms in equations (3.23) and (3.24) by inserting appropriate terms into the equations and eliminating those terms which satisfied equation (3.22). Unfortunatly, the 'Ω' terms were not cancelled out in the resulting equations and accordingly the solution of equation (3.22) is still required to obtain the optimum controller parameter setting. A more elaborate analysis to mathematically simplify the optimum equations appears to be extremely difficult.

An alternate approach is to derive a new set of controller optimum setting equations which would closely approximate the previously derived exact optimum equations over a selected practical range of system parameter values while reducing computation complexity. Such an approach,

which generally requires numerical trial-and-error procedures, has been frequently exploited in the literature.

As indicated by equations (3.22), (3.23) and (3.24) the controller optimum setting is related to the three characteristic parameters of the system by two dimensionless quantities C and D which were defined as:

$$C = \frac{T_1+T_2}{T_1T_2} T_L \quad \text{and} \quad D = \frac{T_L^2}{T_1T_2} \tag{3.6}$$

But C can be expressed in term of D as:

$$C = \frac{T_1+T_2}{\sqrt{T_1T_2}} \sqrt{D} \tag{4.1}$$

This suggests that $(T_1+T_2)/\sqrt{T_1T_2}$ and D be considered as explicit parameters in the development of the new set of equations, rather than T_1, T_2 and T_L individually. For convenience, let

$$E = \frac{T_1+T_2}{\sqrt{T_1T_2}}$$

The following numerical procedure was carried out to investigate, on a quantitative basis, the effects

of E and D on the controller optimum setting through the dimensionless quantities AB and A:

— Select an appropriate system response damping ratio (δ/Ω).

— Assume a constant value for E

— Numerically solve equation (3.22) for a root Ω and compute AB and A from equations (3.23) and (3.24) with different values of D.

— Repeat the same procedure for other values of E.

The variations of AB and A with respect to D are shown in figures 4.3 and 4.4 respectively, where E is considered as parameter. It is to be noted that:

i) A system response damping ratio of $(\delta/\Omega) = 0.4$ which corresponds to a successive amplitude ratio of approximately 25% (see figure 3.3) was selected. Such a successive amplitude ratio was also considered by several authors (References 27, 32 and 36) to result in a good compromise between the response overshoot and transient oscillatory period.

ii) The minimum value of E is 2, which corresponds to

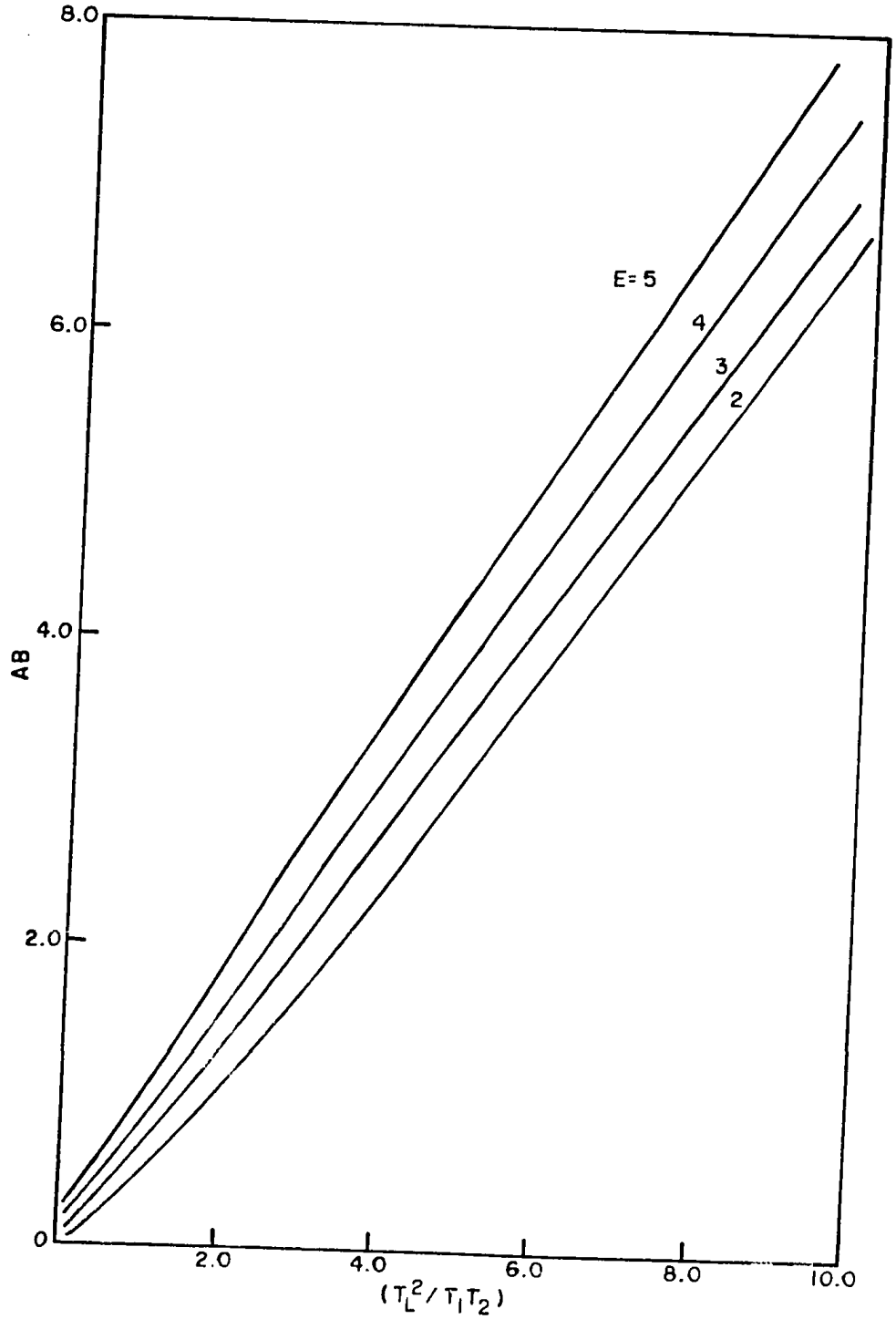

FIGURE 4.3 DEPENDENCY OF AB UPON (T_L^2/T_1T_2)

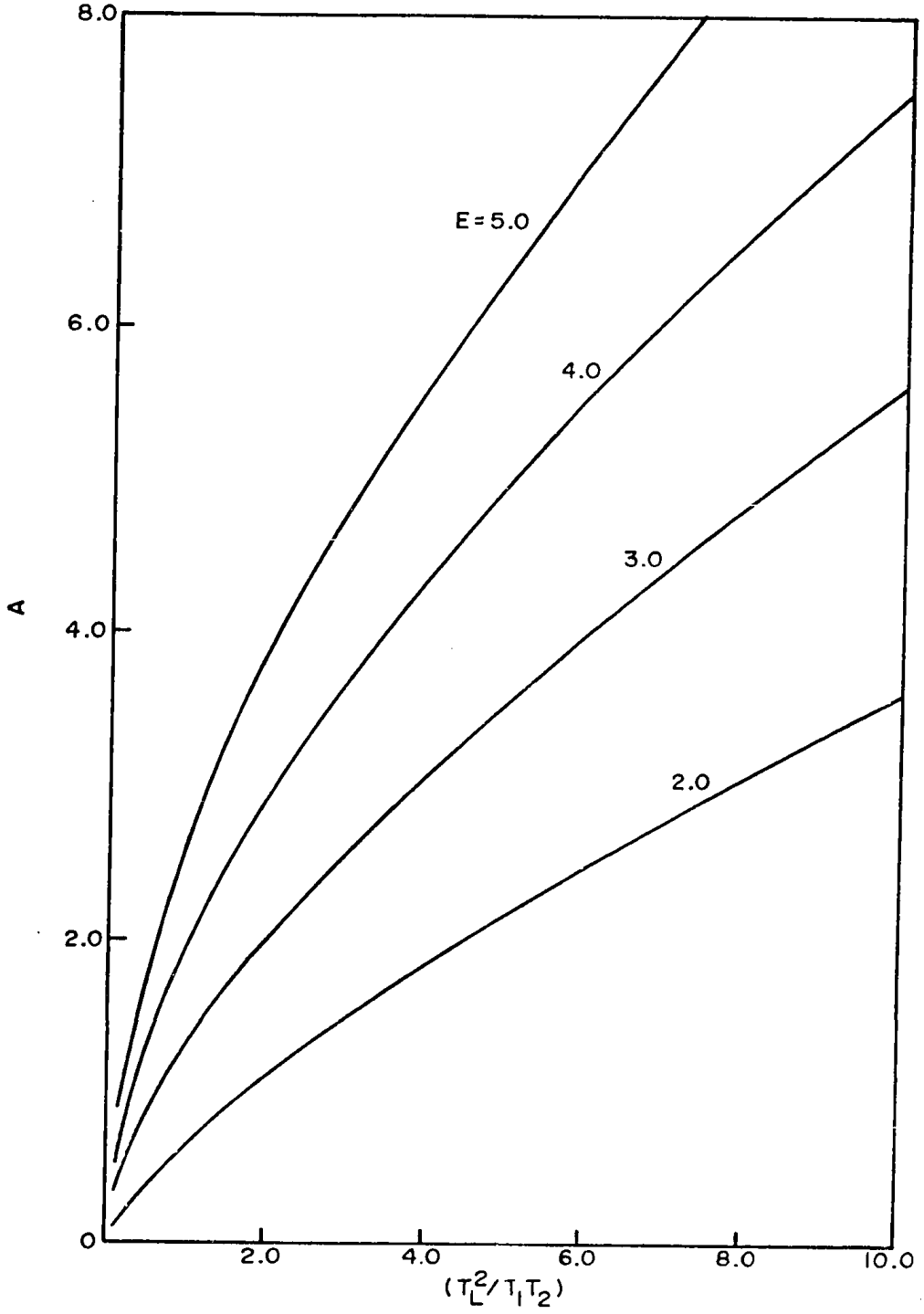

FIGURE 4.4 DEPENDENCY OF A UPON (T_L^2/T_1T_2)

a system where the time constants T_1 and T_2 are of equal magnitude. Although the maximum value of E is infinite, the computation has been limited at E = 5.0 which corresponds to a system where the ratio of (T_1/T_2) or (T_2/T_1) is approximately 25. A greater ratio signifies that one of the system time constants is dominant compared to the other and different criteria developed for systems consisting of one first-order lag and a pure time delay (References 27 and 36) could be realistically used.

The dependencies of AB and A upon D as shown graphically in figures 4.3 and 4.4 suggest the following empirical equations:

$$AB = \alpha_o + \alpha_1 D + \alpha_2 D^2 \qquad (4.2)$$

$$D = \beta_o + \beta_1 A + \beta_2 A^2 \qquad (4.3)$$

where α_o, α_1, α_2 and β_o, β_1, β_2 are functions of E. For each given value of E, the coefficients α_o, α_1 and α_2 were determined by fitting a curve of the form of equation (4.2) through the data points computed from equations (3.22) and (3.23), the curve fitting procedure being based on the principle of least squares. Similarly, the coefficients β_o, β_1 and β_2 were determined for each given value of E by fitting a curve of the form of equation (4.3) through the

data points computed from equations (3.22) and (3.24). The dependencies of these coefficients upon E are shown graphically in figures 4.5 and 4.6.

Thereby, the optimum controller parameter setting could be approximated by the following simplified equations:

$$AB = \alpha_o + \alpha_1 \left[\frac{T_L^2}{T_1 T_2}\right] + \alpha_2 \left[\frac{T_L^2}{T_1 T_2}\right]^2 \qquad (4.5)$$

$$A = \left[-\beta_1 + \sqrt{\beta_1^2 - 4\beta_2(\beta_o - \frac{T_L^2}{T_1 T_2})}\right] \Big/ 2\beta_2 \qquad (4.6)$$

$$K_1 = \frac{T_1 T_2}{T_L^2} A \quad , \quad K_2 = \frac{B}{T_L} \qquad (4.7)$$

where α_o, α_1, α_2 may be determined from figure 4.5 and β_o, β_1, β_2 may be determined from figure 4.6.

4.4 Application of the Simplified Optimum Equations

The performance of the heading reference system with controller parameter setting determined from the simplified optimum equations (4.5), (4.6) and (4.7) was

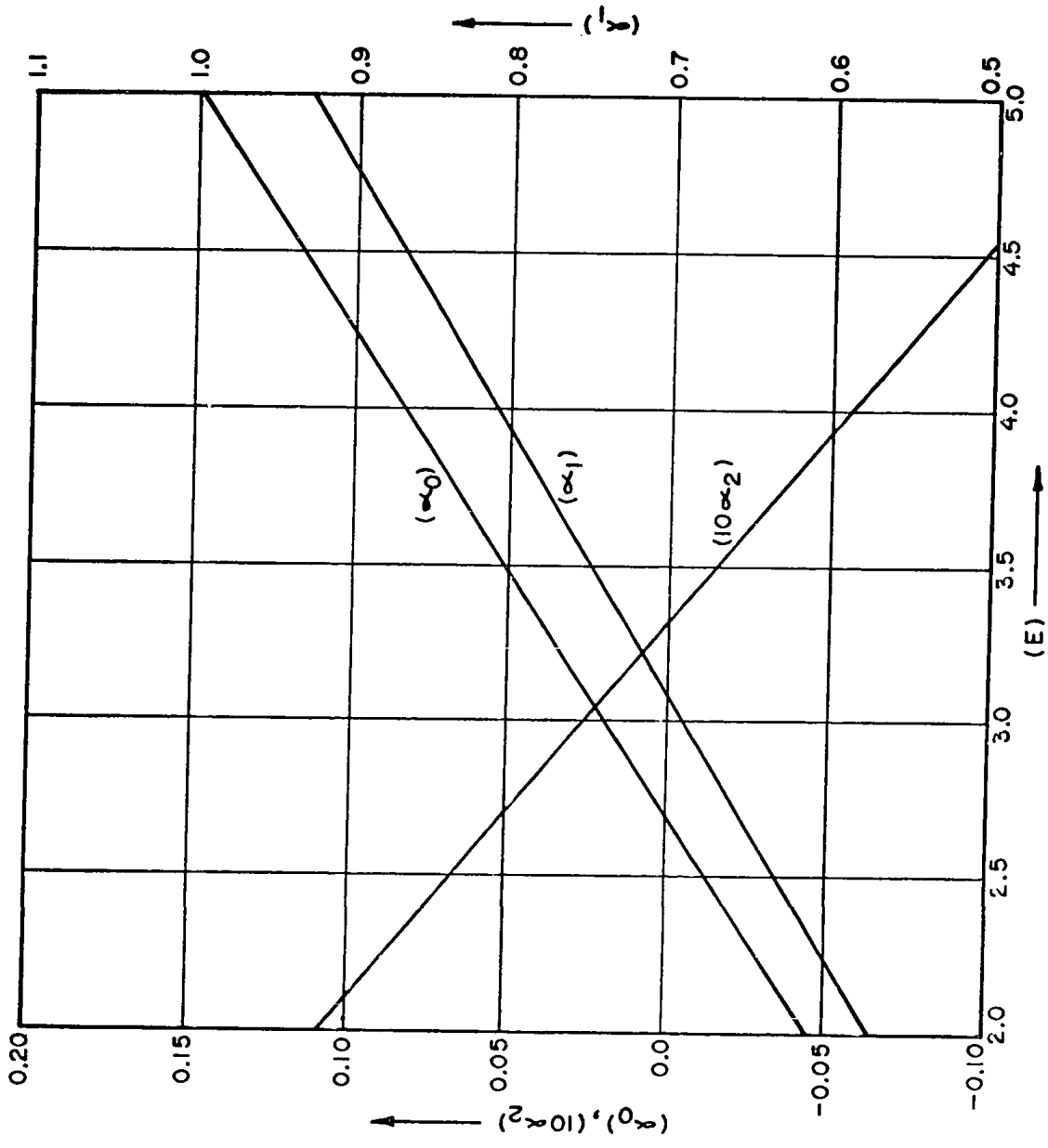

FIGURE 4.5 VALUES OF THE COEFFICIENTS OF EQUATIONS (4.2) AND (4.5)

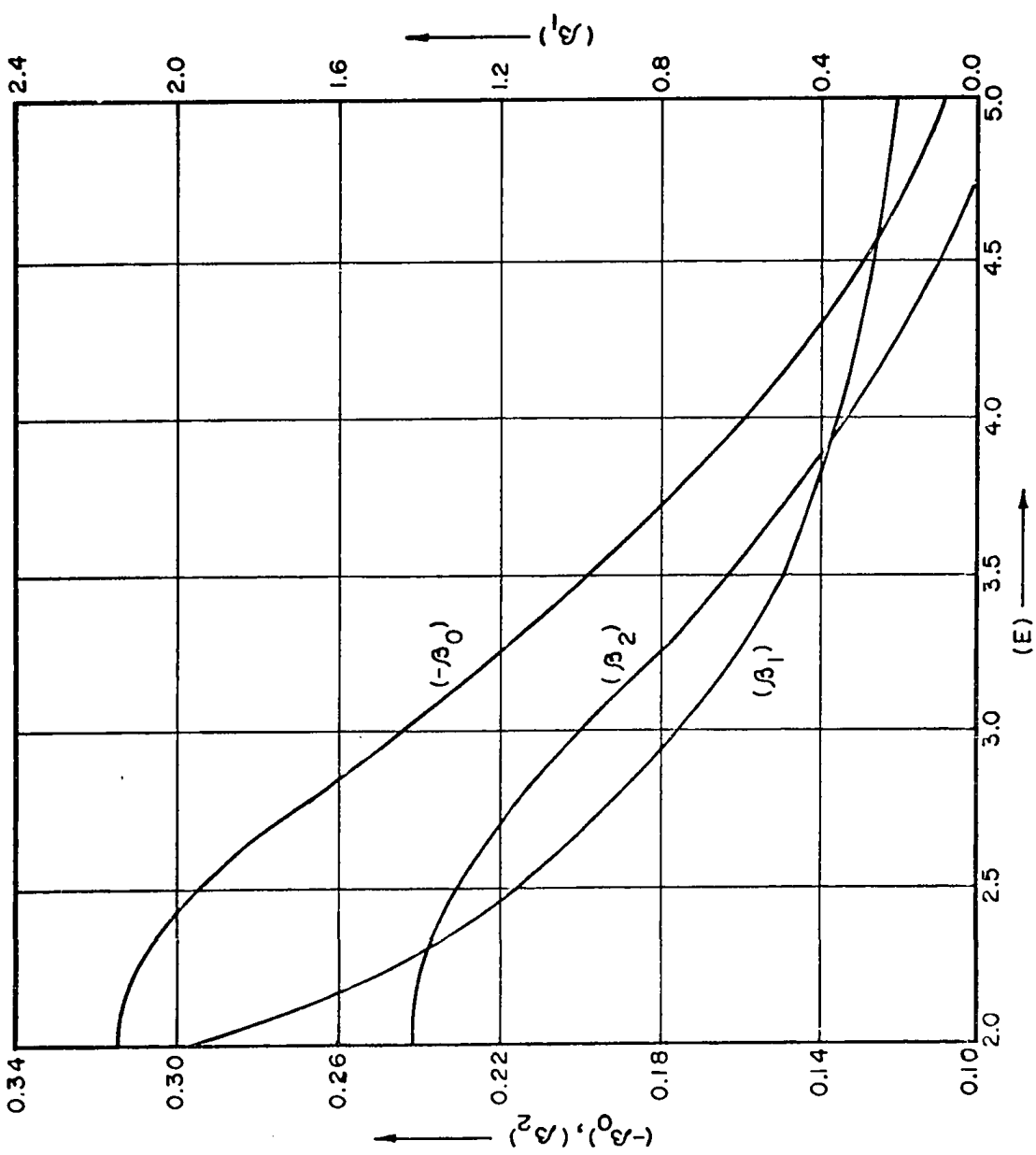

FIGURE 4.6 VALUES OF THE COEFFICIENTS OF EQUATIONS (4.3) AND (4.6)

investigated to determine the validity of the simplified optimum criterion. Three different sets of T_I and T_L values were experimentally attained by varying the rate sensor supply pressure, the appropriate corresponding controller settings being determined in Appendix B. The system performance was initially evaluated using hybrid computer simulation, the system heading error responses to a 10.0 degs./sec. step rate input are shown with the corresponding exact optimum setting responses in figures 4.7, 4.8 and 4.9 respectively for rate sensor supply pressures of 1.0 psi, 5.0 psi and 10.0 psi.

The responses of system with controller parameter settings determined from the simplified optimum equations (4.5), (4.6) and (4.7) correlate reasonably with those obtained with the exact optimum settings. Depending on the values of D and E, the approximately optimized system exhibits either a less oscillatory response with more steady-state error as shown in figure 4.6 or a more oscillatory response with less steady-state error as illustrated in figures 4.7 and 4.8. This variation is attributed to the round-off error resulted from the numerical curve fitting procedure.

The validity of the simplified optimum criterion was also experimentally determined using the experimental system. The heading error responses of the system with

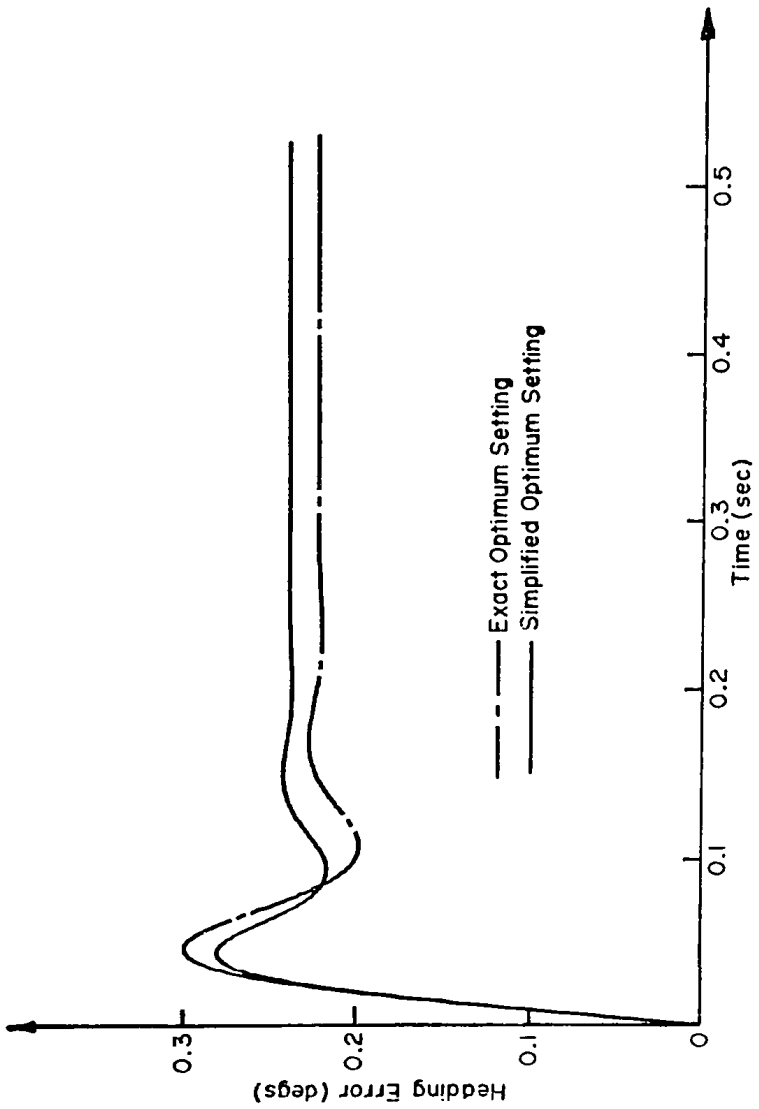

FIGURE 4.7 SYSTEM RESPONSES TO A STEP RATE INPUT OF 10.0 degs/sec
(Rate Sensor Supply Pressure = 1.0 psi)

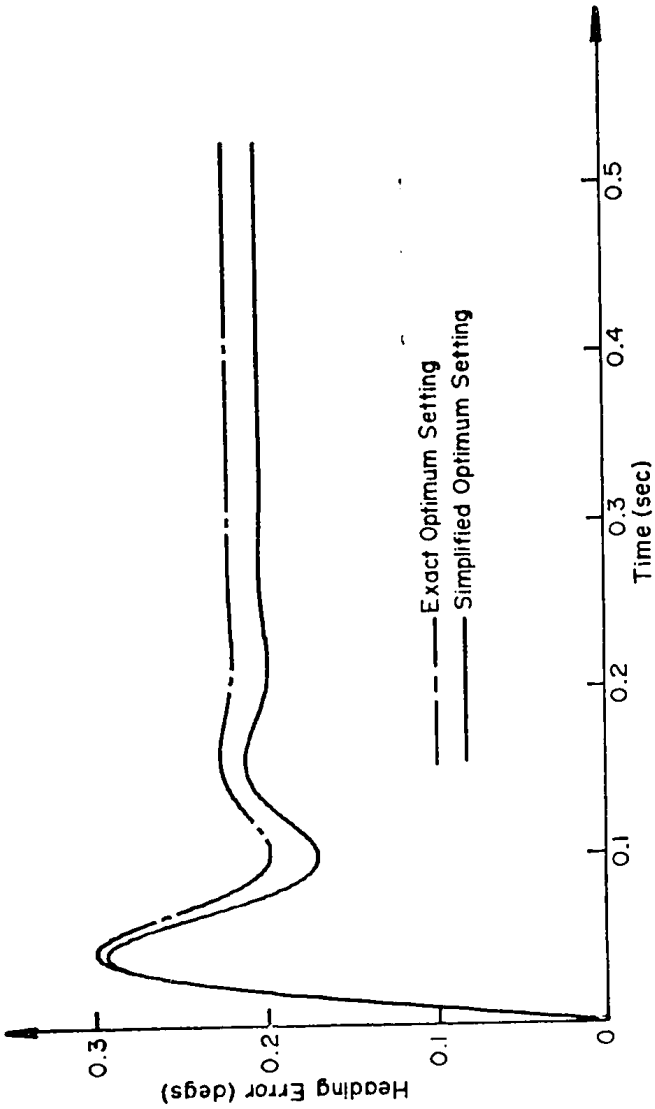

FIGURE 4.8 SYSTEM RESPONSES TO A STEP RATE INPUT OF 10.0 degs/sec
(Rate Sensor Supply Pressure = 5.0 psi)

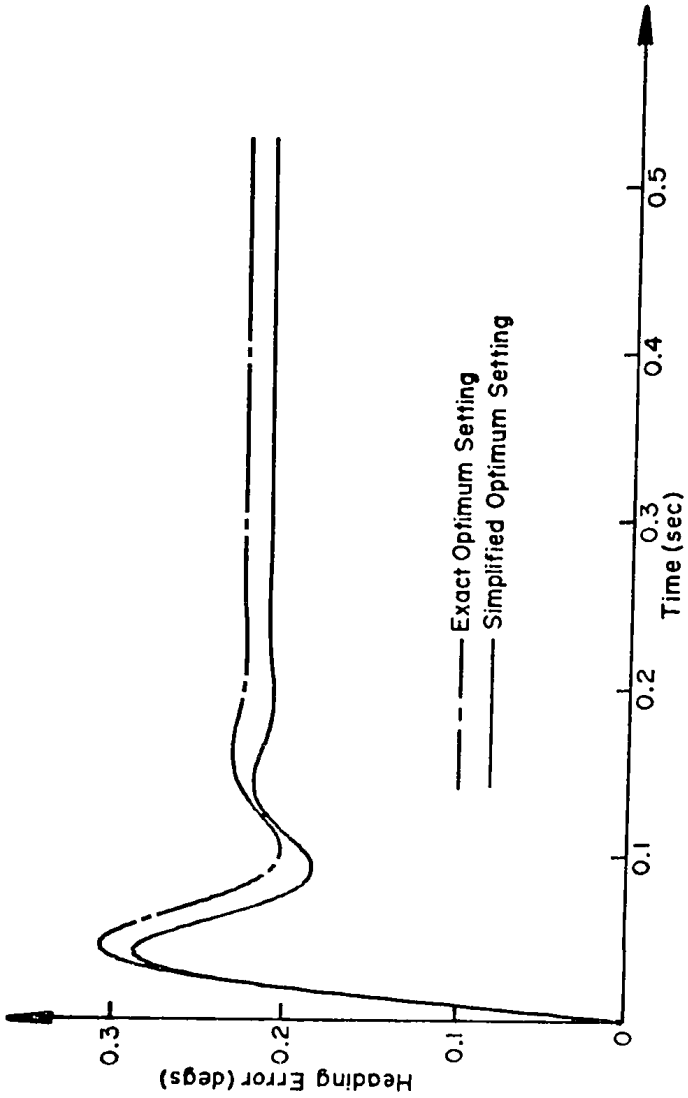

FIGURE 4.9 SYSTEM RESPONSES TO A STEP RATE INPUT OF 10.0 degs/sec
(Rate Sensor Supply Pressure = 10.0 psi)

both the simplified optimum settings and the exact optimum settings are shown in figures 4.10a,b, 4.11a,b and 4.12a,b for a step rate input of 20.0 degs./sec.. The simplified optimum and corresponding exact optimum system responses are also plotted superimposed in figures 4.13, 4.14 and 4.15 to facilitate direct comparison.

It is evident that the errors resulting from the approximation are insignificant compared to those introduced by system hardware components such as noise induced random deviations.

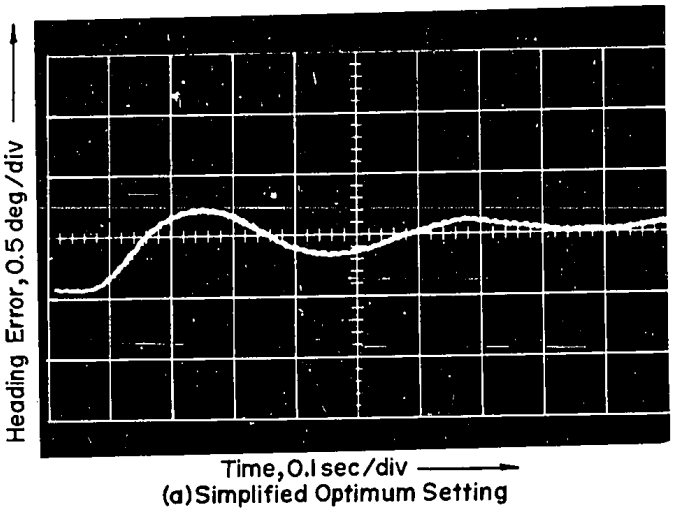

(a) Simplified Optimum Setting

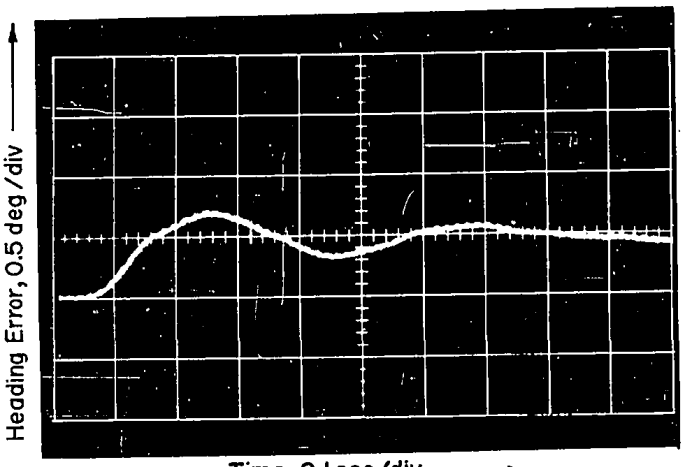

(b) Exact Optimum Setting

FIGURE 4.10 EXPERIMENTAL HEADING RESPONSES TO A STEP RATE INPUT OF 20 degs/sec
(Rate Sensor Supply Pressure = 1.0 psi)

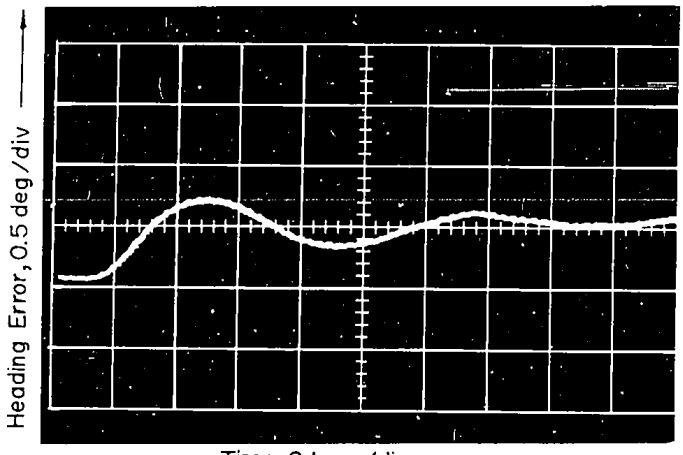

(a) Simplified Optimum Setting

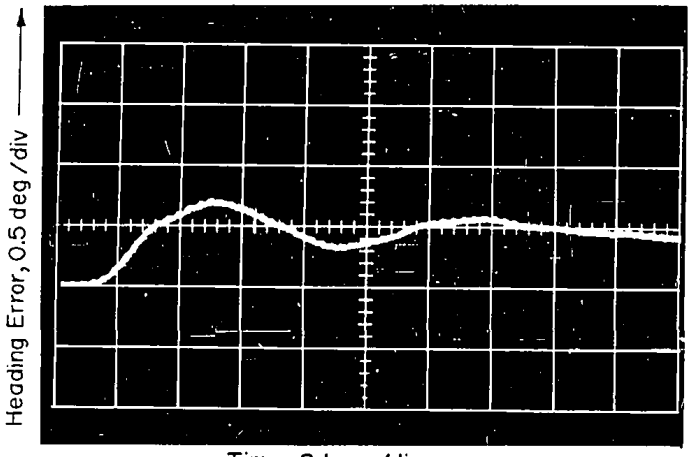

(b) Exact Optimum Setting

FIGURE 4.10 EXPERIMENTAL HEADING RESPONSES TO A STEP RATE INPUT OF 20 degs/sec
(Rate Sensor Supply Pressure = 1.0 psi)

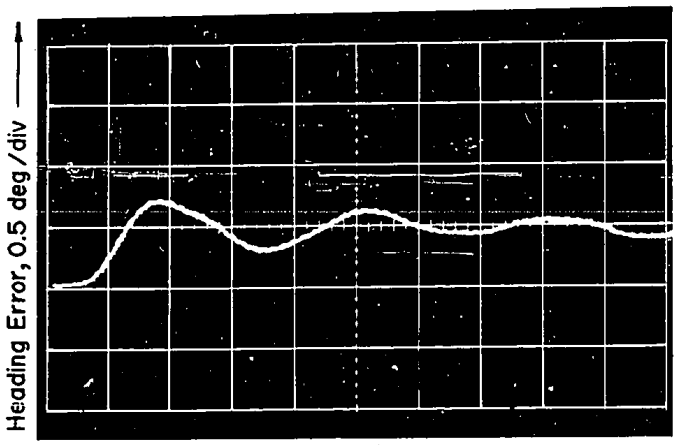

(a) Simplified Optimun Setting

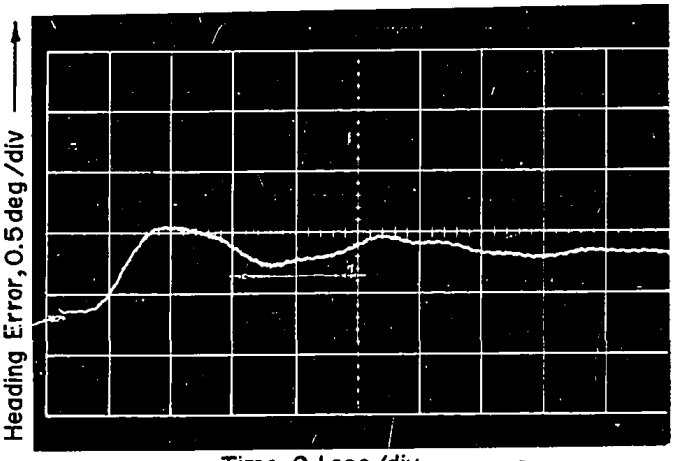

(b) Exact Optimum Setting

FIGURE 4.11 EXPERIMENTAL HEADING RESPONSES TO A STEP RATE INPUT OF 20 degs/sec (Rate Sensor Supply Pressure = 5.0 psi)

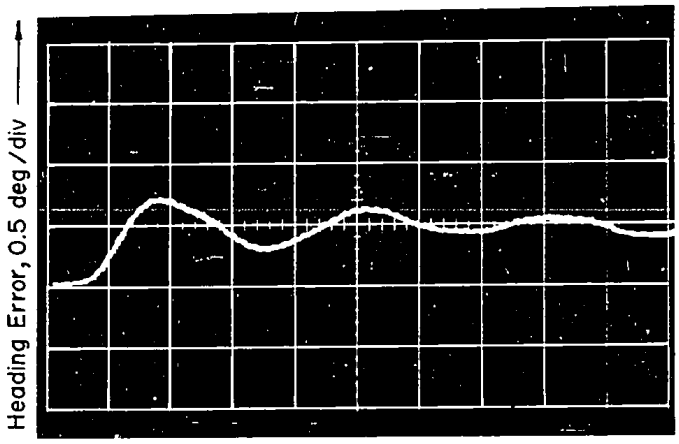

(a) Simplified Optimun Setting

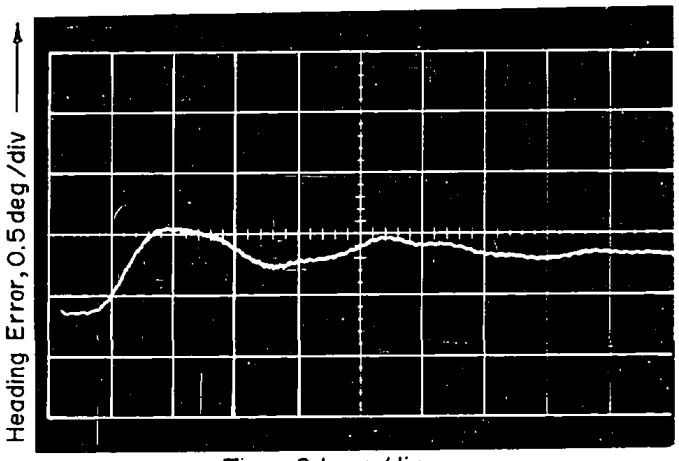

(b) Exact Optimum Setting

FIGURE 4.11 EXPERIMENTAL HEADING RESPONSES TO A STEP RATE INPUT OF 20 degs/sec (Rate Sensor Supply Pressure = 5.0 psi)

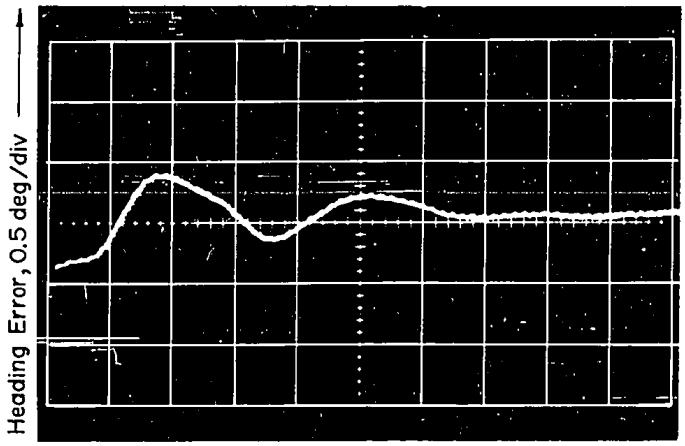

(a) Simplified Optimum Setting

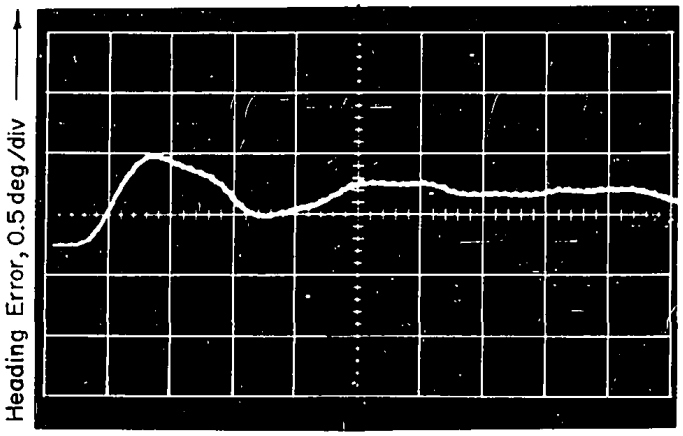

(b) Exact Optimum Setting

FIGURE 4.12 EXPERIMENTAL HEADING RESPONSES TO A STEP RATE INPUT OF 20 degs/sec
(Rate Sensor Supply Pressure = 10.0 psi)

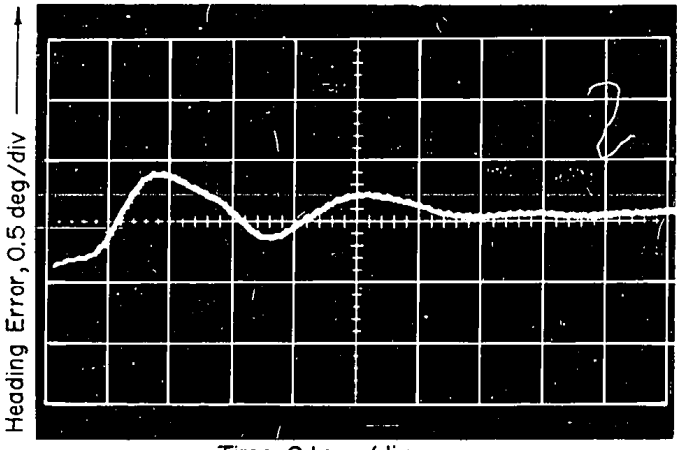

(a) Simplified Optimum Setting

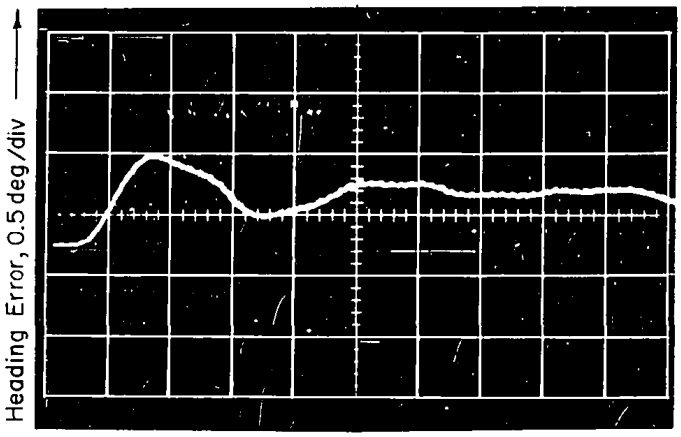

(b) Exact Optimum Setting

FIGURE 4.12 EXPERIMENTAL HEADING RESPONSES TO A STEP RATE INPUT OF 20 degs/sec
(Rate Sensor Supply Pressure = 10.0 psi)

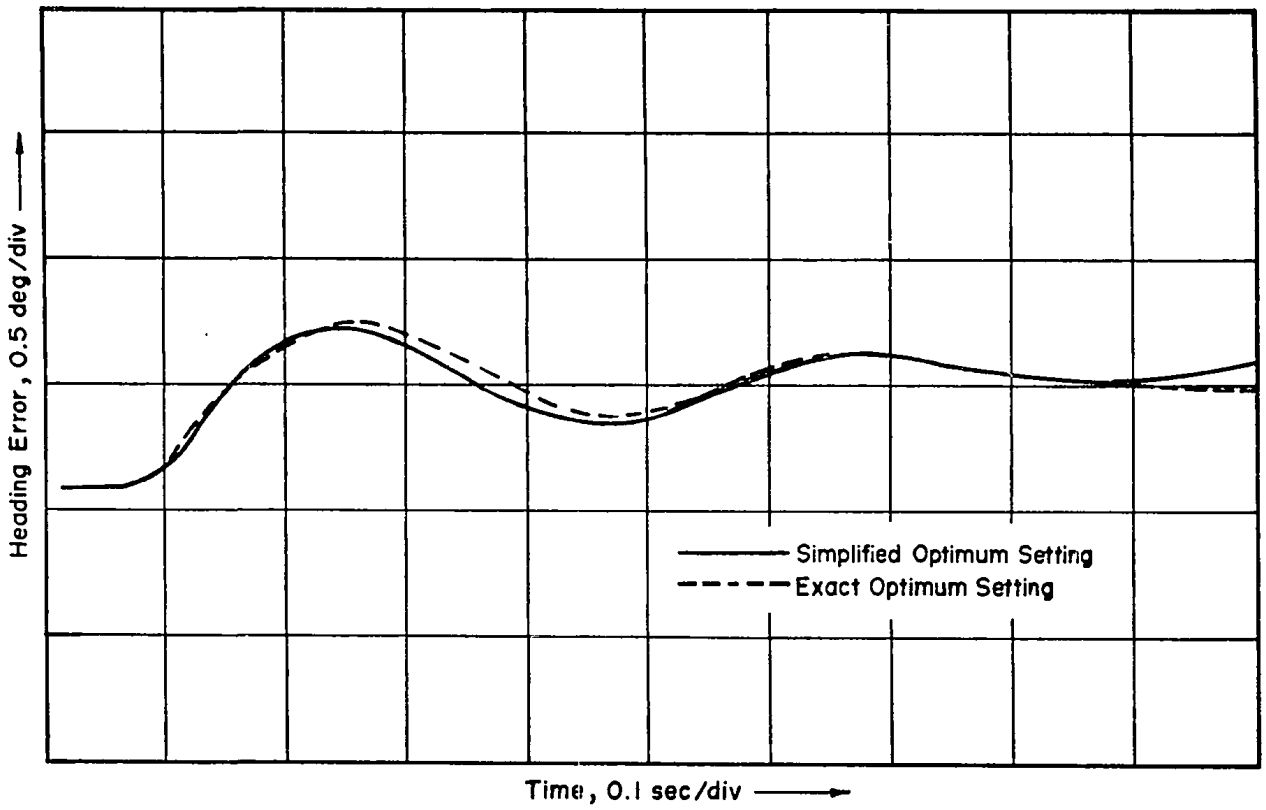

FIGURE 4.13 COMPARISON OF SIMPLIFIED AND EXACT OPTIMUM SETTING SYSTEM RESPONSES
(Rate Sensor Supply Pressure = 1.0 psi)

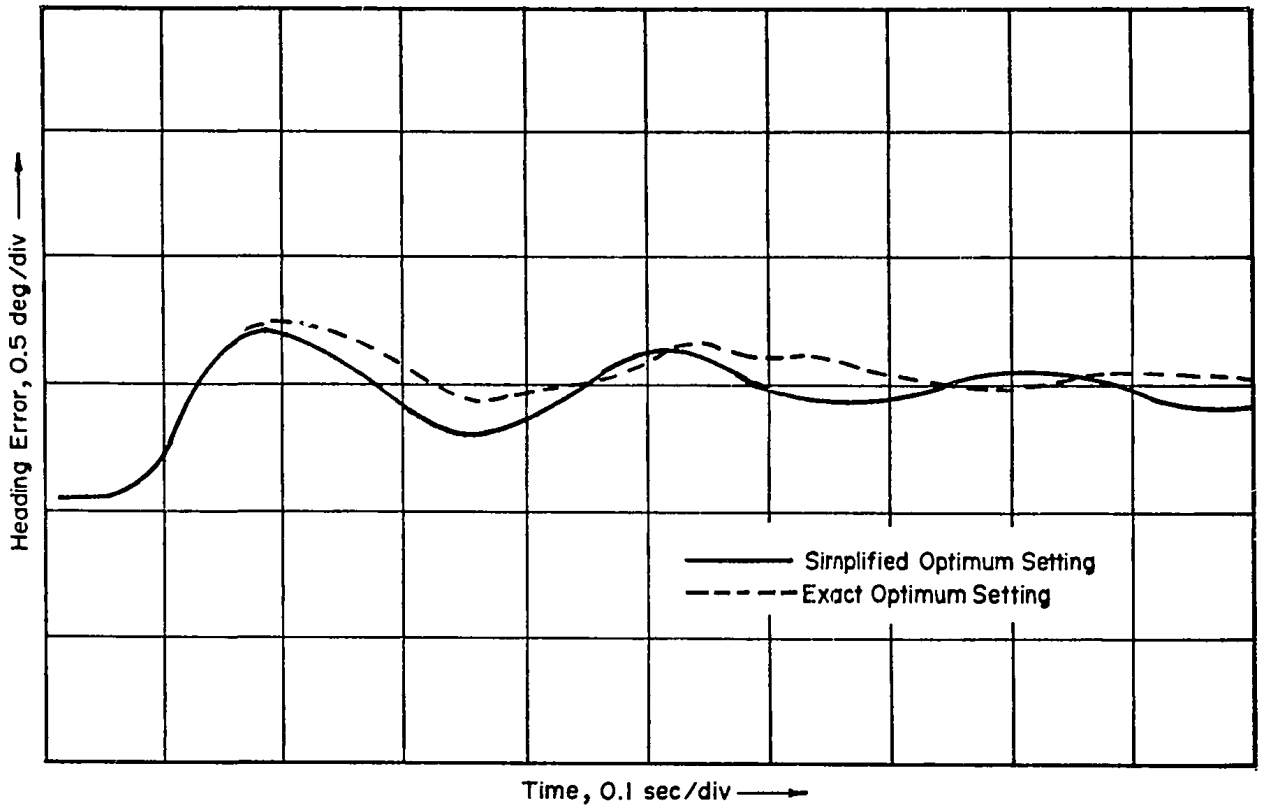

FIGURE 4.14 COMPARISON OF SIMPLIFIED AND EXACT OPTIMUM SETTING SYSTEM RESPONSES
(Rate Sensor Supply Pressure = 5.0 psi)

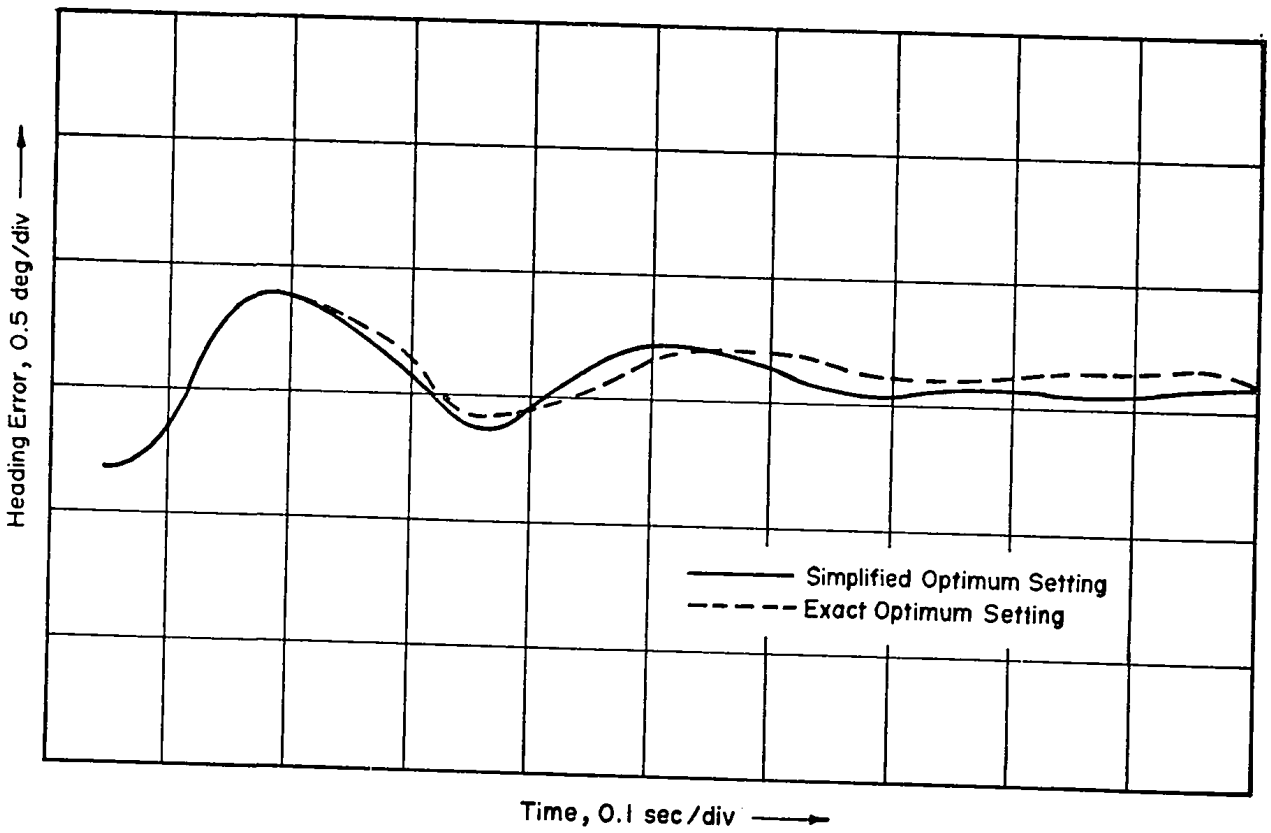

FIGURE 4.15 COMPARISON OF SIMPLIFIED AND EXACT OPTIMUM SETTING SYSTEM RESPONSES
(Rate Sensor Supply Pressure = 10.0 psi)

CHAPTER 5

CONCLUSIONS

The investigation into the hybrid fluidic heading reference system has led to the following conclusions:

— A directional heading reference about a single axis is attainable by incorporating a proportional-integral controller type of compensation in a negative rate feedback servo loop around a rotatable fluidic vortex rate sensor while maintaining transient response heading error and stability margin level acceptable for moderate directional rate of change such as anticipated in land vehicle navigational system application.

— A completely fluidic heading reference system is theoretically feasible by utilizing a reversible impulse turbine as the feedback actuator. This approach would simplify the system hardware requirements and merits further considerations.

— The heading system dynamic performance may be optimized by selecting the controller parameters in accordance with a theoretical optimization technique derived for minimizing the time-integral of error of a generalized negative

feedback control system incorporating a second order lag plus a pure time delay.

— The rigourously derived complex set of equations defining the optimum controller settings may be closely approximated by a much simplified set of equations over a wide range of system transfer function parameter values.

— The optimized time-integral of error varies proportionally with the system pure time delay. Accordingly, the heading system dynamic performance may be improved by reducing the rate sensor time delay independent of the rate sensor time lag as could be attained by rate sensor configuration changes (Reference 44).

— The optimized time-integral of error and the transient duration may be improved by reducing either or both of the time lags from a specific value as defined by the optimization equation for a given system response damping ratio.

— The optimized time-integral of error may be improved by increasing either or both of the time lags from a specific value as defined by the optimization equation for a given system response damping ratio but at the expense of increased system transient duration.

— The second-order lag plus a pure time delay representation of the fluidic rate sensor (Reference 44) may be approximated by a first-order lag plus a pure time delay for purposes of heading reference system performance prediction.

— The application of the heading reference system will be limited not by the transient performance but by the long term drift induced by system noise as evidenced by experimental heading system response random deviations. Accordingly, it is suggested that further investigation of the hybrid heading reference system be concentrated on the identification and subsequent reduction of internally generated system noise in order to attain an acceptable performance over extended duration.

REFERENCES

1) Lock, W.P. and S.W. Gee, " Flight Investigation of a Fluidic Autopilot System ", NASA Technical Note, NASA T N D-5298, July 1969.

2) Ekstrom, U., K.S. Nystrom, Th. Persson and E. Ulen, " An All Fluidic Gyro-Stabilized Platform ", Paper C2, Third Cranfield Fluidics Conference, May 1968, British Hydromechanics Research Association, Cranfield, England.

3) Anonymous, " Rotating-Socket Fluidic Gyro ", Product Engineering, Vol. 40, No. 22, Nov. 1969, pp. 73-74, McGraw-Hill.

4) Haugen, J.L., " A Fluidic Approach to Control of VTOL Aircraft ", AIAA/JACC Guidance and Control Conference, Seatle, Washington, August 1966, pp. 749-756, American Institut of Aeronautics and Astronautics.

5) Ayre, V.H. and P.D. Lee, " An Analysis of a Two Axis Fluid Control System for an Artillery Type Missle", AIAA/ION Guidance and Control Conference, Minneapolis, Minn., August 1965, pp. 210-220.

6) Garner, H.D. and H.V. Fuller, " A Survey of Potential Applications of Fluidics to Spacecraft Attitude Control " NASA Langley Research Center, NASA TMX-59968-03, Acces-

sion No. N68-27381. Presented at SAE Symposium on Fluidics, Oct. 1966, San Francisco, California.

7) Clayton, B.J. and W.M. Posingies, " The Development and Flight Test of Pure Fluidic Missle Control System ", AIAA/ION Guidance and Control Conference, Minneapolis, Min., August 19, 1965, pp. 181-192.

8) Reilly, R.J., " Rate and Attitude Stabilization for Aircraft and Missles ", Fluid Control - Components and Systems, Advisory Group for Aerospace Research and Development, edited by S.Y. Lee, NATO, AGARDograph No. 118, Dec. 1968, Chapter 9.

9) Evans, R.A. and G.W. Fosdick," Hydraulic Fluidics Stabilizes Helicopter ", Hydraulics and Pneumatics, April 1968, pp. 111-115.

10) Keates, A. and C.K. Kwok, " Specification, Dynamic and Static Characteristics for Pure Fluid Vortex Rate Sensor ", Technical Memo-AETM67-095, Aviation Electric Ltd., Montreal.

11) Dransfield, P., Engineering Systems and Automatic Control, Prentice-Hall inc., N.J., 1968.

12) Hayes, W.F. and C.K. Kwok, " Hybrid Fluidic Heading Reference ", Fluidics Quartely, Vol. 2, Issue 5, Dec. 1970, pp. 38-47.

13) Smith, O.J.M. : Feedback Control System, McGraw-Hill, New-York, 1958.

14) Harbert, F.C., " Analogue Computer Techniques ", Electronic Engineering, March 1960.

15) Buckley, D.S., " Automatic Control of Processes with Dead Time ", Automatic and Remote Control, London, Vol. 1, 1960, pp. 33-40.

16) Bauer, P.,"5 Ways to Delay a Signal ", Control Engineering, April 1968, pp. 92.

17) McKinnon, M.G. and J.N. Wilson, " Fluidic Simulation of a Transportation Lag ", paper 69-534, Advances in Instrumentation, Proceedings of ISA Annual Conference, Vol. 24, Oct. 1969.

18) McKinnon, M.G. and J.N. Wilson, " Fluidic Control of Processes with Transportation Lag ", paper D5, Preprints of 2nd IFAC Symposium on Fluidics, Prague, Czechoslovakia, June 1971.

19) Lumper, D.E. and M.W. Oglesby, " The Application of Dead-Time Compensation to a Chemical Reactor for Automatic Control of Production Rate ", IRE Transactions, Vol. 1, No. 1, 1962, pp. 72-80.

20) Tallman, G.H. and O.J.M. Smith, " Analog study of Dead-Beat Posicast Control ", IRE Transactions of Automatic

Control, Vol. AC-4, 1958, pp. 14-21.

21) Truxal, J.G., Automatic Feedback Control System Synthesis, McGraw-Hill, New-York, 1955, pp. 553-558.

22) Oldenbourg, R.C., " Deviation Dependent Step-by-Step Control as Means to Achieve Optimum Control for Plants with Large Distance-Velocity ", Automatic and Manual Control; edited by A. Tustin, Butterworths Scientific Publications, London, 1952, pp. 421-434.

23) Sartorius, H., " Deviation Dependent Step-by-Step Control Systems and their Stability ", Automatic and Manual Control, edited by A. Tustin, Butterworths Scientific Publications, London, 1952, p. 435-447.

24) Balakirev, V.S., " The Principle of the Maximum in the Theory of Second Order Optimal Systems ", Automation and Remote Control, The Soviet Journal Automatika i Telemekhanika in English Translation, Vol, 23, No. 7, July 1962, pp. 948-956.

25) MacKinnon, D., " Optimal Control of Systems with Pure Time Delays Using a Variational Programming Approach ", IEEE Transactions on Automatic Control, Vol. AC-12, No. 3, June 1967.

26) Koepcke, R.W., " On the Control of Linear Systems with Pure Time-Delay ", Proceedings of Joint Automatic Control

Conference, 1964, pp. 397-403.

27) Ziegler, J.G. and N.B. Nichols, " Process Lags in Automatic-Control Circuits ", Transactions of ASME, Vol. 65, 1943, pp. 433-444.

28) Haalman, A., " Adjusting Controllers for a Deadtime Process ", Control Engineering, July 1965, pp. 71-73.

29) Coughanour, D.R. and L.B. Koppel, Process Systems Analysis and Control, McGraw-Hill, New-York, 1965.

30) Barret, J.A. and R.E. Wagner, " Development of a Three Mode Control Using High Gain Fluid Amplifiers ", American Society of Mechanical Engineers, Paper 67-WA/FE-35, Nov. 1967.

31) Chou, Q.B., " Development of a Simple Fluidic Three Mode Controller ", Proceedings of the National Conference on Automatic Control, Alberta, 1969, pp. 3-20.

32) Ziegler, J.G. and N.B. Nichols, " Optimum settings of Automatic Controllers ", Transactions of ASME, Vol. 64, 1942, pp. 759-768.

33) Wolfe, W.A., " Controller Settings for Optimum Control ", Transactions of ASME, Vol. 72, 1951, pp. 413-418.

34) Callender, A., D.R. Hartree and A. Porter, " Time Lag in a Control System ", Phil. Transactions of the Royal

Society of London, Vol. 235, 1936, pp. 415-444.

35) Hartree, D.R., A. Porter and A. Callender, " Time Lag in Control System II ", Proc. of the Royal Society of London, Series A.,Vol. 161, 1937, pp. 460-476.

36) Cohen, G.H. and G.A. Coon, " Theoretical Consideration of Retarded Control ", Transactions of ASME, Vol. 75, 1953, pp. 827-834.

37) Oldenbourg R.C. and H. Sartorius, " A Uniform Approach to the Optimum Adjustment of Control Loops ", Transactions of ASME, Vol. 76, 1954, pp. 211-219.

38) Urbanosky, T.F., " Fluieric Operational Amplifier Survey ", Society of Automotive Engineers, Paper 670707, June 1967.

39) Lequoc, S., W.F. Hayes and C.K. Kwok, " Fluidic Heading Reference System ", Fluidics Quartely, Vol. 3, No. 4, Oct. 1971, pp. 16-29.

40) Graham, D. and R.C. Lathrop, Discussion of the paper " A Uniform Approach to the Optimum Adjustment of Control Loops ", Transactions of ASME, Vol. 76, 1954, pp. 223-224.

41) Nielson, G., " Control of System with Time Delay ", Paper 4.2, Proceedings of the 4th Congress of the In-

ternational Federation of Automatic Control, Warszawa, June 1969.

42) Oldenbourg, R.C. and Sartorious, The Dynamics of Automatic Controls, Translated from German by H.L. Mason, published by ASME, 1948, N.Y.

43) Hayes, W.F. and H. Tucker, " Dynamic Range and Frequency Response of the Vortex Rate Sensor ", Paper E1, Proceedings of the 5th Cransfield Conference on Fluidics, June 1972, Upsala, Sweden.

44) Hayes, W.F., and H. Tucker, " Fluidic Vortex Rate Sensor Transient Response ", Laboratory Technical Report CS-78, Division of Mechanical Engineering, National Research Council of Canada, April 1972.

45) Hayes, W.F. and H. Tucker, " Fluidic Rate Sensor Output Signal Noise Evaluation ", Laboratory Technical Report CS-61, Division of Mechanical Engineering, National Research Council of Canada, Jan. 1972.

46) Ostdiek, A.J., " Viscous Vortex Rate Sensor ", Technical Report HDL-TR-1555, Harry Diamond Laboratories, Washington, D.C., November 1971.

APPENDIX A

NECESSARY MATHEMATICAL DEVELOPMENT FOR SYSTEM HEADING ERROR MINIMIZATION

A.1 Rate Sensor Transfer Function Approximated by a 1st Order Lag Plus a Pure Time Delay

A.1.1 System Closed Loop Transfer Function

From the heading reference system block diagram shown in figure 3.1:

$$\omega_o(s) = \frac{G_1 K_c G_2 e^{-T_L s}\left(\frac{1}{T_I s}+1\right)}{(1+T_1 s)(1+T_2 s)}\left[\omega_i(s)-\omega_o(s)\right] \qquad (A.1)$$

For convenience, let

$$K_1 = G_1 K_c G_2 \quad \text{and} \quad K_2 = \frac{1}{T_I}$$

Introducing the following Laplace auxiliary variable

$$q = T_L s$$

equation (A.1) becomes:

$$\omega_o(s) = \frac{e^{-q}K_1(K_2+\frac{q}{T_L})}{\frac{q}{T_L}(1+T_1\frac{q}{T_L})(1+T_2\frac{q}{T_L})}\left[\omega_i(s)-\omega_o(s)\right]$$

$$= \frac{e^{-q}K_1(K_2T_L+q)T_L^2}{q(T_L+T_1q)(T_L+T_2q)}\left[\omega_i(s) - \omega_o(s)\right]$$

Rearranging the terms gives the equation:

$$\omega_o(s)\left[1+\frac{e^{-q}K_1(K_2T_L+q)T_L^2}{q(T_L+T_1q)(T_L+T_2q)}\right] = \frac{e^{-q}K_1(K_2T_L+q)T_L^2}{q(T_L+T_1q)(T_L+T_2q)}\omega_i(s) \qquad (A.2)$$

Hence, the system closed loop transfer function is given by:

$$\frac{\omega_o(s)}{\omega_i(s)} = \frac{e^{-q}K_1(K_2T_L+q)T_L^2}{q(T_L+T_1q)(T_L+T_2q)+e^{-q}K_1(K_2T_L+q)T_L^2} \qquad (A.3)$$

A.1.2 Heading Rate Error Time Response

For a step rate input:

$$\omega_i(s) = \frac{\omega_i}{s} = \frac{T_L\omega_i}{q}$$

Substituting the value of $\omega_i(s)$ into equation (A.2):

$$\omega_o(s)\left[1+\frac{e^{-q}K_1(K_2T_L+q)T_L^2}{q(T_L+T_1q)(T_L+T_2q)}\right]=\frac{T_L\omega_i}{q}\left[\frac{e^{-q}K_1(K_2T_L+q)T_L^2}{q(T_L+T_1q)(T_L+T_2q)}\right]$$

which gives:

$$\omega_o(s)=\frac{T_L\omega_i}{q}\left[\frac{\dfrac{K_1T_L^2(K_2T_L+q)e^{-q}}{q(T_L+T_1q)(T_L+T_2q)}}{1+\dfrac{K_1T_L^2(K_2T_L+q)e^{-q}}{q(T_L+T_1q)(T_L+T_2q)}}\right] \qquad \text{(A.4)}$$

Since:

$$\omega_e(s)=\omega_i(s)-\omega_o(s)$$

the system rate error will be:

$$\omega_e(s)=\frac{T_L\omega_i}{q}-\frac{T_L\omega_i}{q}\left[\frac{\dfrac{K_1T_L^2(K_2T_L+q)e^{-q}}{q(T_L+T_1q)(T_L+T_2q)}}{1+\dfrac{K_1T_L^2(K_2T_L+q)e^{-q}}{q(T_L+T_1q)(T_L+T_2q)}}\right]$$

Rearranging the terms gives the equation

$$\omega_e(s) = \frac{T_L \omega_i}{q}\left[\frac{1}{1+\frac{K_1 T_L^2(K_2 T_L+q)e^{-q}}{q(T_L+T_1 q)(T_L+T_2 q)}}\right] \qquad (A.5)$$

which verifies equation (3.2) given in chapter 3.

As given by equation (3.9):

$$\frac{\omega_e(\tau)}{\omega_i} = \sum_{n=0}^{\infty}\left[\text{Res.}(q_n)+\text{Res.}(\bar{q}_n)\right] \qquad (A.6)$$

According to the Laurent's series theory, the residues of q_n and $\bar{q}_n$ are determined by:

$$\text{Res.}(q_n)+\text{Res.}(\bar{q}_n) = \lim_{q\to q_n}\frac{(q^2+Cq+D)e^{q\tau}}{q^3+Cq^2+Dq+A(B+q)e^{-q}}(q-q_n) + \lim_{q\to \bar{q}_n}\frac{(q^2+Cq+\bar{D})e^{q\tau}}{q^3+Cq^2+Dq+A(B+q)e^{-q}}(q-\bar{q}_n) \qquad (A.7)$$

Using l'Hospital's rules, equation (A.7) could be rewritten as follows:

$$\text{Res.}(q_n)+\text{Res.}(\bar{q}_n)=\lim_{q\to q_n}\frac{\left[(2q+C)(q-q_n)e^{q\tau}+(q^2+Cq+D)e^{q\tau}+\tau(q^2+Cq+D)(q-q_n)e^{q\tau}\right]}{3q^2+2Cq+D+Ae^{-q}-A(B+q)e^{-q}}$$

$$+\lim_{q\to\bar{q}_n}\frac{\left[(2q+C)(q-\bar{q}_n)e^{q\tau}+(q^2+Cq+D)e^{q\tau}+\tau(q^2+Cq+D)(q-\bar{q}_n)e^{q\tau}\right]}{3q^2+2Cq+D+Ae^{-q}-A(B+q)e^{-q}}$$

or:

$$\text{Res.}(q_n)+\text{Res.}(\bar{q}_n)=\frac{(q_n^2+Cq_n+D)e^{q_n\tau}}{3q_n^2+2Cq_n+D-A(B+q_n-1)e^{-q_n}}$$

$$+\frac{(\bar{q}_n+C\bar{q}_n+D)e^{\bar{q}_n\tau}}{3\bar{q}_n^2+2C\bar{q}_n+D-A(B+\bar{q}_n-1)e^{-\bar{q}_n}}$$

$$=X_n\,e^{q_n\tau}+\bar{X}_n e^{\bar{q}_n\tau} \qquad \text{(A.8)}$$

where

$$X_n=\frac{q_n^2+Cq_n+D}{3q_n^2+2Cq_n+D-A(B+q_n-1)e^{-q_n}} \qquad \text{(A.9)}$$

$$\bar{X}_n=\frac{\bar{q}_n^2+C\bar{q}_n+D}{3\bar{q}_n^2+2C\bar{q}_n+D-A(B+\bar{q}_n-1)e^{-\bar{q}_n}} \qquad \text{(A.10)}$$

Substituting the complex representations for q_n and $\bar{q}_n$, equation (A.8) becomes:

$$\text{Res.}(q_n)+\text{Res.}(\bar{q}_n) = X_n e^{(-\delta_n+i\Omega_n)\tau} + \bar{X}_n e^{(-\delta_n-i\Omega_n)\tau}$$

$$= e^{-\delta_n\tau}\left[X_n e^{i\Omega_n\tau} + \bar{X}_n e^{-i\Omega_n\tau}\right]$$

$$= e^{-\delta_n\tau}\left[X_n(\cos\Omega_n\tau+i\sin\Omega_n\tau) + \bar{X}_n(\cos\Omega_n\tau-i\sin\Omega_n\tau)\right]$$

$$= e^{-\delta_n\tau}\left[(X_n+\bar{X}_n)\cos\Omega_n\tau+i(X_n-\bar{X}_n)\sin\Omega_n\tau\right]$$

(A.11)

Using the identity:

$$a\cos x+ib\sin x = \kappa\cos(x-\xi)$$

(where $\kappa = \sqrt{a^2-b^2}$ and $\xi = \arctan\frac{ib}{a}$)

equation (A.11) could be rewritten as follows:

$$\text{Res.}(q_n)+\text{Res.}(\bar{q}_n)=\left|X_n\right| e^{-\delta_n \tau}\cos(\Omega_n \tau-\phi_n) \tag{A.12}$$

$$\text{where: } \left|X_n\right| = \sqrt{(X_n+\bar{X}_n)^2-(X_n-X_n^2)} = 2\sqrt{X_n \bar{X}_n} \tag{A.13}$$

$$\phi_n = \arctan i \frac{X_n-\bar{X}_n}{X_n+\bar{X}_n} \tag{A.14}$$

Substituting the expressions for X_n and $\bar{X}_n$ defined by equations (A.9) and (A.10) into equations (A.13) and (A.14) gives:

$$\left|X_n\right| = 2\frac{\left[(\delta_n^2+\Omega_n^2)(\delta_n^2+\Omega_n^2+C)-2(\delta_n^2-\Omega_n^2)(C\delta_n-D)-D(2\delta_n-D)\right]^{\frac{1}{2}}}{\left[\begin{array}{l}(\delta_n^2+\Omega_n^2)\left[q(\delta_n^2+\Omega_n^2)+4C^2\right]-6(\delta_n^2-\Omega_n^2)(2C\delta_n-D)-D(4C\delta_n-D)\\ -2Ae^{\delta_n}\cos\Omega_n\left[(B-\delta_n-1)(3\delta_n^2-2C\delta_n-2D)-\Omega_n^2(3B+3\delta_n-2C+3)\right]\\ +2Ae^{\delta_n}\Omega_n\sin\Omega_n\left[3\delta_n(\delta_n-2B-2)+3\Omega_n^2+3C(B-1)+D\right]\end{array}\right]^{\frac{1}{2}}}$$

$$\phi_n = \arctan -\frac{\left[\begin{array}{l}2\Omega_n\left[-C(\Omega_n^2+\delta_n^2)^2+4D\delta_n-CD\right]\\ +2Ae^{\delta_n}\Omega_n\cos\Omega_n\left[\delta_n^2+\Omega_n^2+(C-2\delta_n)(B-1)-D\right]\\ +2Ae^{\delta_n}\sin\Omega\left[(B-\delta_n-1)(\delta_n^2+D-C\delta_n)+\Omega_n^2(-B+1-\delta_n+C)\right]\end{array}\right]}{\left[\begin{array}{l}(\delta_n^2+\Omega_n^2)\left[6(\delta_n^2+\Omega_n^2)-10C\delta_n+4C^2\right]+8(\delta_n^2-\Omega_n^2)D-4CD\delta_n+2D^2\\ -2Ae^{\delta_n}\cos\Omega_n\left[(B-\delta_n-1)(\delta_n^2+D-C\delta_n)+\Omega_n^2(-B+1-\delta_n+C)\right]\\ +2Ae^{\delta_n}\Omega_n\sin\Omega_n\left[\delta_n^2+\Omega_n^2+(C-2\delta_n)(B-1)-D\right]\end{array}\right]}$$

Substituting the residues of q_n and $\bar{q}_n$ defined by equation (A.12) into the heading error time response as given in equation (A.6)

$$\frac{\omega_e(\tau)}{\omega_i} = \sum_{n=0}^{\infty}\left[\text{Res.}(q_n)+\text{Res.}(\bar{q}_n)\right] = \sum_{n\ o}^{\infty} |X_n|\, e^{-\delta_n \tau}\cos(\Omega_n\tau-\phi_n) \qquad (A.15)$$

which verifies equation (3.13) given in chapter 3.

A.1.3 Development of Minimized Heading Error Equations

As given in chapter 3, the characteristic equation was:

$$q^3+Cq^2+Dq+A(B+q)e^{-q} = 0 \qquad (A.16)$$

Let $q = -\delta+i\Omega$ be a root of equation (A.16).

Subtituting this into equation (A.16)

$$(-\delta+i\Omega)^3+C(-\delta+i\Omega)^2+D(-\delta+i\Omega)+A(B-\delta+i\Omega)e^{\Omega-i\delta} = 0$$

Developing the power terms gives the equation:

$$(-\delta^3+3\Omega^2\delta)+i(3\delta^2\Omega-\Omega^3)+C(\delta^2-\Omega^2-2i\delta\Omega)$$
$$+D(-\delta+i\Omega)+Ae^{\delta}(B-\delta+i\Omega)(\cos\Omega-i\sin\Omega) = 0$$

Collecting the real and imaginary parts of the above equation:

$$\left[-\delta^3+3\Omega^2\delta+C(\delta^2-\Omega^2)-D\delta+ABe^{\delta}\cos\Omega+Ae^{\delta}(\Omega\sin\Omega-\delta\cos\Omega)\right]$$
$$+i\left[3\delta^2\Omega-\Omega^3-2C\delta\Omega+D\Omega-ABe^{\delta}\sin\Omega+Ae^{\delta}(\delta\sin\Omega+\Omega\cos\Omega)\right] = 0 \qquad (A.17)$$

The real and imaginary parts of equation (A.17) are equalized to zero to maintain :

$$-\delta^3+3\Omega^2\delta+C(\delta^2-\Omega^2)-D\delta+ABe^{\delta}\cos\Omega+Ae^{\delta}(\Omega\sin\Omega-\delta\cos\Omega) = 0 \qquad (A.18)$$

$$-\Omega^3+3\delta^2\Omega-2C\delta\Omega+D\Omega-ABe^{\delta}\sin\Omega+Ae^{\delta}(\delta\sin\Omega+\Omega\cos\Omega) = 0 \qquad (A.19)$$

Extracting A from equation (A.18) :

$$A = -\frac{-\delta^3+3\Omega^2\delta+C(\delta^2-\Omega^2)-D\delta+ABe^{\delta}\cos\Omega}{e^{\delta}(\Omega\sin\Omega-\delta\cos\Omega)} \qquad (A.20)$$

Substituting A into equation (A.19) :

$$-\Omega^3+3\delta^2\Omega-2C\delta\Omega+D\Omega-ABe^{\delta}\sin\Omega$$
$$-\frac{e^{\delta}(\delta\sin\Omega+\Omega\cos\Omega)\left[-\delta^3+3\Omega^2\delta+C(\delta^2-\Omega^2)-D\delta+ABe^{\delta}\cos\Omega\right]}{e^{\delta}(\Omega\sin\Omega-\delta\cos\Omega)} = 0$$

Rearranging the terms gives:

$$\left\{\begin{array}{l}\left[-\Omega^3+3\delta^2\Omega-2C\delta\Omega+D\Omega\right](\Omega\sin\Omega-\delta\cos\Omega)\\ -\left[-\delta^3+3\Omega^2\delta+C(\delta^2-\Omega^2)-D\delta\right](\delta\sin\Omega+\Omega\cos\Omega)\\ -ABe^{\delta}\left[\sin\Omega(\Omega\sin\Omega-\delta\cos\Omega)+\cos\Omega(\delta\sin\Omega+\Omega\cos\Omega)\right]\end{array}\right\} = 0$$

or:

$$\left\{\begin{array}{l}\left[-\Omega^3+3\delta^2\Omega-2C\delta\Omega+D\Omega\right](\Omega\sin\Omega-\delta\cos\Omega)\\ -\left[-\delta^3+3\Omega^2\delta+C(\delta^2-\Omega^2)-D\delta\right](\delta\sin\Omega+\Omega\cos\Omega)\\ -ABe^{\delta}\left[\Omega\sin^2\Omega-\delta\sin\Omega\cos\Omega+\delta\cos\Omega\sin\Omega+\Omega\cos^2\Omega\right]\end{array}\right\} = 0 \qquad (A.21)$$

Dividing by Ω, equation (A.21) becomes:

$$ABe^{\delta} = \left[-\Omega^3+3\delta^2\Omega-2C\delta\Omega+D\Omega\right](\sin\Omega-\frac{\delta}{\Omega}\cos\Omega) - \left[-\delta^3+3\Omega^2\delta+C(\delta^2-\Omega^2)-D\delta\right](\frac{\delta}{\Omega}\sin\Omega+\cos\Omega) \qquad (A.22)$$

Equation (A.22) could be rewritten as follows:

$$ABe^{(\frac{\delta}{\Omega})\Omega} = \left[\Omega^3(3\frac{\delta^2}{\Omega^2}-1)-2\Omega^2C(\frac{\delta}{\Omega})+\Omega D\right](\sin\Omega-\frac{\delta}{\Omega}\cos\Omega) \left[\Omega^3(3\frac{\delta}{\Omega}-\frac{\delta^3}{\Omega^3})+\Omega^2C(\frac{\delta^2}{\Omega^2}-1)-\Omega D(\frac{\delta}{\Omega})\right](\frac{\delta}{\Omega}\sin\Omega+\cos\Omega)$$

or:

$$AB = \frac{\left\{\begin{array}{l}\left[\Omega^3\left(3\frac{\delta^2}{\Omega^2}-1\right)-2\Omega^2 C\left(\frac{\delta}{\Omega}\right)+\Omega D\right]\left(\sin\Omega-\frac{\delta}{\Omega}\cos\Omega\right) \\ -\left[\Omega^3\left(3\frac{\delta}{\Omega}-\frac{\delta^3}{\Omega^3}\right)+\Omega^2 C\left(\frac{\delta^2}{\Omega^2}-1\right)-\Omega D\left(\frac{\delta}{\Omega}\right)\right]\left(\frac{\delta}{\Omega}\sin\Omega+\cos\Omega\right)\end{array}\right\}}{e^{\left(\frac{\delta}{\Omega}\right)\Omega}} = \frac{u(\Omega)}{v(\Omega)}$$

(A.23)

Since $\left(\frac{\delta}{\Omega}\right)$ is constant for a specified response damping ratio, it is sufficient to differentiate equation (A.23) with respect to Ω and let the derivative equal to zero to obtain a value of Ω which gives a maximum AB.

From equation (A.23):

$$\frac{d(AB)}{d\Omega} = \frac{\frac{du(\Omega)}{d\Omega}\,v(\Omega)-\frac{dv(\Omega)}{d\Omega}\,u(\Omega)}{[v(\Omega)]^2} = 0 \qquad (A.24)$$

Since $v(\Omega) = e^{\left(\frac{\delta}{\Omega}\right)\Omega}$ as defined by equation (A.23), equation (A.24) could be rewritten as follows:

$$\frac{du(\Omega)}{d\Omega}\,e^{\left(\frac{\delta}{\Omega}\right)\Omega}-\left(\frac{\delta}{\Omega}\right)e^{\left(\frac{\delta}{\Omega}\right)\Omega}\,u(\Omega) = 0$$

or:

$$\frac{du(\Omega)}{d\Omega} - \left(\frac{\delta}{\Omega}\right)u(\Omega) = 0 \qquad (A.25)$$

From equation (A.23):

$$u(\Omega) = \left[\Omega^3\left(3\frac{\delta^2}{\Omega^2} - 1\right) - 2\Omega^2 C\left(\frac{\delta}{\Omega}\right) + \Omega D\right]\left(\sin\Omega - \frac{\delta}{\Omega}\cos\Omega\right)$$
$$- \left[\Omega^3\left(3\frac{\delta}{\Omega} - \frac{\delta^3}{\Omega^3}\right) + \Omega^2 C\left(\frac{\delta^2}{\Omega^2} - 1\right) - \Omega D\left(\frac{\delta}{\Omega}\right)\right]\left(\frac{\delta}{\Omega}\sin\Omega + \cos\Omega\right)$$

Collecting the 'sin Ω' and 'cos Ω' terms gives:

$$u(\Omega) = \left\{ \begin{array}{l} \sin\Omega \left\{ \begin{array}{l} \Omega^3\left(3\frac{\delta^2}{\Omega^2} - 1\right) - 2\Omega^2 C\left(\frac{\delta}{\Omega}\right) + \Omega D \\ - \frac{\delta}{\Omega}\left[\Omega^3\left(3\frac{\delta}{\Omega} - \frac{\delta^3}{\Omega^3}\right) + \Omega^2 C\left(\frac{\delta^2}{\Omega^2} - 1\right) - \Omega D\frac{\delta}{\Omega}\right] \end{array} \right\} \\ +\cos\Omega \left\{ \begin{array}{l} - \frac{\delta}{\Omega}\left[\Omega^3\left(3\frac{\delta^2}{\Omega^2} - 1\right) - 2\Omega^2 C\left(\frac{\delta}{\Omega}\right) + \Omega D\right] \\ - \left[\Omega^3\left(3\frac{\delta}{\Omega} - \frac{\delta^3}{\Omega^3}\right) + \Omega^2 C\left(\frac{\delta^2}{\Omega^2} - 1\right) - \Omega D\frac{\delta}{\Omega}\right] \end{array} \right\} \end{array} \right\}$$

or:

$$u(\Omega) = \left\{ \begin{array}{l} \sin\Omega \left\{ \begin{array}{l} 3\Omega^3\frac{\delta^2}{\Omega^2} - \Omega^3 - 2\Omega^2 C\left(\frac{\delta}{\Omega}\right) + \Omega D \\ - \left[3\Omega^3\frac{\delta^2}{\Omega^2} - \Omega^3\frac{\delta^4}{\Omega^4} + \Omega^2 C\frac{\delta^3}{\Omega^3} - \Omega C\frac{\delta}{\Omega} - \Omega D\frac{\delta^2}{\Omega^2}\right] \end{array} \right\} \\ +\cos\Omega \left\{ \begin{array}{l} - 3\Omega^3\frac{\delta^3}{\Omega^3} + \Omega^3\left(\frac{\delta}{\Omega}\right) + 2\Omega^2 C\frac{\delta^2}{\Omega^2} - \Omega D\left(\frac{\delta}{\Omega}\right) \\ - \left[3\Omega^3\frac{\delta}{\Omega} - \Omega^3\frac{\delta^3}{\Omega^3} + \Omega^2 C\frac{\delta^2}{\Omega^2} - C\Omega^2 - \Omega D\frac{\delta}{\Omega}\right] \end{array} \right\} \end{array} \right\}$$

Rearranging the terms gives the equation:

$$u(\Omega) = \left\{ \begin{array}{l} \sin\Omega\left[\Omega^3\left(\frac{\delta^4}{\Omega^4} - 1\right) - \Omega^2\left(\frac{\delta}{\Omega}\right)C\left(\frac{\delta^2}{\Omega^2}+1\right) + \Omega D\left(\frac{\delta^2}{\Omega^2} + 1\right)\right] \\ \quad + \cos\Omega\left[-2\Omega^3\frac{\delta^3}{\Omega^3} - 2\Omega^3\frac{\delta}{\Omega} + \Omega^2 C\frac{\delta^2}{\Omega^2} + C\Omega^2\right] \end{array} \right\}$$

or:

$$u(\Omega) = \left\{ \begin{array}{l} \sin\Omega\left[\Omega^3\left(\frac{\delta^2}{\Omega^2} - 1\right) - \Omega^2\left(\frac{\delta}{\Omega}\right)C + \Omega D\right]\left(\frac{\delta^2}{\Omega^2}+1\right) \\ \quad + \cos\Omega\left[-2\Omega^3\left(\frac{\delta}{\Omega}\right) + \Omega^2 C\right]\left(\frac{\delta^2}{\Omega^2} + 1\right) \end{array} \right\} \qquad (A.26)$$

Differentiating equation (A.26):

$$\frac{du(\Omega)}{d\Omega} = \left\{ \begin{array}{l} \cos\Omega\left[\Omega^3\left(\frac{\delta^2}{\Omega^2} - 1\right) - \Omega^2\left(\frac{\delta}{\Omega}\right)C + \Omega D\right]\left(\frac{\delta^2}{\Omega^2} + 1\right) \\ \quad + \sin\Omega\left[3\Omega^2\left(\frac{\delta^2}{\Omega^2} - 1\right) - 2\Omega C\left(\frac{\delta}{\Omega}\right) + D\right]\left(\frac{\delta^2}{\Omega^2}+1\right) \\ -\sin\Omega\left[-2\Omega^3\left(\frac{\delta}{\Omega}\right) + \Omega^2 C\right]\left(\frac{\delta^2}{\Omega^2} + 1\right) \\ \quad + \cos\Omega\left[-6\Omega^2\left(\frac{\delta}{\Omega}\right) + 2\Omega C\right]\left(\frac{\delta^2}{\Omega^2} + 1\right) \end{array} \right\}$$

Collecting the 'sin Ω' and 'cos Ω' terms gives:

$$\frac{du(\Omega)}{d\Omega} = \left\{ \begin{array}{l} \sin\Omega\left[3\Omega^2\left(\frac{\delta^2}{\Omega^2} - 1\right) - 2\Omega C\left(\frac{\delta}{\Omega}\right) + D + 2\Omega^3\left(\frac{\delta}{\Omega}\right) - \Omega^2 C\right]\left(\frac{\delta^2}{\Omega^2} + 1\right) \\ \quad + \cos\Omega\left[\Omega^3\left(\frac{\delta^2}{\Omega^2} - 1\right) - \Omega^2 C\left(\frac{\delta}{\Omega}\right) + \Omega D - 6\Omega^2\left(\frac{\delta}{\Omega}\right) + 2\Omega C\right]\left(\frac{\delta^2}{\Omega^2} + 1\right) \end{array} \right\}$$

or:

$$\frac{du(\Omega)}{d\Omega} = \left\{ \begin{array}{l} \sin\Omega \left\{ 2\Omega^3(\frac{\delta}{\Omega}) + \Omega^2\left[3(\frac{\delta^2}{\Omega^2} - 1) - C\right] - 2\Omega C(\frac{\delta}{\Omega}) + D \right\} (\frac{\delta^2}{\Omega^2} + 1) \\ + \cos\Omega \left\{ \Omega^3(\frac{\delta^2}{\Omega^2} - 1) - \Omega^2(C+6)(\frac{\delta}{\Omega}) + \Omega(2C+D) \right\} (\frac{\delta^2}{\Omega^2} + 1) \end{array} \right\} \qquad (A.27)$$

Substituting the expressions of $u(\Omega)$ and $\frac{du(\Omega)}{d\Omega}$ defined by equations (A.26) and (A.27) into equation (A.25) gives:

$$\left\{ \begin{array}{l} \sin\Omega(\frac{\delta^2}{\Omega^2} + 1) \left\{ \begin{array}{l} 2\Omega^3(\frac{\delta}{\Omega}) + \Omega^2\left[(3\frac{\delta^2}{\Omega^2} - 1) - C\right] - 2\Omega C(\frac{\delta}{\Omega}) + D \\ -\frac{\delta}{\Omega}\left[\Omega^3(\frac{\delta^2}{\Omega^2} - 1) - \Omega^2 C(\frac{\delta}{\Omega}) + \Omega D\right] \end{array} \right\} \\ + \cos\Omega(\frac{\delta^2}{\Omega^2} + 1) \left\{ \begin{array}{l} \Omega^3(\frac{\delta^2}{\Omega^2} - 1) - \Omega^2(C+6)(\frac{\delta}{\Omega}) + \Omega(2C+D) \\ -\frac{\delta}{\Omega}\left[-2\Omega^3(\frac{\delta}{\Omega}) + \Omega^2 C\right] \end{array} \right\} \end{array} \right\} = 0$$

or:

$$\left\{ \begin{array}{l} \sin\Omega \left\{ \begin{array}{l} 2\Omega^3(\frac{\delta}{\Omega}) + \Omega^2\left[3(\frac{\delta^2}{\Omega^2} - 1) - C\right] \\ -2\Omega C(\frac{\delta}{\Omega}) + D - \Omega^3(\frac{\delta}{\Omega})(\frac{\delta^2}{\Omega^2} - 1) + \Omega^2 C\frac{\delta^2}{\Omega^2} - \Omega D\frac{\delta}{\Omega} \end{array} \right\} \\ \cos\Omega \left\{ \begin{array}{l} \Omega^3(\frac{\delta^2}{\Omega^2} - 1) - \Omega^2(C+6)(\frac{\delta}{\Omega}) \\ +\Omega(2C+D) + 2\Omega^3\frac{\delta^2}{\Omega^2} - \Omega^2 C\frac{\delta}{\Omega} \end{array} \right\} \end{array} \right\} = 0$$

Collecting the terms of equal power Ω's:

$$\sin\Omega\left\{\Omega^3\left(\frac{\delta}{\Omega}\right)\left(3-\frac{\delta^2}{\Omega^2}\right)+\Omega^2\left[3\left(\frac{\delta^2}{\Omega^2}-1\right)-C-C\frac{\delta^2}{\Omega^2}\right]-\Omega\left(\frac{\delta}{\Omega}\right)(2C+D)+D\right\}$$
$$+\cos\Omega\left\{\Omega^3\left(3\frac{\delta^2}{\Omega^2}-1\right)-\Omega^2(2C+6)\left(\frac{\delta}{\Omega}\right)+\Omega(2C+D)\right\}=0$$

which gives:

$$\sin\Omega\left[\Omega^3\left(\frac{\delta}{\Omega}\right)\left(3-\frac{\delta^2}{\Omega^2}\right)+\Omega^2(C+3)\left(\frac{\delta^2}{\Omega^2}-1\right)-\Omega\left(\frac{\delta}{\Omega}\right)(2C+D)+D\right]$$
$$=-\cos\Omega\left[\Omega^3\left(3\frac{\delta^2}{\Omega^2}-1\right)-2\Omega^2(C+3)\left(\frac{\delta}{\Omega}\right)+\Omega(2C+D)\right]$$

The value of Ω which gives a maximum AB will be given by the following equation:

$$\tan\Omega=-\frac{\Omega^3\left(3\frac{\delta^2}{\Omega^2}-1\right)-2\Omega^2(C+3)\left(\frac{\delta}{\Omega}\right)+\Omega(2C+D)}{\Omega^3\left(\frac{\delta}{\Omega}\right)\left(3-\frac{\delta^2}{\Omega^2}\right)+\Omega^2(C+3)\left(\frac{\delta^2}{\Omega^2}-1\right)-\Omega\left(\frac{\delta}{\Omega}\right)(2C+D)+D} \qquad (A.28)$$

This verifies equation (3.22) given in chapter 3.

Once the required root (Ω) is obtained, (AB) is determined by equation (A.23) which is rearranged as follows:

$$AB = \left\{ \begin{array}{c} \left(\frac{\delta^2}{\Omega^2}+1\right)\left[\Omega^3\left(\frac{\delta^2}{\Omega^2}-1\right)-\Omega^2 C\left(\frac{\delta}{\Omega}\right)+\Omega D\right]\sin\Omega \\ \left(\frac{\delta^2}{\Omega^2}+1\right)\left[-2\Omega^3\left(\frac{\delta}{\Omega}\right)+\Omega^2 C\right]\cos\Omega \end{array} \right\} e^{-\left(\frac{\delta}{\Omega}\right)\Omega} \qquad (A.29)$$

From equation (A.18):

$$ABe^{\delta} = -\frac{-\delta^3+3\Omega^2\delta+C(\delta^2-\Omega^2)-D\delta+Ae^{\delta}(\Omega\sin\Omega-\delta\cos\Omega)}{\cos\Omega} \qquad (A.30)$$

Substituting equation (A.30) into equation (A.19) gives:

$$\left[-\Omega^3+3\delta^2\Omega-2C\delta\Omega+D\Omega\right]\cos\Omega + \left[-\delta^3+3\Omega^2\delta+C(\delta^2-\Omega^2)-D\delta+Ae^{\delta}(\Omega\sin\Omega-\delta\cos\Omega)\right]\sin\Omega + Ae^{\delta}(\delta\sin\Omega+\Omega\cos\Omega)\cos\Omega = 0$$

or:

$$\left[-\Omega^3+3\delta^2\Omega-2C\delta\Omega+D\Omega\right]\cos\Omega + \left[-\delta^3+3\Omega^2\delta+C(\delta^2-\Omega^2)-D\delta\right]\sin\Omega+Ae^{\delta}\Omega = 0$$

The above equation may be rearranged as follows:

$$Ae^{\left(\frac{\delta}{\Omega}\right)\Omega}\ \Omega = \left\{ \begin{array}{l} -\left[\Omega^3\left(3\frac{\delta^2}{\Omega^2}-1\right)-2\Omega^2 C\left(\frac{\delta}{\Omega}\right)+D\Omega\right]\cos\Omega \\ -\left[\Omega^3\left(\frac{\delta}{\Omega}\right)\left(3-\frac{\delta^2}{\Omega^2}\right)+\Omega^2 C\left(\frac{\delta^2}{\Omega^2}-1\right)-\Omega D\left(\frac{\delta}{\Omega}\right)\right]\sin\Omega \end{array} \right\}$$

Hence:

$$A = -\left\{ \begin{array}{l} \left[\Omega^2(3\frac{\delta^2}{\Omega^2} -1)-2\Omega C(\frac{\delta}{\Omega})+D\right]\cos\Omega \\ +\left[\Omega^2(\frac{\delta}{\Omega})(3-\frac{\delta^2}{\Omega^2})+\Omega C(\frac{\delta^2}{\Omega^2} -1)-D(\frac{\delta}{\Omega})\right]\sin\Omega \end{array} \right\} e^{-(\frac{\delta}{\Omega})\Omega} \qquad (A.31)$$

This verifies equation (3.24) given in chapter 3.

A.2 Rate Sensor Transfer Function Approximated by a 2nd Order Lag Plus a Pure Time Delay

A.2.1 System Closed Loop Transfer Function

By approximating the rate sensor transfer function by a 2nd order lag plus a pure time delay, the heading reference system can be represented by the block diagram shown in figure A.1. The system heading rate output is given by:

$$\dot{\omega}_o(s) = \frac{G_1K_cG_2\psi_n^2e^{-T_Ls}(\frac{1}{T_Is}+1)}{(s^2+2\zeta\psi_n+\psi_n^2)(1+T_2s)}\left[\omega_i(s)-\omega_o(s)\right] \qquad (A.32)$$

For convenience, let

$$K_1 = G_1K_cG_2, \qquad K_2 = \frac{1}{T_I} \quad \text{and} \quad T_n^2 = \frac{1}{\psi_n^2}$$

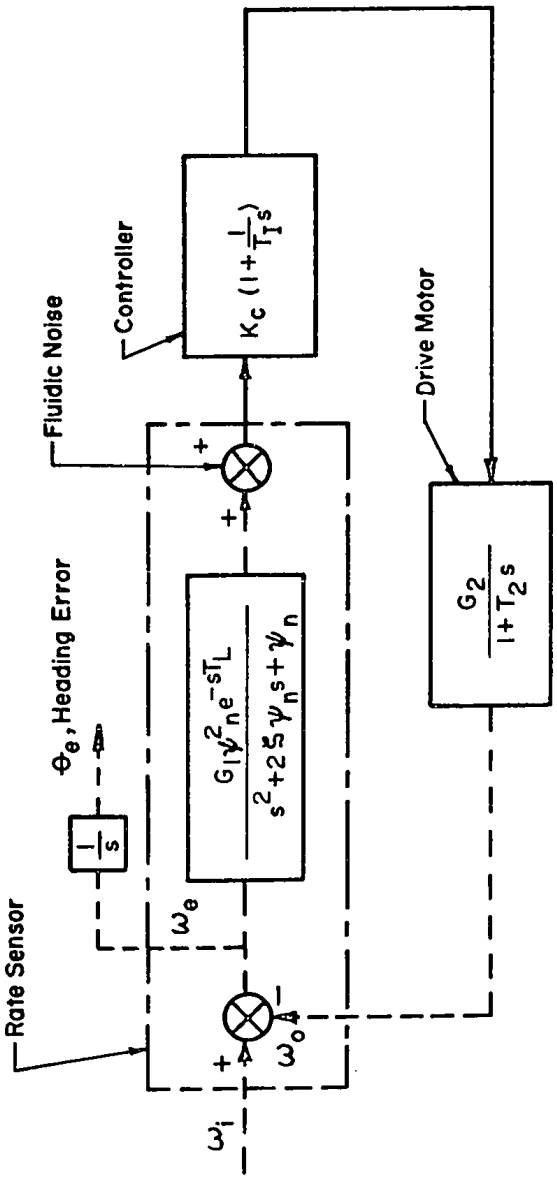

FIGURE A.1 HEADING REFERENCE SYSTEM BLOCK DIAGRAM
(Rate Sensor Transfer Function Represented
by a 2nd Order Lag Plus a Pure Time Delay)

Introducing the auxiliary variable $q = T_L s$, equation (A.32) becomes:

$$\omega_o(s) = \frac{e^{-q}K_1(K_2+\frac{q}{T_L})}{\frac{q}{T_L}(T_n^2\frac{q^2}{T_L^2}+2\zeta T_n\frac{q}{T_L}+1)(1+T_2\frac{q}{T_L})}\left[\omega_i(s)-\omega_o(s)\right]$$

$$= \frac{e^{-q}K_1(K_2T_L+q)T_L^3}{q(T_n^2q^2+2\zeta T_nT_Lq+T_L^2)(T_L+T_2q)}\left[\omega_i(s)-\omega_o(s)\right] \qquad (A.33)$$

Rearranging the terms of equation (A.33) gives:

$$\omega_o(s)\left[1+\frac{e^{-q}K_1(K_2T_L+q)T_L^3}{q(T_n^2q^2+2\zeta T_nT_Lq+T_L^2)(T_L+T_2q)}\right]$$

$$= \frac{e^{-q}K_1(K_2T_L+q)T_L^3}{q(T_n^2q^2+2\zeta T_nT_Lq+T_L^2)(T_L+T_2q)}\omega_i(s) \qquad (A.34)$$

Hence, the system closed loop transfer function is given by:

$$\frac{\omega_o(s)}{\omega_i(s)} = \frac{e^{-q}K_1(K_2T_2+q)T_L^3}{q(T_n^2q^2+2\zeta T_nT_Lq+T_L^2)(T_L+T_2q)+e^{-q}K_1(K_2T_L+q)T_L^3} \qquad (A.35)$$

A.2.2 Steady-State Heading Error

For a step rate input:

$$\omega_i(s) = \frac{\omega_i}{s} = \frac{T_L\omega_i}{q}$$

Substituting the value of $\omega_i(s)$ into equation (A.34):

$$\omega_o(s)\left[1 + \frac{e^{-q}K_1(K_2T_L+q)T_L^3}{q(T_n^2q^2+2\zeta T_nT_Lq+T_L^2)(T_L+T_2q)}\right] = \frac{T_L\omega_i}{q}\left[\frac{e^{-q}K_1(K_2T_L+q)T_L^3}{q(T_n^2q^2+2\zeta T_nT_Lq+T_L^2)(T_L+T_2q)}\right]$$

which gives:

$$\omega_o(s) = \frac{T_L\omega_i}{q}\left[\frac{\dfrac{e^{-q}K_1(K_2T_L+q)T_L^3}{q(T_n^2q^2+2\zeta T_nT_Lq+T_L^2)(T_L+T_2q)}}{1+\dfrac{e^{-q}K_1(K_2T_L+q)T_L^3}{q(T_n^2q^2+2\zeta T_nT_Lq+T_L^2)(T_L+T_2q)}}\right]$$

Since

$$\omega_e(s) = \omega_i(s) - \omega_o(s)$$

the system rate error will be:

$$\omega_e(s) = \frac{T_L\omega_i}{q} - \frac{T_L\omega_i}{q}\left[\frac{\dfrac{e^{-q}K_1(K_2T_L+q)T_L^3}{q(T_n^2q^2+2\zeta T_nT_Lq+T_L^2)(T_L+T_2q)}}{1+\dfrac{e^{-q}K_1(K_2T_L+q)T_L^3}{q(T_n^2q^2+2\zeta T_nT_Lq+T_L^2)(T_L+T_2q)}}\right]$$

$$= \frac{T_L\omega_i}{q}\left[1-\frac{\dfrac{e^{-q}K_1(K_2T_L+q)T_L^3}{q(T_n^2q^2+2\zeta T_nT_Lq+T_L^2)(T_L+T_2q)}}{1+\dfrac{e^{-q}K_1(K_2T_L+q)T_L^3}{q(T_n^2q^2+2\zeta T_nT_Lq+T_L^2)(T_L+T_2q)}}\right]$$

$$= \frac{T_L\omega_i}{q}\left[\frac{1}{1+\dfrac{e^{-q}K_1(K_2T_L+q)T_L^3}{q(T_n^2q^2+2\zeta T_nT_Lq+T_L^2)(T_L+T_2q)}}\right] \qquad (A.36)$$

The heading steady-state error is given by:

$$\theta_e = \int_0^\infty \omega_e(t)dt = \omega_e(s)\Big|_\infty^0 \qquad (A.37)$$

Substituting the expression for $\omega_e(s)$ in equation (A.37):

$$\theta_e = \frac{T_L \omega_i}{q} \left[\frac{1}{1 + \dfrac{e^{-q} K_1 (K_2 T_L + q) T_L^3}{q(T_n^2 q^2 + 2\zeta T_n T_L q + T_L^2)(T_L + T_2 q)}} \right]_{\infty}^{0}$$

Hence:

$$\theta_e = \frac{\omega_i}{K_1 K_2} \qquad (A.38)$$

Equation (A.38) indicated that the system heading steady-state error remains the same for both rate sensor transfer function representations as mentionned in chapter 3.

APPENDIX B

DETERMINATION OF RATE SENSOR PARAMETER VALUES AND OF SIMPLIFIED OPTIMUM CONTROLLER PARAMETER SETTINGS

B.1 Determination of Rate Sensor Parameter Values

As mentionned in chapter 2, the rate sensor transfer function and associated parameter values given by the manufacturer (Reference 10) has been estimated from the experimental frequency response of the rate sensor at 5.0 psi supply pressure. In the absence of a servoed rate table with adequate response capabilities, the rate sensor transient response to an angular rate step input has been investigated in reference 44 in order to determine the rate sensor transfer function at various supply pressures. In this reference, the rate sensor was horizontally suspended from three long lines and the step input of angular rotation was generated by impacting a pendulous mass against a rigid beam radially secured to the sensor. The sensor differential pressure output was detected by a high sensitivity pressure transducer and the step transient response, as taken from reference 44, is shown in figures B.1 and B.2 respectively for rate sensor supply pressures of 1.0 psi and 10.0 psi.

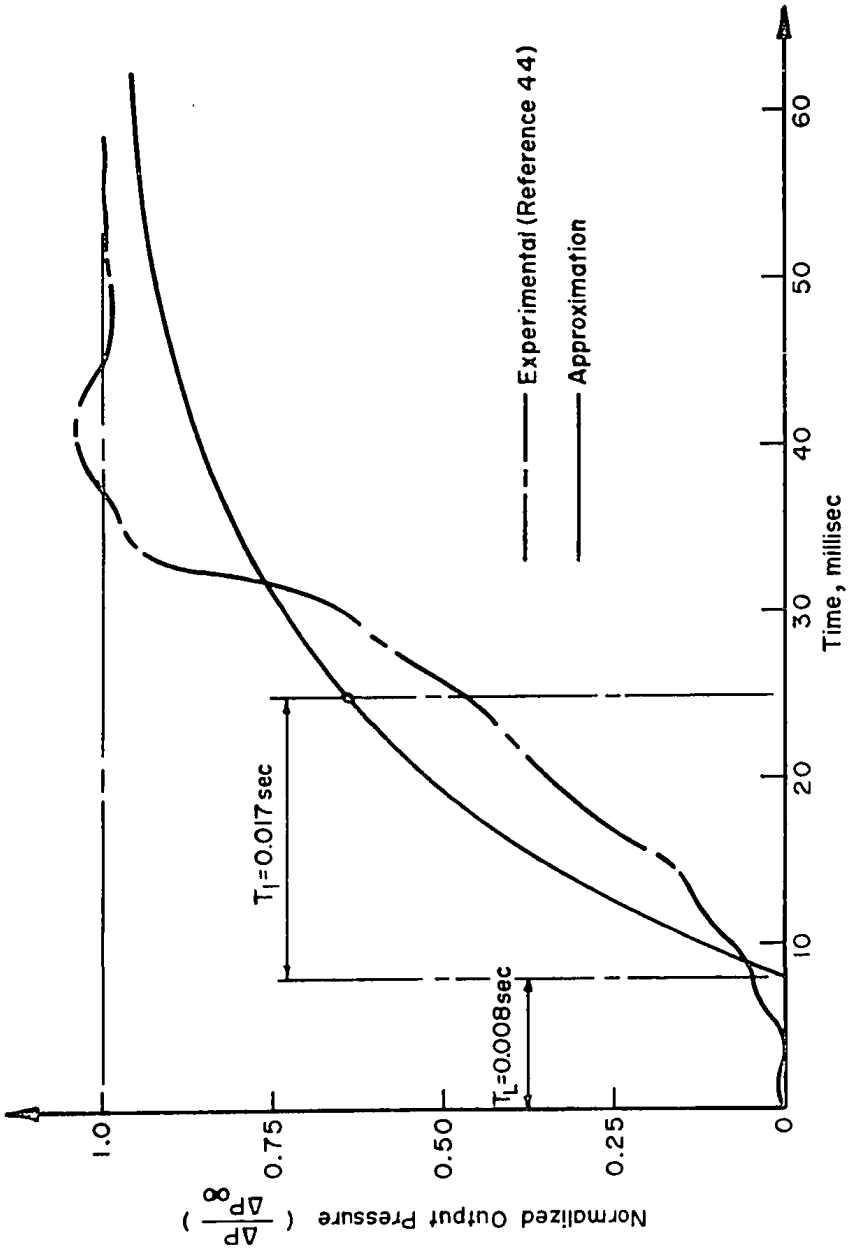

FIGURE B.I RATE SENSOR RESPONSE TO A STEP RATE INPUT (Supply Pressure = 1.0 psi)

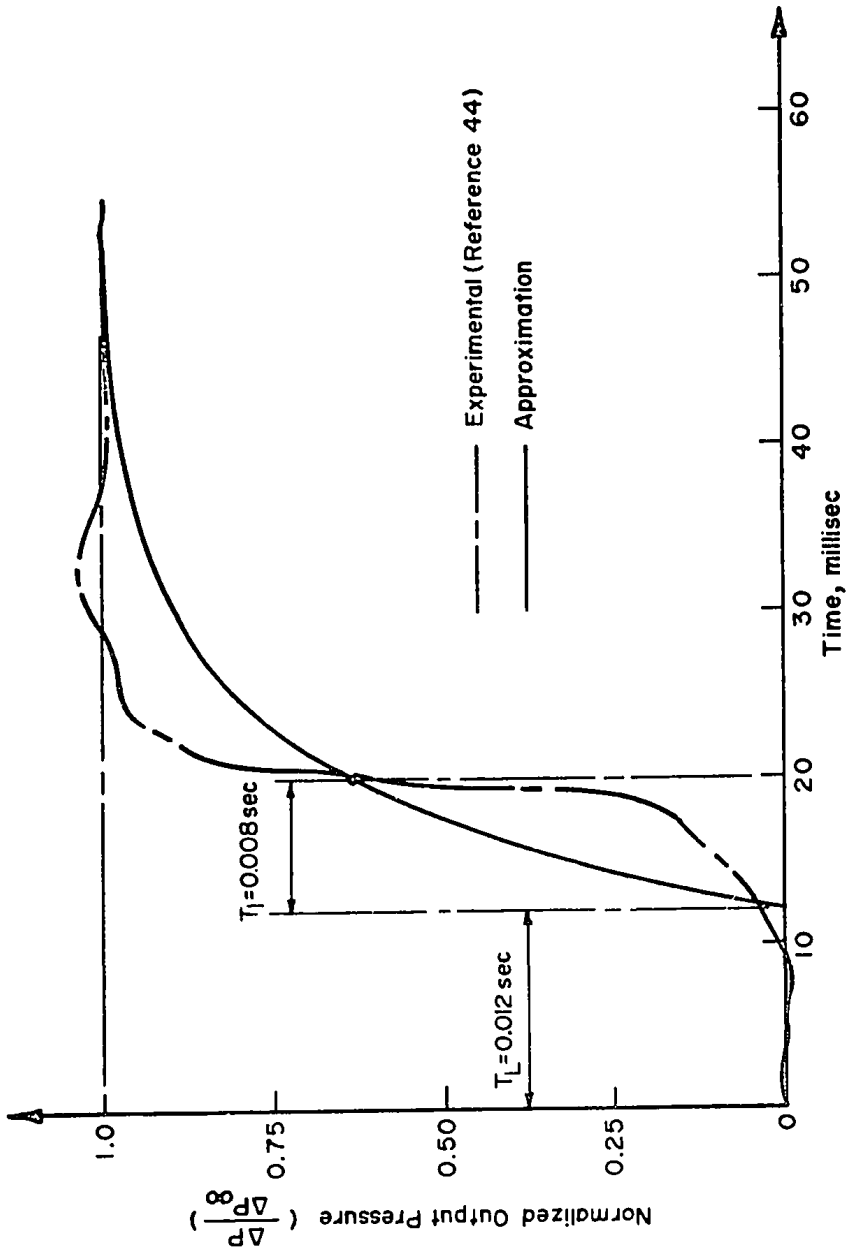

FIGURE B.2 RATE SENSOR RESPONSE TO A STEP RATE INPUT
(Supply Pressure = 10.0 psi)

It is evident from these results that an appropriate transfer function representation of the rate sensor would be by a second-order lag plus a pure time delay. However, as demonstrated in chapter 3, a first-order lag plus a pure time delay with suitably selected parameter values provides an acceptable representation of the rate sensor dynamics for purposes of heading system performance prediction.

From the experimental step transient responses shown in figures B.1 and B.2, the rate sensor transfer function parameter values are estimated to be:

a) At 1.0 psi supply pressure:

$T_L = 0.008$ sec.

$T_1 = 0.017$ sec.

b) At 10.0 psi supply pressure:

$T_L = 0.012$ sec.

$T_1 = 0.008$ sec.

The accuracy with which the assumed transfer function used for the simulated system study represents the actual rate sensor dynamics is indicated in figures B.1 and B.2 where both experimental and corresponding approximate step transient responses are shown superimposed.

B.2 Determination of the Simplified Optimum Controller Parameter Settings

a) System at 1.0 psi supply pressure

As given above:

$$T_1 = 0.017 \text{ sec.}$$
$$T_L = 0.008 \text{ sec.}$$

With $T_2 = 0.020$ sec.

$$D = \frac{T_L^2}{T_1 T_2} = \frac{(0.008)^2}{0.017 \times 0.02} = 0.188$$

$$E = \frac{T_1 + T_2}{\sqrt{T_1 T_2}} \quad \frac{0.017+0.02}{\sqrt{0.017 \times 0.02}} = 2.007$$

From figure 4.5

$$\alpha_o = -0.045, \quad \alpha_1 = 0.572, \quad \alpha_2 = 0.011$$

Substitution of these values into equation (4.5) gives:

$$AB = -0.045 + 0.572(0.188) + 0.011(0.188)^2 = 0.062$$

From figure 4.6

$$\beta_o = -0.314, \quad \beta_1 = 1.96, \quad \beta_2 = 0.240$$

With these values, equation (4.6) gives:

$$A = \frac{-196+\sqrt{1.96^2-4\times0.240(-0.314-0.188)}}{2\times0.240} \doteq 0.245$$

The controller parameter setting are given by:

$$K_1 = \frac{T_1T_2}{T_L^2}A = \frac{1}{0.188}\times 0.245 = 1.303$$

$$K_2 = \frac{B}{T_L} = \frac{AB}{A}\left[\frac{1}{T_L}\right] = \frac{0.062}{0.245}\times\frac{1}{0.008} = 31.63$$

b) System at 5.0 psi supply pressure

As given anteriorly, actual values of T_1 and T_2 were:

$$T_1 = 0.011 \text{ sec.}$$

$$T_L = 0.010 \text{ sec.}$$

With $T_2 = 0.020$ sec.,

$$D = \frac{T_L^2}{T_1T_2} = \frac{(0.01)^2}{0.011\times0.02} = 0.454$$

$$E = \frac{T_1+T_2}{\sqrt{T_1T_2}} = \frac{0.011+0.020}{\sqrt{0.011\times0.020}} = 2.09$$

From figures 4.5 and 4.6

$$\alpha_0 = -0.04, \quad \alpha_1 = 0.58, \quad \alpha_2 = 0.01$$

$$\beta_0 = -0.312, \quad \beta_1 = 1.76, \quad \beta_2 = 0.239$$

By following the same computation procedure as described above, the following controller parameter values are obtained:

$$K_1 = 0.903$$
$$K_2 = 54.87$$

c) System at 10.0 psi supply pressure

From section B.1:

$$T_1 = 0.008 \text{ sec.}$$
$$T_L = 0.012 \text{ sec.}$$

With $T_2 = 0.02$ sec.,

$$D = \frac{T_L^2}{T_1 T_2} = \frac{(0.012)^2}{0.008 \times 0.020} = 0.90$$

$$E = \frac{T_1 + T_2}{\sqrt{T_1 T_2}} = \frac{0.008 + 0.020}{\sqrt{0.008 \times 0.020}} = 2.214$$

With this value of E, figures 4.5 and 4.6 give

$$\alpha_o = -0.034, \quad \alpha_1 = 0.596, \quad \alpha_2 = 0.009$$

$$\beta_o = -0.31, \quad \beta_1 = 1.59, \quad \beta_2 = 0.238$$

The controller parameter setting were determined from equations (4.5), (4.6) and (4.7) as given below:

$$K_1 = 0.98$$
$$K_2 = 48.07$$